

SPIN EVOLUTION OF NEUTRON STARS:
NONLINEAR DEVELOPMENT OF THE R-MODE
INSTABILITY

A Dissertation

Presented to the Faculty of the Graduate School
of Cornell University

in Partial Fulfillment of the Requirements for the Degree of
Doctor of Philosophy

by

Ruxandra Bondarescu

August 2008

© 2008 Ruxandra Bondarescu
ALL RIGHTS RESERVED

SPIN EVOLUTION OF NEUTRON STARS: NONLINEAR DEVELOPMENT
OF THE R-MODE INSTABILITY

Ruxandra Bondarescu, Ph.D.

Cornell University 2008

Rotating neutron stars have modes that are driven unstable by gravitational radiation reaction, principally the r-mode, a Rossby wave with $n = 3, m = 2$, and hence large gravitational radiation reaction. Here n and m label the Legendre functions associated with the mode. The r-mode instability is active when gravitational driving dominates viscous dissipation. It has been suggested that this instability can (1) set the largest angular frequency of rotation of accreting neutron stars and (2) significantly spin down newborn neutron stars preventing them from reaching millisecond periods. Both the maximum frequency that neutron stars can reach and the frequency to which newborn stars can be spun down to in the first few years after formation depend on the neutron star composition via viscous dissipation and neutrino cooling. The nonlinear development of the instability plays a very important role in determining how the saturation process works, and also illustrates how instabilities can saturate at low amplitudes as a consequence of nearly resonant excitation of other modes.

We model the nonlinear interactions between modes together with basic neutron star physics including viscous heating, cooling and spin evolution of the star. The nonlinear effects are included via three-mode couplings. We show that in most scenarios one triplet of modes is sufficient to stop the growth of the instability. To explore possible nonlinear behaviors we parameterize uncertain properties of neutron stars such as the superfluid transition temperature

and the rate at which the star cools via neutrino emission. The average evolution of the mode amplitudes can usually be approximated by quasi-stationary states that change slowly with spin frequency and temperature and can be determined algebraically. The spin and temperature evolution follow or oscillate around trajectories along sequences of quasi-stationary states.

In the Low Mass X-ray Binary (LMXB) case (Chapter 2), after some brief initial oscillations, the modes settle into their quasi-stationary states and the quasi-steady approximation is almost exact. The star heats via viscous dissipation from the three modes and, if this heating is balanced by neutrino cooling, then the evolution will either be stable or enter a slow thermogravitational runaway on a very long timescale of $\approx 10^6$ years. The stable evolutions can be (1) cyclic - with a small cycle size and a typical frequency change of at most 10%, or (2) the star can evolve toward a full equilibrium state in which the accretion torque balances the gravitational radiation emission. Alternatively, if the cooling cannot balance the heating, a faster runaway occurs, the r-mode crosses several parametric instability thresholds, and more modes need to be included.

In the young neutron star case (Chapter 3), the pulsar is hot $T \sim 10^{10}K$ and cools fast. The evolution depends on whether the neutrino cooling can be stopped by viscous heating from the three modes. In this case the evolution is more dynamic. After a short precursor, the modes oscillate around quasi-stationary states and the spin and temperature of the star oscillate around thermal equilibrium. There are three possible outcomes: the neutron star can spin down on different sides of or along the r-mode stability curve. If the viscosity is too low to stop the cooling a runaway occurs.

BIOGRAPHICAL SKETCH

Ruxandra was born in September 1982 in Alexandria, Romania. Her parents are both doctors: her mother is a gynecologist and her father is a retired military doctor. Her grandfather had been an engineer and her grandmother and her great aunt, Tusa Tavi, mathematics teachers. She has one brother, Mihai, who is three years older than her and received his physics Ph.D from Caltech in 2007. She started elementary school in September 1988. In December 1988 Ruxandra and her brother moved to live with their grandparents and Tusa Tavi in Lugoj, a small town in the western part of Romania situated on the banks of the river Timis. They continued school there while their parents were searching for jobs.

Eventually, her parents found jobs during the Romanian Revolution and she and Mihai moved to Timisoara in 1990. There, Ruxandra attended and graduated from General School no. 18 and later the Grigore Moisil Informatics High-school. In this period she and Mihai spent all vacations and weekends in Lugoj swimming all day in summer and bringing stray animals home and then leaving them in the care of their grandmother, who, they believed, was not busy enough when they were away. After passing written examinations, Ruxandra was admitted by three departments at two different universities: (1) the department of control engineering and computer science at the Polytechnic Institute and (2) the department of physics and the department of mathematics and informatics at the West University. Since a fixed curriculum seemed too rigid to her she decided to gain some flexibility by enrolling as a full time student and taking courses in all three departments. The universities were located on the same street within a 5 minute bike ride of each other.

Ruxandra was first introduced to physics research in September 2000 when she and her mother went to visit Mihai in Germany for one week. He was con-

tinuing his undergraduate studies there and had also started research in numerical relativity with Prof. Edward Seidel at the Albert Einstein Institute in Golm, near Berlin. Ruxandra attended Prof. Seidel's group meeting and Mihai introduced her to group members and to Prof. James Bardeen and Luisa Buchman (his graduate student) who were visiting the institute.

At Mihai's advice, she took the GRE Subject Test in Mathematics in addition to the SATs & SAT Subject Tests at the end of highschool and applied to colleges in the US. She was admitted to Reed College, the University of Rochester, Washington College and a few other colleges. By July 2001 she had decided to attend Washington College, received the appropriate visa documents, and was taking her final examinations. In mid July Mihai attended the GR16 conference in South Africa and gave a beautiful talk on his black hole embedding work for which he won the Hartle Award for the best student presentation. There he told Prof. Seidel that 'Ed, if you think I am good, my sister is even better'.

Ruxandra went to Champaign, IL on July 31st, 2001 on a one-way ticket at Prof. Seidel's encouragement and Mihai's advice. Prof. Seidel was visiting the National Center for Supercomputing Applications (NCSA) for a three-week summer vacation to give some momentum to the last year of the Astrophysics Simulation Collaboratory (ASC) project. This was a big project between several institutions in which his group was heavily involved. He and Prof. Paul Saylor tried to convince the University of Illinois in Urbana-Champaign (UIUC) to admit Ruxandra past all deadlines. The university refused, but accepted to enroll her as a part-time, non-degree student and take a maximum of two courses.

She received funding through a Microsoft grant that covered her tuition for Fall 2001 and worked together with Gregory Daues at NCSA on the ASC project. She was admitted as a full time student at UIUC in Spring 2002 and awarded

teaching assistantships that covered her tuition for one year with the condition that she would graduate in this time. With the help and advice of Linda Lorenz, she graduated in December 2002 from UIUC with a major in physics with highest distinction in the curriculum and a double minor in mathematics and computer science. She applied to graduate school and was admitted to UIUC, Caltech, Cornell, Penn State, the University of California San-Diego and a few other universities. She received a masters in physics in August 2003 from UIUC. In the same month she started graduate school at Cornell.

At Cornell Ruxandra worked with Profs. Saul Teukolsky and Ira Wasserman on the effects of nonlinear mode couplings on the R-mode instability. The work is presented in this thesis. Additionally, she collaborated with Andrew Lungren, David Tsang and Mihai Bondarescu on a paper on reducing thermal noise in interferometric detectors that was published in Physical Review D in 2008 [1]. They proved that finite mirror effects are important and need to be taken into account in Mesa mirror design. They matched the phase front of the mirror to that of the finite eigenbeam and found that the diffraction loss was significantly lower, allowing the use of wider beams that have lower noise for the same diffraction loss constraint. She also wrote two papers on numerical simulations of dark matter stars: boson stars (complex scalar field; published in Classical and Quantum Gravity 2006 [2]) and soliton stars (real scalar field; published in Physical Review D 2008 [3]) and studied their behavior under small nonradial perturbations. The LIGO mirror and the scalar field work are not related to the material presented in this thesis and therefore will not be included.

In September Ruxandra will be moving to State College, Pennsylvania and work as a postdoctoral scholar at Penn State.

To Greg and Jaya

ACKNOWLEDGEMENTS

I want to first thank my advisors Ira Wasserman and Saul Teukolsky for being the best advisors I could have possibly had for my Ph.D. They guided my research and they have shown, what seemed to me at times, close to infinite patience. They were there every time I needed advice, encouragement and support. I thank Ritchie Patterson for being on my special committee and for useful discussions and advice.

It is hard to find words to acknowledge Ed Seidel's and Gabrielle Allen's influence on my life. I thank Ed for having faith in an 18 year old who barely spoke English and was in a situation that did not fit any given rule. I still remember the first time I went to the international students office with Ed when I heard him say that he guarantees for everything I do and is convinced that I will be successful. I will continue to believe that you and Gab are among the most amazing people alive. I am grateful to Gab for constantly being there for me and Mihai when we needed advice and help.

I am extremely grateful to Gregory Daues and Jayashree Balakrishna for being my friends as well as my collaborators. They gave up many Christmas and New-Year holidays and also countless weekends and afternoons to work with me. They supported me both as an undergraduate and graduate student and when life seems too hard their support brings me back on track and makes me feel that I cannot fail with such friends. I thank Zorro, my favorite dog in the world, for brightening my stays in Champaign-Urbana and for many pleasant afternoons in open air in various parks spent with him, Greg and Jaya.

I especially want to thank Linda Lorenz for guiding and supporting me as an undergraduate. I am also very grateful to Mark Williams who went well beyond his job requirement to help and advise me. I thank Lance Cooper, Denise Don-

nelly, Gary Gladding, Alan Nathan, Matt Selen, Brad Wind and Galina Wind, Scott Willenbrock, James Wiss, and James Wolfe. Without them my graduation from the University of Illinois would not have been possible.

I thank Doina Costescu, Cornel Costescu and their two daughters: Ruxandra and Ileana for interesting discussions, moral support, very good food, and for making me feel less alone in Champaign-Urbana. I am also grateful to them for hosting me every time I came back to visit from Cornell to work with Greg and Jaya. I have always felt at home when I was with them and they provided good advice and made some of my research projects with Greg and Jaya possible. I am still driving the car that Cornel found for me.

I acknowledge Prof. Dumitru Vulcanov from the West University of Timisoara for valuable advice and support when I was taking college courses in Romania, for inviting me to give my first physics talk at UVT, and for supporting my graduate school applications and later various fellowship applications. He has been a good advisor and friend to both me and Mihai.

I thank my students Elena Caraba (now at LSU; she will be starting graduate school at UIUC later this year), Ana Elena Buleu (now at LSU), Irina Craciun (now at LSU) and Jenica Abrudan (now at the U. of Notre-Dame) for trusting their future in my hands. I thank Ed and Gab for taking the recommendations Mihai and I wrote at face value, for accepting Ana, Elena, Irina, and also Razvan Carbunescu, Florin Mingireanu and Gabriela Turcu (now at the University of Chicago) in their research group at LSU's Center for Computation and Technology, and for being the wonderful advisors they always are.

I am grateful to Jeandrew Brink for many useful conversations and for helping me start the r-modes project. I thank David Tsang and Andrew Lundgren for working with me and Mihai on the LIGO project and for being my friends.

I thank Badri Krishnan for providing the Advanced LIGO and Einstein Telescope noise curves from their paper, and Jocelyn Read for another Advanced LIGO noise curve from David Shoemaker that is not used here. I am grateful to Sharon Morsink for useful discussions when she visited Cornell to give a 2008 astronomy colloquium and especially, for pointing out that higher order frequency corrections are important at non-zero eccentricities when computing frequency differences for mode triplets.

I am also grateful to the sixth floor graduate students who made my stay at Cornell fun and unforgettable. I thank Dave Bernat, Francois Foucart, Paul and Jazz Grabowski, Tanja Hinderer, Rebecca Harbison, Wen Fu, John Karcz, Andrew Lundgren, Zach Medin, Abdul Mroue, Sharvari Nadkarni, Stefan Natu, Nick Taylor, Dave Tsang and Mark Wyman. I am especially grateful to Tanja and Dave T. for watching Kip Thorne's lectures on gravitational waves for almost a whole year and for going on fun hiking trips with me after lectures. I thank my advisors, Mihai, and Andy for carefully proofreading this manuscript.

I thank Kiran Thadani for being my best friend at Cornell and for moral support, housing during my last days in Ithaca and useful discussions.

I also acknowledge my family. I thank Mihai for constant support, for being my role model and my best friend. I am grateful to my parents for believing in me and to my mother for constantly providing strength and giving her best in taking care of us and now of her grandchildren. I thank my sister-in-law Lisa, my nephew David and her yet-to-be-born baby for making me feel at home every time I visited Caltech. I thank my grandparents, Tusa Tavi and their best friends: Tanti Ketu, Tanti Mia and Domnul Costel for helping my parents in bringing Mihai and me up and for making our vacations be like a beautiful dream.

I am very grateful to Richard Price, Pablo Laguna, Ben Owen, and Sam Finn for offering me postdoctoral positions and additionally, I thank Ben for many useful discussions when we met at various conferences and during my latest Penn State visit.

This research was funded by NSF grants AST-0307273, AST-0606710, PHY-0354631, and PHY-0652952. I have also received numerous travel grants from the American Physical Society, the Cornell graduate school, NSF and IU-PAP/ISGRG.

TABLE OF CONTENTS

Biographical Sketch	iii
Dedication	vi
Acknowledgements	vii
Table of Contents	xi
List of Tables	xiii
List of Figures	xiv
1 Introduction	1
2 The Effects of R-mode Instability on the Spin Evolution of Neutron Stars in LMXBs¹	9
2.1 Introduction	9
2.2 Evolution Equations	17
2.2.1 Three mode system: coupling to uniform rotation	17
2.2.2 Temperature and Spin Evolution	20
2.2.3 Temperature and Spin Evolution with the Mode Amplitudes in Quasi-Stationary States	23
2.2.4 Sources of Driving and Dissipation	23
2.3 Summary of Results	27
2.4 Possible Evolution Scenarios	30
2.4.1 Cyclic Evolution	30
2.4.2 Steady State Evolution	33
2.4.3 Thermal Runaway Evolutions	37
2.5 Probability of Detection	41
2.6 Discussion and Concluding Remarks	45
3 The Effects of R-mode Instability on the Spin Evolution of Newborn Neutron Stars	49
3.1 Introduction	49
3.2 Mathematical Background	54
3.2.1 Three-mode Evolution Equations	54
3.2.2 Driving and Damping Rates	55
3.2.3 Angular Momentum and Temperature Evolution	57
3.2.4 Quasi-Stationary Solutions	59
3.3 Brief Summary of Results	60
3.4 Shortcomings of the Model and Possible Improvements	65
3.5 Stable Evolutions	67
3.5.1 Type I	67
3.5.2 Type II	73
3.5.3 Type III	76
3.6 Runaway Evolutions	78
3.7 Detection of Gravitational Waves	79
3.8 Discussion and Concluding Remarks	83

4 Conclusion	85
A Appendices to Chapter 2	90
A.1 Equations of Motion	90
A.2 Stability Around Equilibrium at Constant Angular Velocity	94
B Appendices to Chapter 3	97
B.1 Changes in Mode Frequencies due to Magnetic Fields	97
B.2 Bulk Viscosity Integrals and Viscous Damping Timescales	98
B.3 Boundary Layer Viscosity Integrals	100
B.4 Oscillations Around Thermal Equilibrium: One Mode Evolution .	100
Bibliography	105

LIST OF TABLES

- B.1 Bulk viscosity timescales computed using incompressible stellar modes ($\tau_{\text{bulk } n=0}$; used in this work with a different bulk viscosity coefficient) and $n = 1$ polytrope ($\tau_{\text{bulk } n=1}$) inertial modes for an n-p-e gas. The $n = 1$ polytrope calculation was performed by Lockitch and Friedman [75]. Note that, mathematically, the bulk viscosity damping rate is zero for incompressible stars. We adopt the attitude that the dissipation timescale is computed to leading order in Γ_1 and take $\Gamma_1 = 2$ (for incompressible stars $\Gamma_1 \rightarrow \infty$). The timescales for the two models are roughly within a factor of 2 of each other. 99

LIST OF FIGURES

- 2.1 (a) Typical trajectories for the four observed evolution scenarios are shown in the $\tilde{\Omega} - T_8$ phase space, where $\tilde{\Omega} = \Omega/\Omega_c$. The dashed lines ($H = C$ curves) represent the points in the $\tilde{\Omega} - T_8$ phase space where the dissipative effects of the heating from the three-modes exactly compensate the neutrino cooling for the given set of parameters ($S_{\text{ns}}, f_{\text{dU}}, T_c, \dots$) of each evolution. (b) The corresponding stability regions for which these scenarios occur are plotted at fixed hyperon superfluidity temperature $T_c = 5.0 \times 10^9$ K, while varying f_{dU} and S_{ns} . The position of the initial angular velocity and temperature ($\tilde{\Omega}_{\text{in}}, T_{8 \text{ in}}$) with respect to the maximum of this curve determines the stability of the evolution. (I) $\tilde{\Omega}_{\text{in}} > \tilde{\Omega}_{H=C \text{ max}}$. Trajectory R_1 . Fast Runaway Region. After the r-mode becomes unstable the star heats up, does not find a thermal equilibrium state and continues heating up until a thermogravitational runaway occurs. (II) $\tilde{\Omega}_{\text{in}} < \tilde{\Omega}_{H=C \text{ max}}$. The evolutions are either stable or, if there is a runaway, it occurs on timescales comparable to the accretion timescale. The possible trajectories are (1) Trajectory C. Cycle Region. (2) Trajectories S_1 and S_2 . Steady State Region. (3) Trajectory R_2 . Slow Runaway Region. 28
- 2.2 Two cyclic trajectories in the $\tilde{\Omega} - T_8$ plane are displayed for a star with $T_c = 5.0 \times 10^9$ K and (a) $f_{\text{dU}} = 0.15$ and $S_{\text{ns}} = 0.10$, and (b) $f_{\text{dU}} = 0.142$ and $S_{\text{ns}} = 0.35$, which is close to the border between the stable and unstable region (see Fig. 2.3(b)). The thick solid line labeled as the Heating = Cooling ($H = C$) curve is the locus of points in this phase space where the neutrino cooling is equal to the viscous heating due to the unstable modes. The other solid line representing the r-mode stability curve is defined by setting the gravitational driving rate equal to the viscous damping rate. The part of the curve that decreases with T_8 is dominated by boundary layer and shear viscosity, while the part of the curve that has a positive slope is dominated by hyperon bulk viscosity. In portion $a_1 \rightarrow b_1$ of the trajectory the star heats up at constant $\tilde{\Omega}$. Part $b_1 \rightarrow c_1$ represents the spin down stage, which occurs when the viscous heating is equal to the neutrino cooling. $c_1 \rightarrow d_1$ shows the star cooling back to the initial T_8 . Segment $d_1 \rightarrow a_1$ displays the accretional spin-up of the star back to the r-mode stability curve. The cycle $a_2 \rightarrow d_2$ proceeds in the same way. This cycle is close to the peak of the $H = C$ curve. Configurations above this peak will run away. 31

2.3	<p>(a)The amplitudes of the r-mode C_α and of the $n = 13, m = -3$ and $n = 14, m = 1$ inertial modes C_β and C_γ are shown as a function of time for a star that executes a cyclic evolution (same parameters as in Fig. 2.2). The lowest parametric instability threshold is also displayed. (b)The ratio of the r-mode amplitude to the parametric instability threshold is plotted as a function of time. It can be seen that once the r-mode crosses the parametric instability threshold it remains close to it for the rest of the evolution. (c)The parametric instability threshold is displayed as a function of time. Its value changes as the angular velocity and temperature evolve.</p>	34
2.4	<p>The trajectory of a neutron star in the $\tilde{\Omega}-T_8$ phase space is shown for a model with $T_c = 5.0 \times 10^9$ K, $f_{dU} = 0.03$ and $S_{ns} = 0.03$ that reaches an equilibrium steady state. The star spins up until it crosses the r-mode stability curve and the r-mode becomes unstable. The r-mode then quickly grows to the first parametric instability threshold and excites the daughter modes. In leg $a \rightarrow b$ of the trajectory the star is viscously heated by the mode triplet until the system reaches thermal equilibrium. Segment $b \rightarrow c$ shows the star continuing to heat and spin up in thermal equilibrium until the accretion torque is balanced by the gravitational radiation emission. The r-mode stability curve represents the points in phase space where the viscous driving rate is equal to the gravitational driving rate. The H=C curve is the locus of points where the viscous dissipation due to the mode triplet balances the neutrino cooling.</p>	35
2.5	<p>The $(\tilde{\Omega}, T_8)$ initial values (region delimited by the solid line) that lead to equilibrium steady states and their corresponding final steady state values (region enclosed by the dashed line) are shown. Since both the initial and final values of T_8 are low, these evolutions are roughly independent of T_c.</p>	36
2.6	<p>This plot compares the full evolution resulting from solving Eqs. (2.4),(2.13),(2.18) with the reduced $\Omega - T$ evolution that assumes the amplitudes go through a series of steady states Eqs. (2.19)-(2.20) for a model with $T_c = 5.0 \times 10^9$ K, $f_{dU} = 0.058$ and $S_{ns} = 0.25$. (a) The temperature is displayed as a function of time for the two different methods. (b) The angular velocity $\tilde{\Omega} = \Omega/\Omega_c$ is shown as a function of temperature. The evolution occurs at constant spin frequency. It can be seen that the steady-state amplitude approximation is extremely good. The 'X' shows the point at which the r-mode crosses its second lowest parametric instability threshold, where additional dissipation would become operative.</p>	38

- 2.7 The trajectory of a neutron star in the $\tilde{\Omega}-T_8$ phase space is shown for a model with $T_c = 5.0 \times 10^9$ K, $f_{\text{dU}} = 4.0 \times 10^{-5}$ and $S_{\text{ns}} = 0.02$ that goes through a slow thermogravitational runaway. Portion $a \rightarrow b$ of the trajectory shows the mode triplet heating up the neutron star through boundary layer and shear viscosity until the system reaches thermal equilibrium. Segment $b \rightarrow c$ represents the accretional spin-up of the star in thermal equilibrium. The dotted-dashed line is the locus of points where the viscous dissipation of the mode triplet is equal to the neutrino cooling, and is labeled as the $H = C$ curve. The star reaches the maximum of this curve and fails to reach an equilibrium between the accretion torque and gravitational emission. It then continues heating at constant angular velocity and crosses its second lowest parametric instability threshold, at which point more modes would need to be included to make the evolution accurate. Eventually the star reaches the r-mode stability curve again. 40
- 2.8 The spin-down timescale is shown as slippage factor S_{ns} and fraction of the star subject to direct URCA f_{dU} for cyclic evolutions are varied for a fixed hyperon critical temperature of $T_c = 5.0 \times 10^9$ K. This timescale dominates the heat-up timescale and hence represents the time the star spends above the r-mode instability curve. It increases as the viscosity is lowered and the star gets closer to the steady state region. 42
- 2.9 (a) The stability regions are plotted at fixed hyperon superfluidity temperature $T_c = 6.5 \times 10^9$ K, while varying f_{dU} and S_{ns} . The steady state region remains roughly the same as in Fig. 2.3(b), the slow run-away region disappears, and the cycle region increases dramatically while shrinking the fast-runaway region. (b) The spin-down timescale is shown for the cyclic evolutions in part (a). 43

- 3.1 Typical trajectories for five observed evolution scenarios are shown in the $\tilde{\Omega} - T_9$ plane, where $\tilde{\Omega} = \Omega/\Omega_c$. Stable Evolutions. **Type I:** the star cools until the cooling is balanced by the viscous heating from the three modes and spins down in the first unstable region ($T_9 > T_{9\text{peak}}$) - evolution A. The average trajectory can be determined by using quasi-steady state mode amplitudes until the star intersects the r-mode stability curve. It then cools until it enters the second unstable region: $T_9 < T_{9\text{peak}}$ and spins-down along r-mode stability curve. **Type II:** the star spins down on the r-mode stability curve or oscillates around it - evolutions B and C. In evolution C the thermal oscillations become unstable and the star cools to the next thermal equilibrium region. **Type III:** the star cools until it reaches thermal equilibrium to the left of the r-mode stability curve ($T_9 < T_{9\text{peak}}$) and subsequently spins down on the quasi-steady $H = C$ curve in the second unstable region - evolution D. **Type R:** Runaway evolution. The three-mode system is not sufficient to model this evolution and more modes need to be included. 61
- 3.2 The trajectories in the $\tilde{\Omega} - T_9$ plane for evolutions with different coupling coefficients are shown for three values of κ : 3.95, 1.25 and 0.395. All other parameters are the same. The hyperon superfluidity temperature is $T_h = 6.0 \times 10^9$ K. The cooling is stopped by the heating later for larger κ and the thermal oscillations are smaller. 64
- 3.3 A typical type I trajectory in the $\tilde{\Omega} - T_9$ plane is shown for $T_{\text{ch}} = 6.0 \times 10^9$ K. The evolution starts at $\tilde{\Omega}_i = 0.67$, $T_{9i} = 10$. The star cools down to $T_{9a} = 1.43$ in about 10 minutes. At this point the dissipation heating of the 3-modes balances the cooling and the star spins down, oscillating around its quasi-steady solution for $t_{a \rightarrow b} \approx 0.1$ yr until it intersects the r-mode stability curve at $T_{9b} = 1.25$, $\Omega_b = 0.45$. It then cools down at constant $\tilde{\Omega} = \tilde{\Omega}_b$ until the cooling is again balanced by the viscous heating due to the r-mode. The daughter modes do not get excited in this part of the evolution. The star then spins and cools down in thermal equilibrium on the r-mode stability curve for $t_{c \rightarrow d} \approx 2.8$ yr until it enters the stable region again at $T_d \approx 0.60$, $\tilde{\Omega}_d \approx 0.25$ 68
- 3.4 Mode amplitudes displayed as a function of time for $T_h = 6.0 \times 10^9$ K. (a) Initial evolution. The three modes settle down to their quasi-steady states in the first minute or so and then oscillate around these solutions. (b) Evolution before the r-mode stability curve is reached. (c) The r-mode and its parametric instability threshold amplitude shown as the star crosses from the right to the left side of the r-mode stability curve. 69

- 3.5 The r-mode amplitude for the second part of the evolution ($T_9 < T_{9\text{peak}}$) is shown as a function of T_9 in (a) and as a function of time in (b). Part (a) details the initial oscillation of $|\bar{C}_\alpha|$ around the thermal equilibrium value $|\bar{C}_\alpha|_{H=C \text{ r-mode}}$. The r-mode eventually settle to its equilibrium value and continues spinning down along the r-mode stability curve. Part (b) shows the agreement between the r-mode amplitude from the full evolution code and the thermal equilibrium r-mode amplitude computed on the r-mode stability curve $|\bar{C}_\alpha|_{H=C \text{ r-mode}}(\tilde{\Omega}_{\text{CFS}}, T_{9\text{CFS}})$ with $\tilde{\Omega}$ between $\Omega_c = \Omega_b \approx 0.45$ and $\Omega_d \approx 0.25$ 70
- 3.6 Another type I evolution is shown for a lower hyperon superfluidity temperature $T_h = 2.0 \times 10^9$ K. (a) The trajectory of the star is shown in the $\tilde{\Omega} - T_9$ plane. The star cools from $T_{9i} = 10$, $\tilde{\Omega}_i = 0.67$ to $T_{9a} \approx 1.12$ in about 10 min. At this point the viscous heating is large enough to stop the neutrino cooling. The star then spins down and cools to $\tilde{\Omega}_b \approx 0.27$, $T_{9b} \approx 0.76$ in $t_{a \rightarrow b} \approx 2.5$ yr. At point b the star intersects the r-mode stability curve and the r-mode becomes stable. The star starts cooling at constant angular velocity. At this lower spin frequency the dipole spin-down becomes important and the star spins down at $T_{9c} \approx 0.5$ never reaching the unstable region of the $\tilde{\Omega} - T_9$ plane again. (b) The r-mode and its parametric instability threshold amplitude are shown as a function of time. As before it can be seen that $|\bar{C}_\alpha|_{\text{quasi}} = |\bar{C}_\alpha|_{\text{PIT}}$ is a good approximation for the average r-mode amplitude until the star crosses in the stable region. The oscillations around this quasi-stationary solutions are about 6 times smaller than in the $T_h = 6.0 \times 10^9$ K evolution. 71
- 3.7 The trajectory of the neutron star in the $\tilde{\Omega} - T_9$ plane is shown for evolutions C and D of Fig. 3.1. The star cools to $T_{9a} = 1.82$ in about 6 minutes and crosses the r-mode stability curve for the second time. In evolution C the r-mode reaches large enough amplitudes for the viscous dissipation to balance the cooling. It then settles in thermal equilibrium ($H = C$) and spins down along the r-mode stability curve. It spins down to $\Omega_{b1} = 0.58$, $T_{b1} \approx 1.68$ in $t_{a1 \rightarrow b1} \approx 48$ hours. At this point the temperature of the star starts oscillating and the r-mode amplitude oscillates around the stability curve for $t_{b1 \rightarrow c1} = 6.7 \times 10^5$ sec until $T_{9c1} = 1.53$, $\tilde{\Omega}_{c1} = 0.44$. At this points it cools at constant $\tilde{\Omega}$ for $t_{c1 \rightarrow c2} = 1.2 \times 10^4$ sec to another thermal equilibrium region. The rest of the evolution coincides for C and D. In the case of evolution D the star cools at constant $\tilde{\Omega} = \tilde{\Omega}_i = 0.67$ to $T_{9b2} \approx 1.13$ in about 2 hours and spins down in $t_{b2 \rightarrow e} \approx 3$ yr on a $H = C$ curve determined by the quasi-steady states of all three modes. 74

- 3.8 (a) The r-mode $|\bar{C}_\alpha|$ and daughter mode $|\bar{C}_\beta|, |\bar{C}_\gamma|$ amplitudes are displayed at the beginning of a type II evolution (evolution C in Fig 1). The r-mode is seen to settle to its equilibrium value $|\bar{C}_\alpha|_{H=C_{r\text{-mode}}}$ and the daughter mode oscillations damp to zero. (b) The r-mode and its thermal equilibrium solution $|\bar{C}_\alpha|_{H=C_{r\text{-mode}}}$ are shown for the first part of the evolution (the trajectory oscillates in the $\bar{\Omega} - T_9$ plane around the r-mode stability curve). This equilibrium solution is seen to be a good approximation for the average r-mode amplitude. 75
- 3.9 (a) The amplitudes of the r-mode $|\bar{C}_\alpha|$ and of the two daughter modes $|\bar{C}_\beta|, |\bar{C}_\gamma|$ are shown settling to their quasi-steady states in the first 40 minutes of a type III evolution (evolution D in Fig. 3.1). (b) The r-mode amplitude and its lowest parametric instability threshold (the parametric instability threshold coincides with the r-mode quasi-steady solution) is shown as a function of time for the whole evolution. The quasi-steady solution is a good approximation that maps the evolution with an almost exact agreement in the non-oscillatory part of the trajectory. 77
- 3.10 (a) The growth rate of the r-mode $\tilde{\gamma}_\alpha = \tilde{\gamma}_{GR} - \tilde{\gamma}_{\alpha v}$ and the sum of the viscous damping rates for the two daughter modes $\tilde{\gamma}_\beta + \tilde{\gamma}_\gamma$ are shown versus time. If $\tilde{\gamma}_\alpha > \tilde{\gamma}_\beta + \tilde{\gamma}_\gamma$ the evolution is unstable. (b) The r-mode amplitude $|\bar{C}_\alpha|$ is shown versus time for the two evolutions. In the unstable evolution the r-mode amplitude grows exponentially while for the stable case it oscillates and will eventually settle close to its quasi-steady state. Both evolutions have $T_h = 2 \times 10^9$ K. The viscosity is different with $A_{hb} = 2.9 \times 10^3$ for the unstable case and $A_{hb} = 2.8 \times 10^3$ for the stable case. 80
- 3.11 A similar runaway occurs for low cooling. Here $f_{dU} = 0.0, A_{hb} = 5.0 \times 10^3$ and $T_h = 1.2 \times 10^{10}$ K for both evolutions. The initial amplitudes are $|\bar{C}_\alpha|(0)_{\text{stable}} = 6.0 \times 10^{-5}$ and $|\bar{C}_\alpha|(0)_{\text{unstable}} = 7.0 \times 10^{-5}$. 81

CHAPTER 1

INTRODUCTION

It has been over 26 years since the discovery of the first millisecond radio pulsar in 1982 by Backer *et al* [4]. This pulsar, labeled as PSR B1937+21, has a spin rate of 642 Hz and remains one of the fastest known spinning neutron stars. Since then powerful telescopes and observatories have revolutionized the field of observational astronomy. A large number of millisecond pulsars have been identified, with the majority located in globular clusters.

Globular clusters have high stellar densities and make the existence of binary systems more likely. The globular cluster location together with the inferred low magnetic fields of accreting millisecond pulsars compared to young neutron stars favor the 'recycling' theory as an explanation for their formation. In this scenario an old, slowly rotating neutron star is spun up or recycled through accretion from a companion star.

Neutron stars are the most compact stars in the observable universe. They are about as massive as the sun and have a radius roughly between 10 – 20 km, depending on the equation of state [5]. Since they are very compact they have high gravitational fields, and in a binary accreted material spirals towards the neutron star with angular momentum that is too high to hit the tiny star directly. It instead orbits in a disk around the compact object. The gas then heats due to viscosity as it spirals inward emitting X-rays. Eventually, the matter reaches the surface of the neutron star and transfers angular momentum to the neutron star increasing the rotation rate. The recycling process ends when the pulsar is revitalized and has reached millisecond periods, and the companion is almost emptied and turned into a white dwarf or brown dwarf. At this point the in-

fall of matter stops, the X-ray emission declines, and the neutron star becomes a radio millisecond pulsar. In dense globular clusters the neutron star can also swap companion stars. One such example was observed by the Chandra X-ray Telescope in Tuc 47 W in 2005 [6]. This binary contains a millisecond pulsar with a period of $T = 2.35$ ms and a normal companion star of about $0.12M_{\odot}$. It is believed that this star has been captured recently, and is not the original companion that spun up the pulsar. A shock wave is observed around the millisecond pulsar as its companion is trying to dump more matter on the already fast spinning object. In contrast with this system, SAX J1808.4-3658 has a similar pulsation period, but it is located outside a globular cluster [7]. Its companion is a depleted star with a mass of only $0.05M_{\odot}$. This pulsar is likely with its original companion.

SAX J1808.4-3658 was also the first millisecond pulsar discovered in an X-ray binary, and was considered to be direct proof of pulsar recycling [8]. It is a transient source and recent XMM-Newton and Gemini observations studied its behavior in quiescence (see Heinke *et al.* (2006) [9].) They found that the binary exhibits particularly low X-ray luminosity and relatively high optical luminosity. The strong heating of its companion star, inferred from the optical luminosity, could suggest that radio emission turns on when accretion turns off [9]. This would make the binary a transition object between accreting X-ray binaries and millisecond radio pulsars. On the other hand, the low X-ray luminosity provides evidence for enhanced neutrino cooling in its core.

The spin rates of radio-quiet neutron stars in X-ray binaries can be estimated using emitted X-ray oscillations. There are three different types of oscillations. The spin of the neutron star can be measured directly if there are fixed hot spots

on the star by observing the rise and fall of the surface temperature as the hot spots appear and disappear due to rotation. The hot spots are believed to occur at the magnetic footpoints, where the electromagnetic radiation is funneled back into the surface of the star. Hot spots were first observed in 2005 by the XMM-Newton satellite on the surfaces of three nearby neutron stars. Currently, there are 10 sources that exhibit such behavior with spin frequencies between 182–599 Hz [13]. The other measures of spins are indirect. The second is through X-ray burst oscillations. These are coherent millisecond pulsations during type I X-ray bursts, which are explosive thermonuclear reactions on the surface of the neutron star. When enough accreted material (degenerate gas) is compressed against the surface of the neutron star thermal instabilities set off exothermic nuclear fusion reactions. The explosive burning occurs when the layer of helium formed near the surface of the neutron star ignites. Three sources were found to exhibit both burst oscillations and hot spots and in those cases the burst oscillation frequency is very close to the spin frequency with frequency drifts of up to a few Hz [10, 11, 12]. There are almost 20 neutron stars that display burst oscillations [13]. They have frequencies ranging from 45 – 620 Hz. Some of these sources have oscillations that have been detected at the same frequency in multiple bursts. Others have been seen in only one burst or part of one burst and are not yet reliable such as the 1122 Hz transient source in XTE J1739-285 [14]. The third and last type of oscillations are Quasi-Periodic Oscillations (QPOs) in the X-ray brightness of the binary system. These oscillations are dominated by two kHz frequencies. The highest kHz QPO may reflect the orbital frequency of the gas in the disk near the neutron star. The separation between the two kHz QPOs varies as the accretion rate changes and some models predict that this separation is related to the stellar spin [15].

The speed record of the first millisecond pulsar discovered held for 24 years and was broken in 2006 by another radio pulsar spinning at 716 Hz. This 24 year gap between detections suggests that neutron stars spinning this fast are rare. Moreover, based on a Bayesian statistical analysis of the spin frequencies of 11 accretion powered millisecond pulsars whose spin periods are known from burst oscillations, Chakrabarty *et al.* [10] claimed a cutoff limit of $\nu_{\max} = 760$ Hz (95% confidence). A more recent analysis, which added two more pulsars to the sample, found $\nu_{\max} = 730$ Hz [11]. Instruments have no significant selection effects against detecting burst oscillations at frequencies well above 1 kHz [11].

Theoretically, the recycling model of pulsars allows for spins as high as 1.6 kHz depending on the equation of state. Cook, Shapiro and Teukolsky [16, 17] model the recycling of pulsars to millisecond periods via accretion from a Keplerian disk onto a bare, non-spinning neutron star with $M = 1.4M_{\odot}$. Depending on the equation of state they find that spin frequencies of between ≈ 670 Hz and 1600 Hz could be achieved before mass shedding or radial instability set in (these calculations predated the realization that the r-mode instability could limit the spin frequency). So, one question is what is the mechanism that limits the rotation rate of neutron stars. This limiting frequency ν_{\max} will depend on the internal neutron star physics such as cooling, dissipation and strength of magnetic fields, and so it is a probe of the high density nuclear physics of neutron stars.

At first sight, one might conclude that mass shedding or radial instability sets ν_{\max} , and that it is just above the record $\nu = 716$ Hz determined for PSR J1748-2446ad [18, 19]. However, the nuclear equations of state consistent with this picture all have rather large radii $\approx 16 - 17$ km for non-rotating $1.4 M_{\odot}$.

models; see Table 1 in Cook *et al.* [16]. For these equations of state, the r-mode instability should lead to ν_{\max} somewhat below 716 Hz; see Eq. (2.33) in Chapter 2 below. We conjecture that the r-mode instability always leads to limiting frequencies below mass shedding or radial instability. In other words, the detection of the 716 Hz rotator is consistent with accretion spin-up mitigated by the r-mode instability only for equations of state for which mass shedding or radial instability would permit even faster rotation. Ultimately, this may be turned into useful constraints on nuclear equations of state. However, at present the uncertainty in the physics of internal dissipation is a significant hindrance in establishing such constraints.

The youngest supernova in our galaxy was discovered in 2008 and the star is believed to have exploded less than 150 years ago [20]. Neutron stars are born in the aftermath of core-collapse supernova explosions as the stellar remnant becomes gravitationally decoupled from the stellar ejecta. An interesting and timely question is whether they are born spinning at millisecond periods or spinning closer to the observed periods of young pulsars. Theoretically, following the collapse, a $8 - 30M_{\odot}$ progenitor can easily lead to neutron stars rotating with periods of ~ 1 ms. Observationally, the fastest known young pulsar is the Large Magellanic Cloud supernova remnant N157B, which has a rotation period of 16 ms. Another fast young neutron star is the Crab pulsar. It is the best known pulsar and has a period of 33 ms. Assuming the rotational spin-down is well described by a power law $\dot{\Omega} \propto -\Omega^n$, Lyne *et al.* find the braking index of the pulsar to be $n = 2.51 \pm 0.01$ [21]. Using this braking index and the current period of the pulsar one can estimate the initial period to be 19 ms [22]. Another way to predict the distribution of initial pulsar periods is through population synthesis studies. These studies generally use present day observations with

some assumption of their time evolution to reconstruct the birth distributions of periods and magnetic fields of the pulsars. They currently favor initial periods in the range of several tens to several hundreds of milliseconds [23, 24]. The apparent discrepancy between the theoretically expected fast rotation rates and the observed slow rotation could be reconciled if the r-mode instability or some other mechanism could spin the stars down efficiently, preventing them from reaching millisecond periods [25].

One mechanism that could slow down newborn neutron stars and explain the sub-breakup spin frequencies of millisecond pulsars is the r-mode instability. R-modes are oscillations in rotating fluids that occur due to the Coriolis effect. They are subject to the classical Chandrasekhar-Friedman-Shutz (CFS) instability [26, 27], which is driven by the gravitational radiation backreaction force. In the absence of fluid dissipation, the CFS mechanism causes any mode that is retrograde in the co-rotating frame, but prograde in the inertial frame to grow as it emits gravitational radiation [28, 29]. The principal unstable r-mode is the $n = 3, m = 2$ mode, where n and m label the Legendre functions associated with the mode. In the rotating frame the r-mode has an angular velocity of $\omega_r = 2\Omega/3$ and is retrograde, while in the inertial frame it has an angular velocity of $\omega_i = \omega - m\Omega = (2/3 - 2)\Omega = -4\Omega/3$, and is prograde.

In more realistic situations, there is a competition between the internal viscous dissipation and gravitational driving [28, 29, 30, 31, 32, 33]. The r-mode is linearly unstable when the gravitational driving dominates the viscous dissipation. This happens above a critical curve in the angular velocity-temperature $(\Omega - T)$ plane along which the damping and driving rates are equal. Once the r-mode is unstable, it grows exponentially. Soon it may enter a regime where

other inertial modes that couple to the r-mode become excited and nonlinear effects become important. Roughly speaking, nonlinear effects first become significant as the amplitude passes its first parametric instability threshold. This threshold amplitude depends on the detuning, the strength of the mode coupling and the viscosity of the inertial modes, and is typically low ($< 10^{-3}$). Modeling and understanding the nonlinear effects is crucial in determining (1) the final saturation amplitude of the r-mode, (2) the limiting spin frequency that neutron stars can achieve, and (3) the frequency to which newborn neutron stars can be spun down if they are born at millisecond periods. The r-mode amplitude and the duration of the instability are also important in determining whether the associated gravitational radiation could be detectable by gravitational wave detectors on Earth.

The oscillation frequencies and the eigenfunctions of the modes themselves can also be affected by effects such as those due to magnetic fields and buoyancy. An r-mode oscillation perturbs the magnetic field inside the star, and the resulting magnetic stress acts as a restoring force for the oscillation [34]. Following Morsink and Reznia [35], we perform a quick calculation in Chapter 2 (see Appendix B.2.) in which we assume that the eigenfrequencies are unchanged, and compute the frequency corrections perturbatively for a constant internal magnetic field. We find that these corrections are less than $2.0 \times 10^{-6}\Omega$ for a magnetic field of 10^{13} G and this suggests that we can neglect the effect. The buoyancy effects become important when the spin frequencies of the star become comparable with the Brunt-Vaisala frequency at roughly 100 Hz. This region of frequency space is relevant once the young neutron star has spun down significantly. For g-modes, Lai has shown that there exists a zero inertial frequency line $\omega_i = 0$ between 50 – 100 Hz above which the CFS instability is active

[36]. For $n = m + 1$ r-modes A. Passamonti *et al.* [37] have shown that the mode frequencies are roughly unaffected by buoyancy. While it does seem to turn the instability off buoyancy significantly affects inertial mode frequencies and hence three-mode resonances. In this work, we do not reach frequencies below 200 Hz and do not include buoyancy effects. Reaching lower spin frequencies requires low enough viscosity for the gravitational driving to dominate viscous dissipation at those frequencies. Low mode viscosity also makes the instability harder to stop and our simple three-mode model is no longer sufficient to model the instability. We focus on understanding possible nonlinear behavior using one mode triplet and leave the inclusion of multiple mode triplets to future studies.

The rest of the thesis is structured as follows. In Chapter 2 we discuss our model for the r-mode instability in neutron stars in Low Mass X-ray Binaries (LMXBs). We use one triplet of modes: the r-mode and the first two inertial modes that are excited at the lowest parametric instability threshold. The coupled equations of the three-mode system are evolved numerically in conjunction with the spin and temperature of the star. We include neutrino cooling, accretional spin-up, gravitational radiation spin-down due to the unstable r-mode and viscous heating due to the three modes. In Chapter 3 the same model is applied to young neutron stars. We add dipole spin-down due to large magnetic fields and remove the accretion terms. Chapter 4 includes concluding remarks.

CHAPTER 2

THE EFFECTS OF R-MODE INSTABILITY ON THE SPIN EVOLUTION OF NEUTRON STARS IN LMXBS¹

2.1 Introduction

The r-mode instability has been proposed as an explanation for the sub-breakup spin rates of neutron stars in LMXBs [28, 29, 42]. Cook, Shapiro and Teukolsky [16, 17] model the recycling of pulsars to millisecond periods via accretion from a Keplerian disk onto a bare neutron star with $M = 1.4M_{\odot}$ when $\Omega = 0$. Depending on the equation of state they found that spin frequencies of between ≈ 670 Hz and 1600 Hz could be achieved before mass shedding or radial instability set in (these calculations predated the realization that the r-mode instability could limit the spin frequency). We conjecture that the limiting spin frequency arising from the r-mode instability is always below that from mass shedding or radial instability. Observationally, the highest observed spin rate of millisecond pulsars is 716 Hz for PSR J1748-2446ad [18, 19]. PSR B1937+21, which was discovered in 1982, was the previous fastest known radio pulsar with a spin rate of 642 Hz [4]; that this “speed” record stood for 24 years suggests that neutron stars rotating this fast are rare. Moreover, based on a Bayesian statistical analysis of the spin frequencies of the 11 nuclear-powered millisecond pulsars whose spin periods are known from burst oscillations, Chakrabarty *et al.* [10] claimed a cutoff limit of $\nu_{\max} = 760$ Hz (95% confidence); A more recent analysis, which added two more pulsars to the sample, found $\nu_{\max} = 730$ Hz [11].

¹Published with minor modifications in R. Bondarescu, S. Teukolsky and I. Wasserman, Phys. Rev. D **76**, 064019 (2007).

Since a physical model to follow the nonlinear phase of the evolution was initially unavailable, Owen *et al.* [32] proposed a simple one-mode evolution model in which they assumed that nonlinear hydrodynamics effects saturate the r-mode amplitude at some arbitrarily fixed value. According to their model, once this maximum allowed amplitude is achieved, the r-mode amplitude remains constant and the star spins down at this fixed amplitude (see Eqs. (3.16) and (3.17) in Ref. [32]). They used this model to study the impact of the r-mode instability on the spin evolution of young hot neutron stars assuming normal matter. In their calculation they include the effects of shear viscosity and n-p-e bulk viscosity. They found that the star would cool to approximately 10^9 K and spin down from a frequency close to the Kepler frequency to about 100 Hz in a period of ~ 1 yr [32].

Most subsequent investigations that did not perform direct hydrodynamic simulations used the one-amplitude model of Ref. [32] for studying the r-mode instability. Levin [38] used this model to study the limiting effects of the r-mode instability on the spin evolution of LMXBs, assuming an r-mode saturation amplitude of ~ 1 ; he adopted a modified shear viscosity to match the maximum LMXB spin frequency of 330 Hz known in 1999. Levin found that the neutron star followed a cyclic evolution in the $\Omega - T$ phase plane. The star spins up for several million years until it crosses the r-mode stability curve, whereupon the r-mode becomes unstable and the star is viscously heated for a fraction of a year until the r-mode reaches its saturation amplitude (~ 1). At this point the spin and r-mode amplitude evolution equations are changed, following the prescription of Ref. [32] to ensure constant amplitude. The star then spins down by emitting gravitational radiation for another fraction of a year until it crosses the r-mode stability curve again and the instability shuts off. The time period dur-

ing which the r-mode is unstable was found to be about 10^{-6} times shorter than the spin-up time, and Levin concluded that it is unlikely that any neutron stars in LMXBs in our galaxy are currently spinning down and emitting gravitational radiation. However, following work by Arras *et al.* [39] showing that nonlinear effects become significant at small r-mode amplitude, Heyl [40] varied the saturation amplitude, and found that the duration of the spin-down depends sensitively on it. He predicted that the unstable phase could be as much as 30% of the cyclic evolution for an r-mode saturation amplitude of $\alpha \approx 10^{-5}$, and that this would make some of the fastest spinning LMXBs in our galaxy detectable by interferometers on Earth.

Jones [41] and Lindblom and Owen [46] pointed out that if the star contains exotic particles such as hyperons (massive nucleons where an up or down quark is replaced with a strange quark), internal processes could lead to a very high coefficient of bulk viscosity in the cores of neutron stars. While this additional high viscosity coefficient could eliminate the instability altogether in newly born neutron stars [41, 46, 47, 48], Nayyar and Owen [48] proposed that it would enhance the probability of detection of gravitational radiation from LMXBs by blocking the thermal runaway.

The cyclic evolution found by Levin [38] and generalized by Heyl [40] arises when shear or boundary layer viscosity dominates the r-mode dissipation. In the evolutionary picture of Nayyar and Owen [48], the r-mode first becomes unstable at a temperature where shear and boundary layer viscosity dominate, but the resulting thermal runaway halts once hyperon bulk viscosity becomes dominant. The key feature behind the runaway is that shear and boundary layer viscosities both decrease with increasing temperature, so the instability speeds

up as the star grows hotter. However, if the bulk viscosity is sufficiently large the star can cross the r-mode stability curve at a point where the viscosity is an increasing function of temperature. Such scenarios were studied by Wagoner [50] for hyperon bulk viscosity with low hyperon superfluid transition temperature; similar evolution was found for strange stars by Andersson, Jones and Kokkotas [49]. In this picture, the star evolves near the r-mode stability curve until an equilibrium between accretion spin-up and gravitational radiation spin-down is achieved. The value of the r-mode amplitude remains below the lowest instability threshold found by Brink *et al.* [51, 52, 53] for modes with $n < 30$, and hence in this regime nonlinear effects may not play a role.

Schenk *et al.* [54] developed a formalism to study the nonlinear interaction of the r-mode with other inertial modes. They assumed a small r-mode amplitude and treated the oscillations of the modes with weakly nonlinear perturbation theory via three-mode couplings. This assumption was tested by Arras *et al.* [39] and Brink *et al.* [51, 52, 53]. Arras *et al.* proposed that a turbulent cascade would develop in the strong driving regime. They estimated that r-mode amplitude was small and could have values between $10^{-1} - 10^{-4}$. Brink *et al.* modeled the star as incompressible and calculated the coupling coefficients analytically. They computed the interaction of about 5000 modes via approximately 1.3 million couplings of the 10^9 possible couplings among the modes with $n \leq 30$. The couplings were restricted to mode triplets with a fractional detuning $\delta\omega/(2\Omega) < 0.002$ since near-resonances promote modal excitation at very small amplitudes. Brink *et al.* showed that the nonlinear evolution saturates at a very small amplitude, generally comparable to the lowest parametric instability threshold that controls the initiation of energy sharing among the sea of inertial modes. However, Brink *et al.* did not model accretion spin-up or

neutrino cooling in their calculation and only included minimal dissipation via shear viscosity.

In this chapter we begin a more complete study of the saturation of the r-mode instability including accretion spin up and neutrino cooling. We use a simple model in which we parameterize uncertain properties of the star such as the rate at which it cools via neutrino emission and the rate at which the energy in inertial modes dissipates via boundary layer effects [42] and bulk viscosity. In order to exhibit the variety of possible nonlinear behaviors, we explore a range of models with different neutrino cooling and viscous heating coefficients by varying the free parameters of our model. In particular, we vary: (1) the slippage factor S_{ns} , which regulates the boundary layer viscosity, between 0 and 1 (see for example [43, 44, 45] for some models of the interaction between the oscillating fluid core and an elastic crust); (2) the fraction of the star that is above the density threshold for direct URCA reactions f_{dU} , which is taken to be between 0 (0% of the star cools via direct URCA) and 1 (100% of the star is subjected to direct URCA reactions), and in general depends on the equation of state used; and (3) the hyperon superfluidity temperature T_c , which is believed to be between $10^9 - 10^{10}$ K (We use a single, effective T_c rather than modelling its spatial variation.) We focus on $T_c \gtrsim 5 \times 10^9$ K for which nonlinear effects are important. For low $T_c \lesssim 3 \times 10^9$ K, Wagoner [50] showed that the evolution reaches a steady state at amplitudes below the lowest parametric instability threshold found by Brink *et al.* [53]. It is important to note that all our evolutions start on the part of the r-mode stability curve that decreases with temperature and that the bulk viscosity does not play a role in any of our bound evolutions.

We include three modes: the r-mode at $n = 3$ and the two inertial modes

at $n = 13$ and $n = 14$ that become unstable at the lowest parametric instability threshold found by Brink *et al.* [53]. We evolve the coupled equations for the three-mode system numerically in conjunction with the spin and temperature evolution equations. The lowest parametric instability threshold provides a physical cutoff for the r-mode amplitude. In all cases we investigate, the growth of the r-mode is initially halted by energy transfer to the two daughter modes. We observe that the mode amplitudes settle into a series of quasi-stationary states within a period of a few years after the spin frequency of the star has increased above the r-mode stability curve. These quasi-stationary states are algebraic solutions of the three-mode amplitude equations (see Eqs. (2.6)) and change slowly as the spin and the temperature of the star evolve. Using these solutions for the mode amplitudes, one can reduce the eight evolution equations (six for the real and imaginary parts of the mode amplitudes, which are complex [54]; one for the spin, and one for the temperature) to two equations governing the rotational frequency and the temperature of the star. Our work can be regarded as a minimal physical model for modeling amplitude saturation realistically.

The outcome of the evolution is crucially dependent on whether the star can reach a state of thermal equilibrium. This can be predicted by finding the curve where the viscous heating by the three modes balances the neutrino cooling, referred to below as the Heating = Cooling ($H = C$) curve. The $H = C$ curve can be calculated prior to carrying out an evolution using the quasi-stationary solutions for the mode amplitudes. If the spin frequency of the star upon becoming unstable is below the peak of the $H = C$ curve, then the star will reach a state of thermal equilibrium. When such a state is reached we find several possible scenarios. The star can: (1) undergo a cyclic evolution; (2) reach a true

equilibrium in which the accretion torque is balanced by the rate of loss of angular momentum via gravitational radiation; or (3) evolve in thermal equilibrium until it reaches the peak of the $H = C$ curve, which occurs on a timescale of about 10^6 yr, and subsequently enter a regime of thermal runaway. On the other hand, if the star cannot find a state of thermal equilibrium, then it enters a regime of thermogravitational runaway within a few hundred years of crossing the r-mode stability curve. When this happens, the r-mode amplitude increases beyond the second parametric instability, and more inertial modes would need to be included to correctly model the nonlinear effects. This is beyond the scope of this work.

This chapter focuses on showing how nonlinear mode couplings affect the evolution of the temperature and spin frequency of a neutron star once it becomes prone to the r-mode CFS instability. We do this in the context of three mode coupling, which may be sufficient for large enough dissipation. To illustrate the types of behavior that arise, we adopt a very specific model in which the mode frequencies and couplings are computed for an incompressible star, modes damp via shear viscosity, boundary layer viscosity and hyperon bulk viscosity, and the star cools via a mixture of fast and slow processes. This model involves several parameters that are uncertain, and we vary these to find ‘phase diagrams’ in which different generic types of behavior are expected. Moreover, the model itself is simplified: (1) A more realistic treatment of the modes could include buoyant forces, and also mixtures of superfluids or of superfluid and normal fluid in different regions. (2) Dissipation rates, particularly from bulk viscosity, depend on the composition of high density nuclear matter, which could differ from what we assume.

Nevertheless, although the quantitative details may differ from what we compute, we believe that many features of our calculations ought to be robust. More sophisticated treatment of the modes of the star will still find a dense set of modes confined to a relatively small range of frequencies. Most importantly, this set will exhibit numerous three mode resonances, which is the prerequisite for strong nonlinear effects at small mode amplitudes. Thus, whenever the unstable r-mode can pass its lowest parametric instability threshold, it must start exciting its daughters. Whether or not that occurs depends on the temperature dependence of the dissipation rate of the r-mode; for the models considered here, where bulk viscosity is relatively unimportant, soon after the star becomes unstable its r-mode amplitude passes its first parametric instability threshold. Once that happens, the generic types of behavior we find - cycles, steady states, slow and fast runaway - ought to follow suit. The details of when different behaviors arise will depend on the precise features of the stellar model, but the principles we outline here (parametric instability, quasisteady evolution, competition between heating and cooling) ought to apply quite generally.

In Sec. 2.2 we describe the evolution equations of the three modes, the angular frequency and the temperature of the neutron star. We first show how the equations of motion for the modes of Schenk *et al.* couple to the rotational frequency of the star in the limit of slow rotation. We then give a short review of the parametric instability threshold and the quasi-stationary solutions of the three-mode system. The thermal and spin evolution of the star is discussed next. This is followed by a description of the driving and damping rates used. Sec. 2.3 provides an overview of the results, which includes a discussion of each evolution scenario and of the initial conditions and input physics that lead to each scenario. Sec. 2.4.1 discusses cyclic evolution in more detail. An evolution that

leads to an equilibrium steady state is presented next in Sec. 2.4.2. The two types of thermal runaway are then discussed in Sec. 2.4.3. The prospects for detecting gravitational radiation for the evolutions in which the three-mode system correctly models the nonlinear effects are considered in Sec. 2.5. We summarize the results in the conclusion. Appendix A.1 sketches a derivation of the equations of motion for the three modes and Appendix A.2 contains a stability analysis of the evolution equations around the thermal equilibrium state.

2.2 Evolution Equations

2.2.1 Three mode system: coupling to uniform rotation

In this section we review the equations of motion for the three-mode system in the limit of slow rotation. In terms of rotational phase τ for the time variable with $d\tau = \Omega dt$ Eq. (2.49) of Schenk *et al.* [54] can be rewritten as

$$\begin{aligned}\frac{dC_\alpha}{d\tau} &= i\tilde{\omega}_\alpha C_\alpha + \frac{\gamma_\alpha}{\Omega} C_\alpha - \frac{2i\tilde{\omega}_\alpha \tilde{\kappa}}{\sqrt{\Omega}} C_\beta C_\gamma, \\ \frac{dC_\beta}{d\tau} &= i\tilde{\omega}_\beta C_\beta - \frac{\gamma_\beta}{\Omega} C_\beta - \frac{2i\tilde{\omega}_\beta \tilde{\kappa}}{\sqrt{\Omega}} C_\alpha C_\gamma^*, \\ \frac{dC_\gamma}{d\tau} &= i\tilde{\omega}_\gamma C_\gamma - \frac{\gamma_\gamma}{\Omega} C_\gamma - \frac{2i\tilde{\omega}_\gamma \tilde{\kappa}}{\sqrt{\Omega}} C_\alpha C_\beta^*.\end{aligned}\tag{2.1}$$

Here the scaled frequency $\tilde{\omega}_j$ is defined to be $\tilde{\omega}_j = \omega_j/\Omega$, the dissipation rates of the daughter modes are γ_β and γ_γ , γ_α is the sum of the driving and damping rates of the r-mode $\gamma_\alpha = \gamma_{GR} - \gamma_{\alpha v}$, and the dimensionless coupling is $\tilde{\kappa} = \kappa/(MR^2\Omega^2)$. These amplitude variables are complex and can be written in terms of the variables of Ref. [54] as $C_j(t) = \sqrt{\Omega(t)}c_j(t)$ (see Appendix A.1 for a derivation of Eqs. 2.1). The index j loops over the three modes $j = \alpha, \beta, \gamma$, where α labels the r-

mode or parent mode and β and γ label the two daughter modes in the mode triplet.

When the daughter mode amplitudes are much smaller than that of the parent mode, one can approximate the parent mode amplitude as constant. Under this assumption one performs a linear stability analysis on Eqs. (2.1) and finds the r-mode amplitude when the two daughter modes become unstable (see Eqs. (B5-B7) of Ref. [53] for a full derivation). This amplitude is the parametric instability threshold

$$|C_\alpha|^2 = \frac{\gamma_\beta \gamma_\gamma}{4\tilde{\kappa}^2 \tilde{\omega}_\beta \tilde{\omega}_\gamma \Omega} \left[1 + \Omega^2 \left(\frac{\delta\tilde{\omega}}{\gamma_\beta + \gamma_\gamma} \right)^2 \right], \quad (2.2)$$

where the fractional detuning is $\delta\tilde{\omega} = \tilde{\omega}_\alpha - \tilde{\omega}_\beta - \tilde{\omega}_\gamma$. Thorough explorations of the phase space of damped three-mode systems were performed by Dimant [55] and Wersinger *et al.* [56].

For the three modes at the lowest parametric instability threshold, $\tilde{\omega}_\alpha \approx 0.66$, $\tilde{\omega}_\beta \approx 0.44$, $\tilde{\omega}_\gamma \approx 0.22$, $\tilde{\kappa} \approx 0.19$ and $|\delta\tilde{\omega}| \approx 3.82 \times 10^{-6}$. Note that $\tilde{\omega}$ is twice the w of Brink *et al.* [51, 52, 53]. Here β labels the mode with $n = 13, m = -3$ and γ labels the $n = 14, m = 1$ mode. The amplitude the r-mode has to reach before exciting these two daughter modes is $|C_\alpha| \approx 1.5 \times 10^{-5} \sqrt{\Omega}$ [53].

We next rescale the rotational phase τ by the fractional detuning as $\tilde{\tau} = \tau|\delta\tilde{\omega}|$ and the mode amplitudes by

$$\begin{aligned} |C_\alpha|_0 &= \frac{|\delta\tilde{\omega}| \sqrt{\Omega_c}}{4\tilde{\kappa} \sqrt{\tilde{\omega}_\beta \tilde{\omega}_\gamma}}, & |C_\beta|_0 &= \frac{|\delta\tilde{\omega}| \sqrt{\Omega_c}}{4\tilde{\kappa} \sqrt{\tilde{\omega}_\alpha \tilde{\omega}_\gamma}}, \\ |C_\gamma|_0 &= \frac{|\delta\tilde{\omega}| \sqrt{\Omega_c}}{4\tilde{\kappa} \sqrt{\tilde{\omega}_\beta \tilde{\omega}_\alpha}}, \end{aligned} \quad (2.3)$$

which for the r-mode is, up to a factor of $\sqrt{\tilde{\Omega}} = \sqrt{\Omega/\Omega_c}$, the no-damping limit of the parametric instability threshold below which no oscillations will occur. The

coupled equations become

$$\begin{aligned}
\frac{d\bar{C}_\alpha}{d\tilde{\tau}} &= \frac{i\tilde{\omega}_\alpha}{|\delta\tilde{\omega}|}\bar{C}_\alpha + \frac{\tilde{\gamma}_\alpha}{|\delta\tilde{\omega}|\tilde{\Omega}}\bar{C}_\alpha - \frac{i}{2\sqrt{\tilde{\Omega}}}\bar{C}_\beta\bar{C}_\gamma, \\
\frac{d\bar{C}_\beta}{d\tilde{\tau}} &= \frac{i\tilde{\omega}_\beta}{|\delta\tilde{\omega}|}\bar{C}_\beta - \frac{\tilde{\gamma}_\beta}{|\delta\tilde{\omega}|\tilde{\Omega}}\bar{C}_\beta - \frac{i}{2\sqrt{\tilde{\Omega}}}\bar{C}_\alpha\bar{C}_\gamma^*, \\
\frac{d\bar{C}_\gamma}{d\tilde{\tau}} &= \frac{i\tilde{\omega}_\gamma}{|\delta\tilde{\omega}|}\bar{C}_\gamma - \frac{\tilde{\gamma}_\gamma}{|\delta\tilde{\omega}|\tilde{\Omega}}\bar{C}_\gamma - \frac{i}{2\sqrt{\tilde{\Omega}}}\bar{C}_\alpha\bar{C}_\beta^*,
\end{aligned} \tag{2.4}$$

with $\bar{C}_j = C_j/|C_j|_0$ and $\tilde{\gamma}_j = \gamma_j/\Omega_c$ being the newly rescaled amplitudes and dissipation/driving rates, respectively.

Quasi-Stationary Solution

In terms of amplitudes and phase variables $C_j = |C_j|e^{i\phi_j}$ Eqs. (2.4) can be rewritten as

$$\begin{aligned}
\frac{d|\bar{C}_\alpha|}{d\tilde{\tau}} &= \frac{\tilde{\gamma}_\alpha}{\tilde{\Omega}|\delta\tilde{\omega}|}|\bar{C}_\alpha| - \frac{\sin\phi|\bar{C}_\beta||\bar{C}_\gamma|}{2\sqrt{\tilde{\Omega}}}, \\
\frac{d|\bar{C}_\beta|}{d\tilde{\tau}} &= -\frac{\tilde{\gamma}_\beta}{\tilde{\Omega}|\delta\tilde{\omega}|}|\bar{C}_\beta| + \frac{\sin\phi|\bar{C}_\alpha||\bar{C}_\gamma|}{2\sqrt{\tilde{\Omega}}}, \\
\frac{d|\bar{C}_\gamma|}{d\tilde{\tau}} &= -\frac{\tilde{\gamma}_\gamma}{\tilde{\Omega}|\delta\tilde{\omega}|}|\bar{C}_\gamma| + \frac{\sin\phi|\bar{C}_\alpha||\bar{C}_\beta|}{2\sqrt{\tilde{\Omega}}}, \\
\frac{d\phi}{d\tilde{\tau}} &= \frac{\delta\tilde{\omega}}{|\delta\tilde{\omega}|} - \frac{\cos\phi}{2\sqrt{\tilde{\Omega}}}\left(\frac{|\bar{C}_\beta||\bar{C}_\gamma|}{|\bar{C}_\alpha|} - \frac{|\bar{C}_\alpha||\bar{C}_\gamma|}{|\bar{C}_\beta|} - \frac{|\bar{C}_\beta||\bar{C}_\alpha|}{|\bar{C}_\gamma|}\right),
\end{aligned} \tag{2.5}$$

where we have defined the relative phase difference as $\phi = \phi_\alpha - \phi_\beta - \phi_\gamma$. These equations have the stationary solution

$$\begin{aligned}
|\bar{C}_\alpha|^2 &= \frac{4\tilde{\gamma}_\beta\tilde{\gamma}_\gamma}{\tilde{\Omega}|\delta\tilde{\omega}|^2}\left(1 + \frac{1}{\tan^2\phi}\right), \\
|\bar{C}_\beta|^2 &= \frac{4\tilde{\gamma}_\alpha\tilde{\gamma}_\gamma}{\tilde{\Omega}|\delta\tilde{\omega}|^2}\left(1 + \frac{1}{\tan^2\phi}\right), \\
|\bar{C}_\gamma|^2 &= \frac{4\tilde{\gamma}_\alpha\tilde{\gamma}_\beta}{\tilde{\Omega}|\delta\tilde{\omega}|^2}\left(1 + \frac{1}{\tan^2\phi}\right), \\
\tan\phi &= \frac{\tilde{\gamma}_\beta + \tilde{\gamma}_\gamma - \tilde{\gamma}_\alpha}{\tilde{\Omega}|\delta\tilde{\omega}|}.
\end{aligned} \tag{2.6}$$

Note that in the limit in which $\gamma_\beta + \gamma_\gamma \gg \gamma_\alpha$ the stationary solution for the r-mode amplitude $|C_\alpha|$ is the same as the parametric instability threshold.

2.2.2 Temperature and Spin Evolution

The spin evolution equation is obtained from conservation of total angular momentum J , where

$$J = I\Omega + J_{\text{phys}}. \quad (2.7)$$

Following Eq (K39-K42) of Schenk *et al.* [54] the physical angular momentum of the perturbation can be written as

$$\begin{aligned} \Omega J_{\text{phys}} &= \sum_{AB} C_B^* C_A \int d^3x \rho [(\hat{\Omega} \times \xi_B^*) \cdot (\hat{\Omega} \times \xi_A) \\ &\quad - i \frac{(\tilde{\omega}_A + \tilde{\omega}_B)}{2} \xi_B^* \cdot (\hat{\Omega} \times \xi_A)]. \end{aligned} \quad (2.8)$$

Since the eigenvectors $\xi_A \propto e^{im_A\phi}$ the cross-terms will vanish for modes with different magnetic quantum numbers m as $\int e^{i(m_A - m_B)\phi} d\phi = 0$ for $m_A \neq m_B$. Eq. (2.8) can be re-written for our triplet of modes as

$$J_{\text{phys}} = MR^2(k_{\alpha\alpha}|C_\alpha|^2 + k_{\beta\beta}|C_\beta|^2 + k_{\gamma\gamma}|C_\gamma|^2), \quad (2.9)$$

where $k_{\alpha\alpha}$ is defined as

$$k_{\alpha\alpha} = \frac{1}{MR^2} \int d^3x \rho [(\hat{\Omega} \times \xi_\alpha^*) \cdot (\hat{\Omega} \times \xi_\alpha) - i\tilde{\omega}_\alpha \xi_\alpha^* \cdot (\hat{\Omega} \times \xi_\alpha)] \quad (2.10)$$

and similarly for $k_{\beta\beta}$ and $k_{\gamma\gamma}$. In terms of the scaled variables $\bar{C}_j = C_j/|C_j|_0$ (with $|C_j|_0$ defined in Eq. (2.3)) the angular momentum of the perturbation can be written as

$$\begin{aligned} J_{\text{phys}} &= \frac{MR^2\Omega_c|\delta\tilde{\omega}|^2}{(4\tilde{k})^2\tilde{\omega}_\alpha\tilde{\omega}_\beta\tilde{\omega}_\gamma} (k_{\alpha\alpha}|\bar{C}_\alpha|^2\tilde{\omega}_\alpha \\ &\quad + k_{\beta\beta}|\bar{C}_\beta|^2\tilde{\omega}_\beta + k_{\gamma\gamma}\tilde{\omega}_\gamma|\bar{C}_\gamma|^2). \end{aligned} \quad (2.11)$$

We chose the same normalization for the eigenfunctions as Refs. [54, 39, 51, 52, 53] so that at unit amplitude all modes have the same energy $\epsilon_\alpha = MR^2\Omega^2$. The energy of a mode α is $E_\alpha = MR^2\Omega^2|c_\alpha|^2 = MR^2\Omega|C_\alpha|^2$. The rotating frame energy is the same as the canonical energy and physical energy [54]. The canonical angular momentum and the canonical energy of the perturbation satisfy the general relation $E_c = -(\omega/m)J_c$ [27].

Angular momentum is gained because of accretion and lost via gravitational waves emission

$$\frac{dJ}{dt} = 2\gamma_{GR}J_{c \text{ rmode}} + \dot{M} \sqrt{GMR}, \quad (2.12)$$

where $J_{c \text{ rmode}} = -(m_\alpha/\omega_\alpha)\epsilon_\alpha|c_\alpha|^2 = -3MR^2\Omega|c_\alpha|^2 = -3MR^2|C_\alpha|^2$. Eq. (2.12) can be rewritten in terms of the scaled variables above as

$$\frac{dJ}{d\tilde{\tau}} = -\frac{6\tilde{\gamma}_{GR}}{\tilde{\Omega}} \frac{MR^2\Omega_c|\delta\tilde{\omega}|}{(4\tilde{k})^2\tilde{\omega}_\beta\tilde{\omega}_\gamma} |\tilde{C}_\alpha|^2 + \frac{\dot{M} \sqrt{GMR}}{\Omega_c\tilde{\Omega}|\delta\tilde{\omega}|}. \quad (2.13)$$

Thermal energy conservation gives the temperature evolution equation

$$\begin{aligned} C(T) \frac{dT}{dt} &= \sum_j 2E_j\gamma_j + K_n\dot{M}c^2 - L_\nu(T), \\ &= 2MR^2\Omega(\gamma_{\alpha\nu}|C_\alpha|^2 + \gamma_\beta|C_\beta|^2 \\ &\quad + \gamma_\gamma|C_\gamma|^2) + K_n\dot{M}c^2 - L_\nu(T). \end{aligned} \quad (2.14)$$

The three terms on the right hand side of the equation represent viscous heating, nuclear heating and neutrino cooling. The specific heat is taken to be $C(T) \approx 1.5 \times 10^{38} T_8 \text{ erg K}^{-1}$, where $T = T_8 \times 10^8 \text{ K}$. Nuclear heating occurs because of pycnonuclear reactions and neutron emission in the inner crust [57]. At large accretion rates such as that of the brightest LMXBs of $\dot{M} \approx 10^{-8} M_\odot/\text{yr}$, the accreted helium and hydrogen burns stably and most of the heat released in the crust is conducted into the core of the neutron star, where neutrino emission is assumed to regulate the temperature of the star [57, 58]. The nuclear heat-

ing constant is taken to be $K_n \approx 1 \times 10^{-3}$ [57]. Following Ref. [50], we take the neutrino luminosity to be

$$\begin{aligned} L_\nu &= L_{\text{dU}} T_8^6 R_{\text{dU}}(T/T_p) + L_{\text{mU}} T_8^8 R_{\text{mU}}(T/T_p) \\ &+ L_{\text{e-i}} T_8^6 + L_{\text{n-n}} T_8^8 + L_{\text{Cp}} T_8^7, \end{aligned} \quad (2.15)$$

where the constants for the modified and direct URCA reactions are defined by $L_{\text{mU}} = 1.0 \times 10^{32} \text{ erg sec}^{-1}$, $L_{\text{dU}} = f_{\text{dU}} \times 10^8 L_{\text{mU}}$ [59, 60], and the electron-ion, neutron-neutron neutrino bremsstrahlung and Cooper pairing of neutrons are given by $L_{\text{e-i}} = 9.1 \times 10^{29} \text{ erg sec}^{-1}$ [57], $L_{\text{n-n}} \approx 0.01 L_{\text{mU}}$, $L_{\text{Cp}} = 8.9 \times 10^{31} \text{ erg sec}^{-1}$ [61]. The fraction of the star f_{dU} that is above the density threshold for direct URCA reactions is in general dependent on the equation of state [62] and in this work we treat f_{dU} a free parameter with values between 0 and 1.

The proton superfluid reduction factors for the modified and direct URCA reactions are taken from Ref. [60] (see Eqs. (32) and (51) in Ref. [60]):

$$\begin{aligned} R_{\text{dU}}(T/T_p) &= \left[0.2312 + \sqrt{(0.76880)^2 + (0.1438\nu)^2} \right]^{5.5} \\ &\times \exp\left(3.427 - \sqrt{(3.427)^2 + \nu^2}\right), \\ R_{\text{mU}}(T/T_p) &= \left(0.2414 + \sqrt{(0.7586)^2 + (0.1318\nu)^2} \right)^7, \\ &\times \exp\left(5.339 - \sqrt{(5.339)^2 + (2\nu)^2}\right) \end{aligned} \quad (2.16)$$

where the dimensionless gap amplitude ν for the singlet type superfluidity is given by

$$\nu = \sqrt{1 - \frac{T}{T_p}} \left(1.456 - 0.157 \sqrt{\frac{T_p}{T}} + 1.764 \frac{T_p}{T} \right). \quad (2.17)$$

Similar to Ref. [50], we use $T_p = 5.0 \times 10^9 \text{ K}$. In terms of the scaled variables Eq. (2.14) becomes

$$\begin{aligned} C(T) \frac{dT}{d\tilde{\tau}} &= \frac{2MR^2 \Omega_c^2 |\delta\tilde{\omega}|}{(4\tilde{\kappa})^2 \tilde{\omega}_\alpha \tilde{\omega}_\beta \tilde{\omega}_\gamma} (\tilde{\omega}_\alpha \tilde{\gamma}_{\alpha\nu} |\bar{C}_\alpha|^2 + \tilde{\omega}_\beta \tilde{\gamma}_\beta |\bar{C}_\beta|^2 \\ &+ \tilde{\omega}_\gamma \tilde{\gamma}_\gamma |\bar{C}_\gamma|^2) + \frac{K_n \dot{M} c^2 - L_\nu(T)}{\Omega_c \tilde{\Omega} |\delta\tilde{\omega}|}. \end{aligned} \quad (2.18)$$

2.2.3 Temperature and Spin Evolution with the Mode Amplitudes in Quasi-Stationary States

Assuming that the amplitudes evolve through a series of spin- and temperature-dependent steady states, i.e., $dC_i/d\tilde{\tau} \approx 0$, the spin and thermal evolution equations can be rewritten by taking $J \approx I\Omega$ and using Eqs. (2.6) in Eq. (2.13).

$$\frac{d\tilde{\Omega}}{d\tilde{\tau}} = -\frac{6\tilde{\gamma}_{\text{GR}}}{\tilde{\Omega}^2|\delta\tilde{\omega}|} \frac{\tilde{\gamma}_\beta\tilde{\gamma}_\gamma}{4\tilde{k}^2\tilde{I}\tilde{\omega}_\beta\tilde{\omega}_\gamma} k_{\alpha\alpha} \left(1 + \frac{1}{\tan^2\phi}\right) + \frac{\dot{M}}{\Omega_c^2} \frac{\sqrt{GMR}}{MR^2\tilde{I}\tilde{\Omega}|\delta\tilde{\omega}|}, \quad (2.19)$$

where $\tilde{I} = I/(MR^2)$. The thermal evolution of the system is given by

$$C(T) \frac{dT}{d\tilde{\tau}} = \frac{2MR^2\Omega_c^2}{(4\tilde{k})^2\tilde{\omega}_\alpha\tilde{\omega}_\beta\tilde{\omega}_\gamma} \frac{\tilde{\gamma}_\alpha\tilde{\gamma}_\beta\tilde{\gamma}_\gamma}{\tilde{\Omega}|\delta\tilde{\omega}|} \left(\frac{\tilde{\omega}_\alpha\tilde{\gamma}_{\alpha,v}}{\tilde{\gamma}_\alpha} + \tilde{\omega}_\beta + \tilde{\omega}_\gamma \right) \left(1 + \frac{1}{\tan^2\phi}\right) + \frac{K_n\dot{M}c^2 - L_v(T)}{\Omega_c\tilde{\Omega}|\delta\tilde{\omega}|}. \quad (2.20)$$

By setting the right hand side of the above equation to zero, one can find the Heating = Cooling ($H = C$) curve. Below, we find that Eqs. (2.19)-(2.20) describe the evolution very well throughout the unstable regime. These equations are a minimal physical model for the effects of nonlinear coupling on r-mode evolution.

2.2.4 Sources of Driving and Dissipation

The damping mechanisms are shear viscosity, boundary layer viscosity and hyperon bulk viscosity; for modes $j = \alpha, \beta, \gamma$ we write

$$\gamma_{jv}(\Omega, T) = \gamma_{j\text{sh}}(T) + \gamma_{j\text{bl}}(\Omega, T) + \gamma_{j\text{hb}}(\Omega, T). \quad (2.21)$$

The r-mode is driven by gravitational radiation and damped by these dissipation mechanisms, while the pair of daughter modes ($n = 13, m = -3$ labeled as β and $n = 14, m = 1$ labeled as γ) is affected only by the viscous damping. Brink *et al.* [51, 52, 53] determined that this pair of modes is excited at the lowest parametric instability threshold. Their model uses the Bryan [63] modes of an incompressible star, which has the advantage that the mode eigenfrequencies (and eigenfunctions) are known analytically. This enables them to find near resonances efficiently. We are using their results, but we include more realistic effects such as bulk viscosity, whose effect vanishes in the incompressible limit ($\Gamma_1 \rightarrow \infty$ in Eq. (2.29))

For our benchmark calculations, we adopt the neutron star model of Owen *et al.* Ref. [30] ($n = 1$ polytrope, $M = 1.4M_\odot$, $\Omega_c = 8.4 \times 10^3$ rad sec $^{-1}$ and $R = 12.53$ km) and use their gravitational driving rate and shear viscous damping rate for the r-mode

$$\begin{aligned}\gamma_{GR}(\Omega) &\simeq \frac{\tilde{\Omega}^6}{3.26} \text{sec}^{-1}, \\ \gamma_{\alpha \text{ sh}}(T) &\simeq \frac{1}{\tau_{\text{sh}}} \frac{1}{T_8^2},\end{aligned}\tag{2.22}$$

where $\tau_{\text{sh}} = 2.56 \times 10^6$ sec. (In Sec. 2.5 we consider approximate scalings with M and R .)

The damping rate due to shear viscosity for the two daughter modes is calculated using the Bryan modes for a star with the same mass and radius

$$\begin{aligned}\gamma_{\beta \text{ sh}}(T) &\simeq 3.48 \times 10^{-4} \text{sec}^{-1} \frac{1}{T_8^2}, \\ \gamma_{\gamma \text{ sh}}(T) &\simeq 4.52 \times 10^{-4} \text{sec}^{-1} \frac{1}{T_8^2}.\end{aligned}\tag{2.23}$$

The geometric contribution γ_{sh}/η of the individual modes increases significantly with the degree n of the mode scaling approximatively like n^3 for large n (see Eq. (29) of Brink *et al.* [52] for an analytic fit to the shear damping rates computed for the 5,000 modes in their network), and hence the inertial modes with $n = 13$ and $n = 14$ have shear damping rates about three orders of magnitude larger than that of the r-mode.

The damping due to boundary layer viscosity is calculated using Eq. (4) of Ref. [42],

$$\begin{aligned}\gamma_{\alpha \text{ bl}}(T, \Omega) &\simeq 0.009 \text{ sec}^{-1} S_{\text{ns}}^2 \frac{\sqrt{\tilde{\Omega}}}{T_8}, \\ \gamma_{\beta \text{ bl}}(T, \Omega) &\simeq 0.028 \text{ sec}^{-1} S_{\text{ns}}^2 \frac{\sqrt{\tilde{\Omega}}}{T_8}, \\ \gamma_{\gamma \text{ bl}}(T, \Omega) &\simeq 0.021 \text{ sec}^{-1} S_{\text{ns}}^2 \frac{\sqrt{\tilde{\Omega}}}{T_8}.\end{aligned}\tag{2.24}$$

Analogous to Wagoner [50], we allow the slippage factor S_{ns} to vary. The slippage factor is defined by Refs. [50, 43, 67] to be $S_{\text{ns}}^2 = (2S_n^2 + S_s^2)/3$, with S_n being the fractional difference in velocity of the normal fluid between the crust and the core [43] and S_s the fractional degree of pinning of the vortices in the crust [67]. Note that $\gamma_{\beta \text{ bl}}$ and $\gamma_{\gamma \text{ bl}}$ are both greater than $2 \times \gamma_{\alpha \text{ bl}}$ and can easily be comparable to γ_{GR} in the unstable regime.

The damping rate due to bulk viscosity produced by out-of-equilibrium hyperon reactions for the r-mode is found by fitting the results of Nayyar and Owen [48]. This rate is taken to have a form similar to that taken by Wagoner [50]

$$\gamma_{\alpha \text{ hb}} = f_{\text{hb}} \frac{t_{0\alpha}^{-2} \tau(T) \tilde{\Omega}^4}{1 + (\tilde{\omega}_\alpha \Omega \tau(T))^2},\tag{2.25}$$

and for the daughter modes

$$\gamma_{\beta \text{ hb}} = f_{\text{hb}} \frac{t_{0\beta}^{-2} \tau(T) \tilde{\omega}_\beta^2}{1 + (\tilde{\omega}_\beta \Omega \tau(T))^2},\tag{2.26}$$

and similarly for $\gamma_{\gamma \text{ hb}}$. The relaxation timescale

$$\tau(T) = \frac{t_1 T_8^{-2}}{R_{\text{hb}}(T/T_c)} \quad (2.27)$$

The reduction factor is taken to be the product of two single-particle reduction factors [47, 48]

$$R_{\text{hb single}}(T/T_c) = \frac{a^{5/4} + b^{1/2}}{2} \exp\left(0.5068 - \sqrt{0.5068^2 + y^2}\right) \quad (2.28)$$

where $a = 1 + 0.3118y^2$, $b = 1 + 0.2566y^2$ and $y = \sqrt{1.0 - T/T_c}(1.456 - 0.157\sqrt{T_c/T} + 1.764T_c/T)$. The constants $t_1 \approx 10^{-4}$ sec and $t_{0\alpha} \approx 0.00058$ sec are found by fitting the results of Ref. [48]. The factor f_{hb} allows for physical uncertainties; we take $f_{\text{hb}} = 1$ throughout the body of the paper since T_c , which enters $\gamma_{j \text{ hb}}$ exponentially, is also uncertain. For the daughter modes, the dissipation energy due to bulk viscosity is calculated using the modes for the incompressible star. In the slow rotation limit, it is given to leading order in Γ_1^{-2} by

$$-\dot{E}_{Bj} = \left(\frac{\zeta\omega_j^2}{\Gamma_1^2}\right) \int d^3x \left|\frac{\xi_j \cdot \nabla p}{p}\right|^2. \quad (2.29)$$

This approximation was proposed by Cutler and Lindblom [65] and adopted by Kokkotas and Stergioulas [66] for the r-mode and by Brink *et al.* [52] for the inertial modes. The adiabatic index Γ_1 is regarded as a parameter; we use $\Gamma_1 \approx 2$.

The damping rate is

$$\gamma_{j \text{ hb}} = -\frac{\dot{E}_{Bj}}{\epsilon}, \quad (2.30)$$

where $\epsilon = MR^2\Omega^2$ is the mode's energy in the rotating frame at unit amplitude and $j = \beta, \gamma$. Using this procedure, we calculate

$$t_{0\beta} \approx 1.4 \times 10^{-5} \text{ sec}, \quad (2.31)$$

$$t_{0\gamma} \approx 1.0 \times 10^{-5} \text{ sec}.$$

2.3 Summary of Results

Fig. 2.3(a) shows possible evolutionary trajectories of a neutron star in the angular velocity-temperature $\tilde{\Omega} - T_8$ plane, where $T = T_8 \times 10^8$ K is the core temperature, and $\tilde{\Omega} = \Omega/\Omega_c = \Omega/\sqrt{\pi G \bar{\rho}}$ with $\bar{\rho}$ the mean density of the neutron star. Fig. 2.3(b) displays the regions in $f_{\text{dU}} - S_{\text{ns}}$ in which the trajectories occur. Here f_{dU} represents the fraction of the star that is above the density threshold for direct URCA reactions and S_{ns} is the slippage factor that reduces the relative motion between the crust and the core taking into account the elasticity of the crust [43]. The stability regions are shown at fixed hyperon superfluidity temperature, $T_c = 5.0 \times 10^9$ K. The initial part of the evolution is similar in all scenarios and can be divided into phases.

Phase 0. Spin up below the r-mode stability curve at $T_8 = T_{8\text{in}}$ such that nuclear heating balances neutrino cooling.

Phase 1. Linear regime. The r-mode amplitude grows exponentially. The phase ends when the r-mode reaches the parametric instability.

Phase 2. The triplet coupling leads to quasi-steady mode amplitudes. The star is secularly heated at approximately constant Ω because of viscous dissipation in all three modes.

Phase 3. Several trajectories are possible depending on how the previous phase ends.

a. Fast Runaway. The star fails to reach thermal equilibrium when the trajectory passes over the peak of the Heating = Cooling ($H = C$) curve. This leads to rapid runaway. The daughter modes damp eventually as bulk viscosity becomes important, and the r-mode grows exponentially until the trajectory hits the r-mode stability curve again. This scenario ends as predicted by Nayyar and Owen [48].

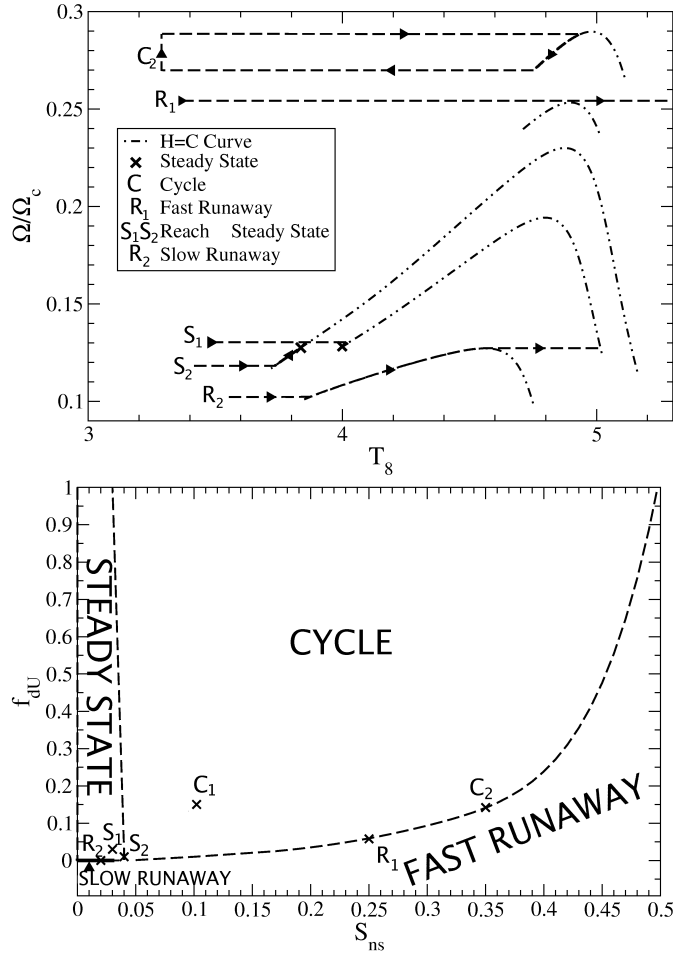


Figure 2.1: (a) Typical trajectories for the four observed evolution scenarios are shown in the $\tilde{\Omega} - T_8$ phase space, where $\tilde{\Omega} = \Omega/\Omega_c$. The dashed lines ($H = C$ curves) represent the points in the $\tilde{\Omega} - T_8$ phase space where the dissipative effects of the heating from the three-modes exactly compensate the neutrino cooling for the given set of parameters ($S_{ns}, f_{dU}, T_c, \dots$) of each evolution. (b) The corresponding stability regions for which these scenarios occur are plotted at fixed hyperon superfluidity temperature $T_c = 5.0 \times 10^9$ K, while varying f_{dU} and S_{ns} . The position of the initial angular velocity and temperature ($\tilde{\Omega}_{in}, T_{8\ in}$) with respect to the maximum of this curve determines the stability of the evolution. (I) $\tilde{\Omega}_{in} > \tilde{\Omega}_{H=C\ max}$. Trajectory R_1 . Fast Runaway Region. After the r-mode becomes unstable the star heats up, does not find a thermal equilibrium state and continues heating up until a thermogravitational runaway occurs. (II) $\tilde{\Omega}_{in} < \tilde{\Omega}_{H=C\ max}$. The evolutions are either stable or, if there is a runaway, it occurs on timescales comparable to the accretion timescale. The possible trajectories are (1) Trajectory C. Cycle Region. (2) Trajectories S_1 and S_2 . Steady State Region. (3) Trajectory R_2 . Slow Runaway Region.

However, the r-mode passes its second parametric instability threshold soon after it starts growing again. This requires the inclusion of more modes to follow the evolution, which is the subject of future work.

b. The star reaches thermal equilibrium. There are then three possibilities:

(i) Cycle. The star cools and spins down slowly, descending the $H = C$ curve until it crosses the r-mode stability curve again. At this point the instability shuts off. The star cools back to $T_{8\text{in}}$ at constant $\tilde{\Omega}$ and then the cycle repeats itself. At $T_c = 5.0 \times 10^9$ K this scenario occurs for values of $S_{\text{ns}} < 0.50$ and large enough values of f_{dU} . However, if T_c is larger, the cycle region in the $f_{\text{dU}}-S_{\text{ns}}$ phase space increases dramatically (see Fig. 2.9(a)). Note that our cycles are different from those obtained by Levin [38] in that the spin-down phase does not start when the r-mode amplitude saturates (or in our case when it reaches the parametric instability threshold), but rather when the system reaches thermal equilibrium. The r-mode amplitude does not grow significantly above its first parametric instability threshold, remaining close to $\sim 10^5$ and so the part of the cycle in which the r-mode is unstable also lasts longer than in Ref. [38]. Also, our cycles are narrow. During spin-down the temperature changes by less than 20 % and $\tilde{\Omega}$ changes by less than 10% of the initial value. (See Sec. 2.2 for a detailed example.)

(ii) Steady State. For small S_{ns} and large enough f_{dU} ($f_{\text{dU}} \gtrsim 5 \times 10^{-5}$, $S_{\text{ns}} \lesssim 0.04$; see Fig. 2.3(b)) the star evolves towards an $\tilde{\Omega}$ equilibrium. The trajectory either ascends or descends the $H = C$ curve (spins up and heats or spins down and cools). The evolution stops when the accretion torque equals the gravitational radiation emission.

(iii) Slow Runaway. For small S_{ns} and very small f_{dU} ($S_{\text{ns}} \lesssim 0.03$, $f_{\text{dU}} < 5 \times 10^{-5}$) the star ascends the $H = C$ curve until the peak is overcome and subsequently a

runaway occurs. The daughter modes eventually damp and the r-mode grows exponentially until it crosses its second parametric instability threshold and more modes need to be included.

Bulk viscosity only affects the runaway evolutions; the cyclic and steady state evolutions found here would be the same if there were no hyperon bulk viscosity. For large $T_c \sim 10^{10}$, or for models with no hyperons at all, there would be no runaway region (See Fig. 2.9(a) for an $f_{\text{dU}} - S_{\text{ns}}$ scenario space with a larger $T_c = 6.5 \times 10^9$ K where the fast runaway region has shrunk dramatically and the slow runaway region has disappeared.)

2.4 Possible Evolution Scenarios

In this section we examine examples of the different types of evolution in more detail. We assume $\dot{M} = 10^{-8} M_{\odot}/\text{yr}$ and $T_c = 5.0 \times 10^9$ K.

2.4.1 Cyclic Evolution

In this sub-section we present the features of typical cyclic trajectories of neutron stars in the angular velocity temperature plane in more detail. We focus on two cases: (C1) $S_{\text{ns}} = 0.10$ and $f_{\text{dU}} = 0.15$ and (C2) $S_{\text{ns}} = 0.35$ and $f_{\text{dU}} = 0.142$. In this scenario the 3-mode system is sufficient to model the nonlinear effects and successfully stops the thermal runaway. The numerical evolution is started once the star reaches the r-mode stability curve. The initial temperature of the star is at the point where nuclear heating equals neutrino cooling in Eq. (2.18) that

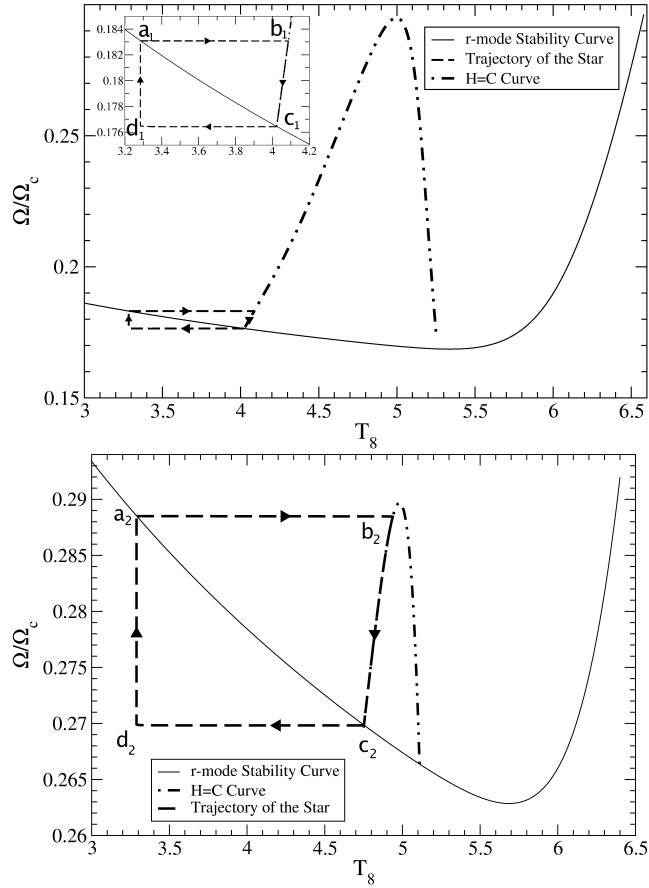


Figure 2.2: Two cyclic trajectories in the $\tilde{\Omega}-T_8$ plane are displayed for a star with $T_c = 5.0 \times 10^9$ K and (a) $f_{dU} = 0.15$ and $S_{ns} = 0.10$, and (b) $f_{dU} = 0.142$ and $S_{ns} = 0.35$, which is close to the border between the stable and unstable region (see Fig. 2.3(b)). The thick solid line labeled as the Heating = Cooling ($H = C$) curve is the locus of points in this phase space where the neutrino cooling is equal to the viscous heating due to the unstable modes. The other solid line representing the r-mode stability curve is defined by setting the gravitational driving rate equal to the viscous damping rate. The part of the curve that decreases with T_8 is dominated by boundary layer and shear viscosity, while the part of the curve that has a positive slope is dominated by hyperon bulk viscosity. In portion $a_1 \rightarrow b_1$ of the trajectory the star heats up at constant $\tilde{\Omega}$. Part $b_1 \rightarrow c_1$ represents the spin down stage, which occurs when the viscous heating is equal to the neutrino cooling. $c_1 \rightarrow d_1$ shows the star cooling back to the initial T_8 . Segment $d_1 \rightarrow a_1$ displays the accretional spin-up of the star back to the r-mode stability curve. The cycle $a_2 \rightarrow d_2$ proceeds in the same way. This cycle is close to the peak of the $H = C$ curve. Configurations above this peak will run away.

is approximately $T_{8\text{in}} \approx 3.29$ for both cases. The initial Ω is the angular velocity that corresponds to this temperature on the r-mode stability curve, which differs for the different S_{ns} ($\tilde{\Omega}_{\text{in}} = 0.183$ for C_1 and $\tilde{\Omega}_{\text{in}} = 0.288$ for C_2).

Figs. 2.2(a) and (b) display the cyclic evolution for trajectories C_1 and C_2 of Fig. 2.3(b). In leg $a_1 \rightarrow b_1$ of the trajectory the r-mode and, once the r-mode amplitude increases above the first parametric instability threshold, the two daughter modes it excites, viscously heat up the star until point b_1 when the neutrino cooling balances the viscous dissipation. This part of the evolution occurs at constant angular velocity over a period of $t_{\text{heat-up}} \approx 100$ yr and a total temperature change $(\Delta T)_{a_1-b_1} \approx 0.80$ ($\approx 24\%$ of $T_{8\text{in}}$). The points where the viscous heating compensates the neutrino cooling are represented by the Heating = Cooling ($H = C$) curve. This is determined by setting Eq. 2.18 to zero and using the quasi-stationary solutions given by Eq. (2.6) for the three modes on the right hand side. The star continues to evolve on the $H = C$ curve for part $b_1 \rightarrow c_1$ of the trajectory as it spins down and cools down back to the r-mode stability curve. This spin-down stage lasts a time $t_{\text{spin-down } b_1-c_1} \approx 23,000$ yr that is much longer than the heat-up period. This timescale is very sensitive to changes in the slippage factor and can reach 10^6 yr for smaller values of S_{ns} that are close to boundary of the steady state region. The cycle is very narrow in angular velocity with a total angular velocity change of less than 4%, $(\Delta\tilde{\Omega})_{b_1-c_1} \approx 0.0066$. The temperature also changes by only about 2%, $(\Delta T_8)_{b_1-c_1} \approx 0.08$ in this spin-down period. Segment $c_1 \rightarrow d_1$ represents the cooling of the star to the initial temperature on a timescale of $\sim 2,000$ yr. In part $d_1 \rightarrow a_1$ the star spins up by accretion at constant temperature back to the original crossing point on the r-mode stability curve. This last part of the trajectory is the longest-lasting one, taking $\approx 200,000$ yr at our chosen \dot{M} of $10^{-8} M_{\odot}\text{yr}^{-1}$. The cycle C_2 in Fig. 2.2(b)

proceeds in a similar fashion. It is important to note that this configuration is close to the border between the “FAST RUNAWAY” and “CYCLE” regions and therefore close to the peak of the $H = C$ curve. Configurations above this peak (e.g., with the same f_{dU} and higher S_{ns}) will go through a fast runaway.

Fig. 2.3(a) shows the evolution of the three modes in the first few years after the star first reaches the r-mode stability curve. In this region the r-mode is unstable and initially grows exponentially. Once it has increased above the first parametric instability threshold the daughter modes are excited. The oscillations of the three modes display some of the typical dynamics of a driven three-mode system. When the r-mode transfers energy to the daughter modes they increase exponentially while the r-mode decreases. Similarly, when daughter modes decrease the r-mode increases. The viscosity damps the oscillations and the r-mode amplitude settles at a value close to the parametric instability threshold. Fig. 2.3(b) displays the evolution of the r-mode amplitude divided by the parametric instability threshold on a longer timescale. It can be seen that the r-mode never grows significantly beyond this first threshold. Fig. 2.3(c) shows the evolution of the parametric instability threshold as a function of time. The threshold increases as the temperature increases and the star is viscously heated by the three modes. When the star spins down in thermal equilibrium, the threshold decreases to a value close to its initial value.

2.4.2 Steady State Evolution

This sub-section focuses on evolutions that lead to a steady equilibrium state in which the rate of accretion of angular momentum is balanced by the rate of

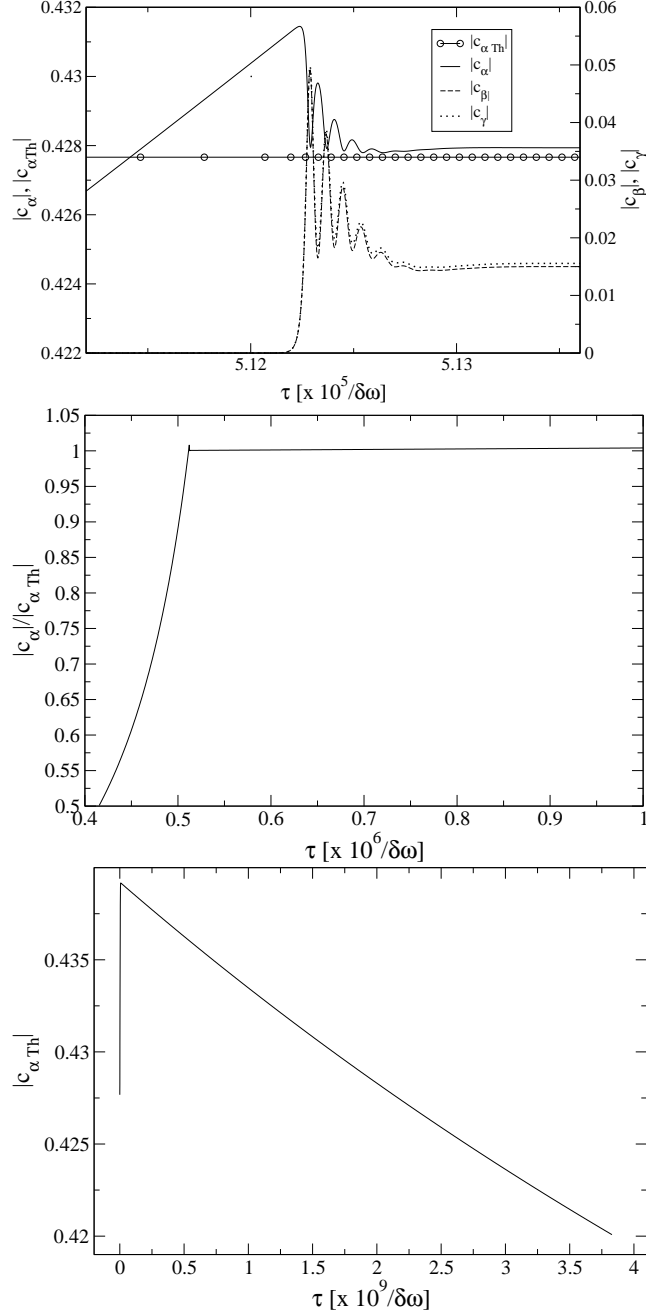


Figure 2.3: (a) The amplitudes of the r-mode $|C_\alpha|$ and of the $n = 13, m = -3$ and $n = 14, m = 1$ inertial modes $|C_\beta|$ and $|C_\gamma|$ are shown as a function of time for a star that executes a cyclic evolution (same parameters as in Fig. 2.2). The lowest parametric instability threshold is also displayed. (b) The ratio of the r-mode amplitude to the parametric instability threshold is plotted as a function of time. It can be seen that once the r-mode crosses the parametric instability threshold it remains close to it for the rest of the evolution. (c) The parametric instability threshold is displayed as a function of time. Its value changes as the angular velocity and temperature evolve.

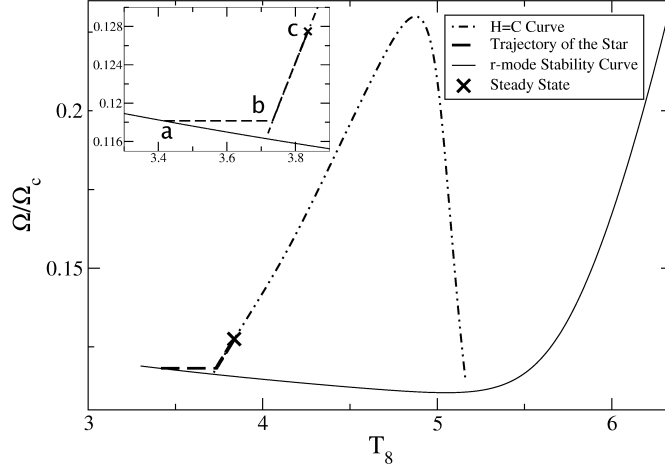


Figure 2.4: The trajectory of a neutron star in the $\tilde{\Omega} - T_8$ phase space is shown for a model with $T_c = 5.0 \times 10^9$ K, $f_{dU} = 0.03$ and $S_{ns} = 0.03$ that reaches an equilibrium steady state. The star spins up until it crosses the r-mode stability curve and the r-mode becomes unstable. The r-mode then quickly grows to the first parametric instability threshold and excites the daughter modes. In leg $a \rightarrow b$ of the trajectory the star is viscously heated by the mode triplet until the system reaches thermal equilibrium. Segment $b \rightarrow c$ shows the star continuing to heat and spin up in thermal equilibrium until the accretion torque is balanced by the gravitational radiation emission. The r-mode stability curve represents the points in phase space where the viscous driving rate is equal to the gravitational driving rate. The H=C curve is the locus of points where the viscous dissipation due to the mode triplet balances the neutrino cooling.

loss via gravitational radiation emission. This scenario is restricted to stars with small slippage factor ($S_{ns} \lesssim 0.04$, see Fig. 2.3(b)) and boundary layer viscosity. A typical trajectory of a star that reaches such an equilibrium is shown in Fig. 2.4. As always, we start the evolution at the point on the r-mode stability curve at which the nuclear heating balances neutrino cooling. Above the r-mode stability curve the gravitational driving rate is greater than the viscous damping rate and the r-mode grows exponentially until nonlinear effects become important. In this case, as in the cyclic evolution, the triplet of modes at the lowest parametric instability threshold is sufficient to stop the thermal runaway. The r-mode remains close to the first instability threshold for the length of the evolution and

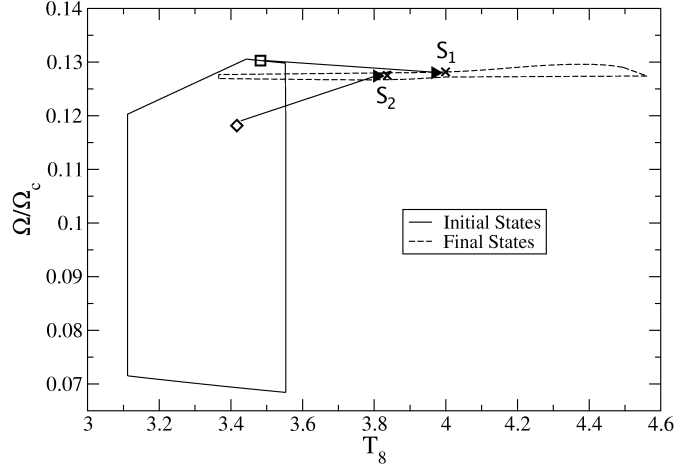


Figure 2.5: The $(\tilde{\Omega}, T_8)$ initial values (region delimited by the solid line) that lead to equilibrium steady states and their corresponding final steady state values (region enclosed by the dashed line) are shown. Since both the initial and final values of T_8 are low, these evolutions are roughly independent of T_c .

after a few oscillations the three modes settle into their quasi-stationary states, which change only secularly as the spin and temperature of the star evolve. The modes heat the star viscously at constant $\tilde{\Omega}$ in segment $a \rightarrow b$ of the trajectory for $t_{\text{heat-up}} \approx 1, 100$ yr. At point b , the star reaches a state of thermal balance. In leg $b \rightarrow c$ the star continues its evolution in thermal equilibrium and slowly spins up due to accretion until the angular velocity evolution also reaches an equilibrium. The timescale to reach an equilibrium steady state is $t_{\text{steady}} \approx 3.5 \times 10^6$ yr for this set of parameters.

Fig. 2.5 displays the possible initial values for the angular velocity $\tilde{\Omega}$ and temperature T_8 of the star that lead to a balancing between the accreted angular momentum and the angular momentum emitted in gravitational waves. The fraction of the star that is above the threshold for direct URCA reactions and the slippage factor are varied within the corresponding “STEADY STATE” region of Fig. 2.3(b). The final equilibrium values are also displayed and cluster in

a narrower region than the initial values. Because viscosity is so small in this regime, the values of Ω also tend to be small. Thus, although an interesting physical regime, this case is most likely not relevant to recycling by accretion to create pulsars with spin frequencies as large as 716 Hz. Note that a steady state can be achieved when $S_{\text{ns}} = 0$. This is the probable end state of the problem first calculated by Levin [38]. The reason we do not find a cycle at low S_{ns} is twofold: (1) the shear viscosity we are using is lower (shear viscosity in Ref. [38] is amplified by a factor of 244), and (2) the nonlinear couplings keep all mode amplitudes small.

2.4.3 Thermal Runaway Evolutions

We now consider evolutions in which the three-mode system is not sufficient to halt the thermal runaway. We observe two such scenarios. In the first scenario, the star is unable to reach thermal equilibrium. The runaway occurs on a period much shorter than the accretion timescale and so the whole evolution is at approximately constant angular frequency. In the second scenario, the star reaches a state of thermal equilibrium but the spin evolution does not reach a steady state. The star continues to spin up by accretion until it climbs to the peak of the $H = C$ curve, thermal equilibrium fails and a runaway occurs.

Fast Runaway

A typical trajectory of a star that goes through a rapid thermal runaway is displayed in Fig. 2.6. This star has $S_{\text{ns}} = 0.25$ and $f_{\text{dU}} = 0.058$. Initially, the growth of the r-mode is halted by the two daughter modes once the lowest parametric in-

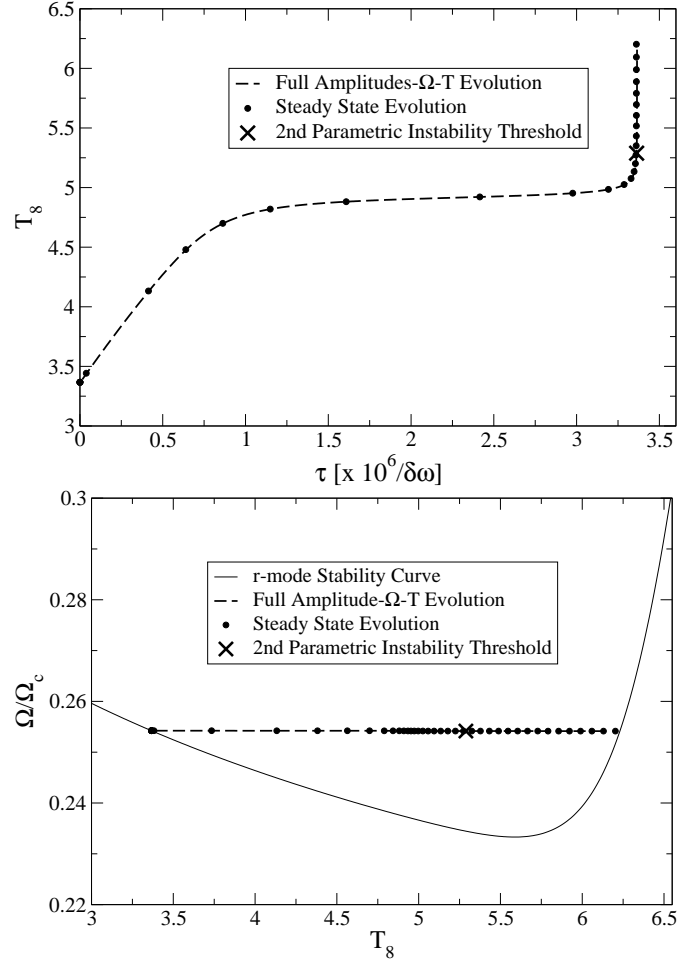


Figure 2.6: This plot compares the full evolution resulting from solving Eqs. (2.4),(2.13),(2.18) with the reduced $\Omega - T$ evolution that assumes the amplitudes go through a series of steady states Eqs. (2.19)-(2.20) for a model with $T_c = 5.0 \times 10^9$ K, $f_{aU} = 0.058$ and $S_{ns} = 0.25$. (a) The temperature is displayed as a function of time for the two different methods. (b) The angular velocity $\tilde{\Omega} = \Omega/\Omega_c$ is shown as a function of temperature. The evolution occurs at constant spin frequency. It can be seen that the steady-state amplitude approximation is extremely good. The 'X' shows the point at which the r-mode crosses its second lowest parametric instability threshold, where additional dissipation would become operative.

stability threshold is crossed, and the three modes settle in the (Ω, T) -dependent quasi-stationary states of Eqs. (2.6). They viscously heat up the star until hyperon bulk viscosity becomes important for the daughter modes. As the amplitudes of the daughter modes decrease the coupling is no longer strong enough to drain enough energy to stop the growth of the r-mode. The daughter modes are completely damped and the r-mode increases exponentially. The system goes back to the one-mode evolution described by Ref. [48].

Fig. 2.6(a) and (b) compare both the temperature evolution and the trajectory in the $\tilde{\Omega}-T_8$ plane of the star for a simulation solving the full set of equations to a simulation that assumes quasi-stationary solutions for the three amplitudes and evolves only the angular velocity and temperature of the star. It can be seen that the steady state approximation is very good until the thermal runaway occurs. Afterward, the temperature evolution of the reduced equations is offset slightly from the quasi-steady result and intersects the r-mode instability curve sooner. This evolution is similar to that described by Nayyar and Owen [48]. However, the r-mode crosses its second lowest parametric instability much earlier in the evolution (see the 'X' in the figure), and at that point more modes need to be included to model the instability accurately. Thus, we cannot be sure that a runaway must occur in this case. We shall return to this issue in a subsequent paper.

Slow Runaway

In this section we examine evolutions in which the neutron star has both a very small slippage factor, $S_{\text{ns}} \lesssim 0.03$, and only a small percentage of the star is above the threshold for direct URCA reactions, $f_{\text{dU}} < 5 \times 10^{-5}$. A trajectory for this kind

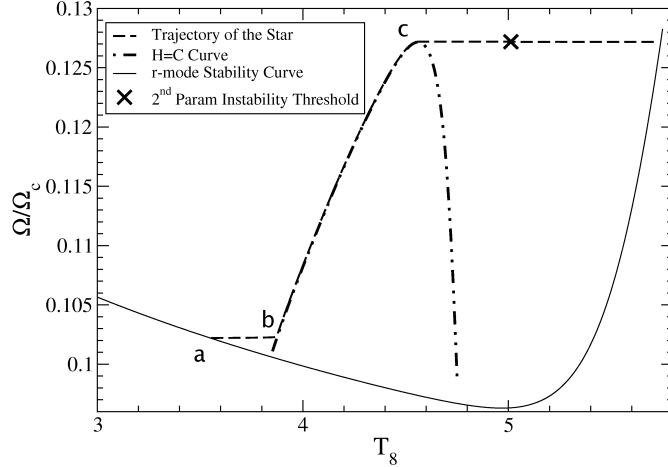


Figure 2.7: The trajectory of a neutron star in the $\tilde{\Omega} - T_8$ phase space is shown for a model with $T_c = 5.0 \times 10^9$ K, $f_{dU} = 4.0 \times 10^{-5}$ and $S_{ns} = 0.02$ that goes through a slow thermogravitational runaway. Portion $a \rightarrow b$ of the trajectory shows the mode triplet heating up the neutron star through boundary layer and shear viscosity until the system reaches thermal equilibrium. Segment $b \rightarrow c$ represents the accretional spin-up of the star in thermal equilibrium. The dotted-dashed line is the locus of points where the viscous dissipation of the mode triplet is equal to the neutrino cooling, and is labeled as the $H = C$ curve. The star reaches the maximum of this curve and fails to reach an equilibrium between the accretion torque and gravitational emission. It then continues heating at constant angular velocity and crosses its second lowest parametric instability threshold, at which point more modes would need to be included to make the evolution accurate. Eventually the star reaches the r-mode stability curve again.

of evolution is displayed in Fig. 2.7. After the star crosses the r-mode stability curve, the r-mode increases beyond the first parametric instability threshold, and its growth is temporarily stopped by energy transfer to the daughter modes. As in the previous scenarios, the star is viscously heated by the mode triplet at constant Ω in part $a \rightarrow b$ of the trajectory on a timescale of about 5,000 yr. At point b , it reaches thermal equilibrium. In leg $b \rightarrow c$ of the trajectory, the star continues its evolution by ascending the $H = C$ curve and spinning up because of accretion for about 2×10^6 yr without finding an equilibrium state for the angular momentum evolution. Once it reaches the peak of the $H = C$ curve, the

cooling is no longer sufficient to stop the temperature from increasing exponentially and a thermal runaway occurs. The cross mark ‘X’ on the trajectory shows the point at which the r-mode amplitude crosses its second lowest parametric instability threshold. At this stage more inertial modes need to be included to model the rest of this evolution correctly. As for the cases that evolve to steady states, these long-timescale runaways tend to occur at low spin rates.

2.5 Probability of Detection

Fig. 2.8 shows how the time the star spends above the r-mode stability curve changes when S_{ns} and f_{dU} are varied. For large enough values of S_{ns} the boundary layer viscosity dominates. In this region of phase space the spin-down timescale can be approximated by

$$\begin{aligned}
 t_{\text{spin-down}} &= \int_b^c \frac{dt}{d\tilde{\Omega}} d\tilde{\Omega} & (2.32) \\
 &\approx \frac{\tilde{I}\tau_{\text{GR}}^0}{6} \frac{(4\tilde{\kappa})^2 \tilde{\omega}_\beta \tilde{\omega}_\gamma}{|\delta\tilde{\omega}|^2} \frac{1}{|\bar{C}_\alpha|^2} \frac{\Delta\tilde{\Omega}}{\langle\tilde{\Omega}\rangle^6} \\
 &\approx 250 \text{ yr} \frac{\Delta\nu_{\text{kHz}}}{\langle\nu_{\text{kHz}}\rangle^7} \frac{1}{M_{1.4} R_6^4} \left(\frac{|c_\alpha^{\text{th}}|}{|c_\alpha|} \right)^2,
 \end{aligned}$$

where $M_{1.4} = M/(1.4M_\odot)$, $R_6 = R/(10^6 \text{ cm})$, $\nu_{\text{kHz}} = \nu/1 \text{ kHz}$, $\tilde{I} = 0.261$ [?], the r-mode amplitude at its parametric instability threshold $|c_\alpha^{\text{th}}| \approx |\delta\tilde{\omega}|/(4\tilde{\kappa}\sqrt{\tilde{\omega}_\beta\tilde{\omega}_\gamma}) \approx 1.5 \times 10^{-5}$, and $\bar{C}_\alpha = \sqrt{\tilde{\Omega}}|c_\alpha|/|c_\alpha^{\text{th}}|$. This approximation agrees with spin-up timescales obtained from our simulations to $\sim 25\%$.

The maximum ν is approximately the same as the initial frequency, and can be determined by equating the driving and damping rate of the r-mode, since it

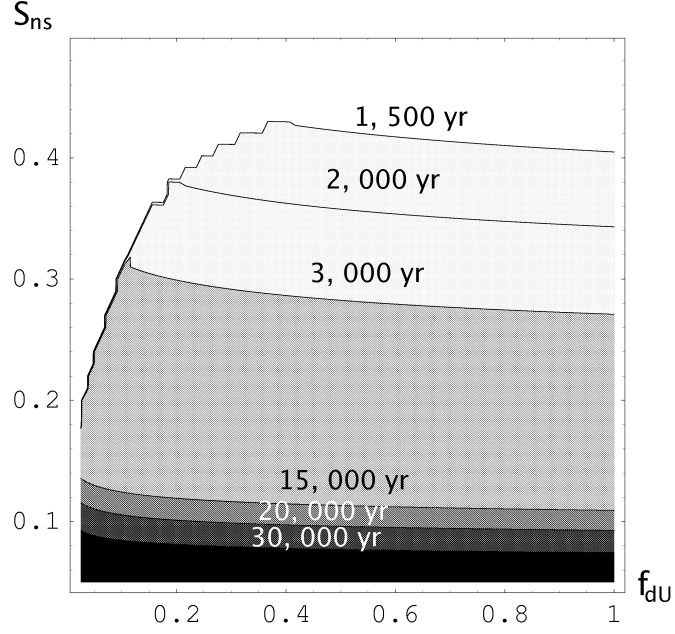


Figure 2.8: The spin-down timescale is shown as slippage factor S_{ns} and fraction of the star subject to direct URCA f_{dU} for cyclic evolutions are varied for a fixed hyperon critical temperature of $T_c = 5.0 \times 10^9$ K. This timescale dominates the heat-up timescale and hence represents the time the star spends above the r-mode instability curve. It increases as the viscosity is lowered and the star gets closer to the steady state region.

is on the r-mode stability curve

$$\nu_{\text{max}} \approx 800 \text{Hz} \left(\frac{S_{\text{ns}}}{M_{1.4} R_6} \right)^{4/11} \frac{1}{T_8^{2/11}}. \quad (2.33)$$

Thus, the spin-down timescale is very sensitive to the slippage factor $t_{\text{spin-down}} \propto S_{\text{ns}}^{-24/11} (\Delta\nu_{\text{kHz}}/\nu_{\text{kHz}})$. The dependences on f_{dU} and accretion rate \dot{M} are much weaker; a rough approximation, obtained by matching direct URCA cooling and nuclear heating, is $T_{8\text{in}} \propto \dot{M}^{1/6} f_{\text{dU}}^{-1/6} R_6^{-1/6} M_{1.4}^{-1/9}$, and $\nu_{\text{max}} \propto S_{\text{ns}}^{4/11} f_{\text{dU}}^{1/33} \dot{M}^{-1/33} R_6^{-1/3} M_{1.4}^{-34/99}$. The gravitational wave amplitude measured at distance d [69, 70] is

$$h \approx 1.6 \frac{R}{d} \sqrt{\frac{GM}{\tau_{\text{GR}}^0 c^3}} \tilde{\Omega}^3 |c_\alpha| \quad (2.34)$$

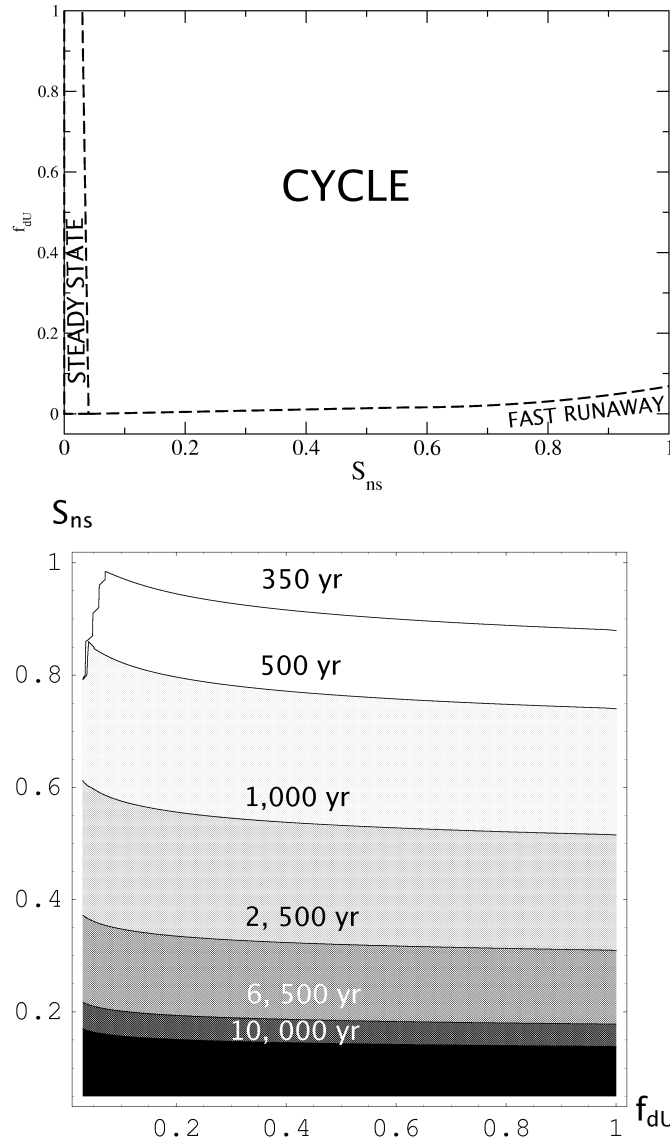


Figure 2.9: (a) The stability regions are plotted at fixed hyperon superfluidity temperature $T_c = 6.5 \times 10^9$ K, while varying f_{dU} and S_{ns} . The steady state region remains roughly the same as in Fig. 2.3(b), the slow run-away region disappears, and the cycle region increases dramatically while shrinking the fast-runaway region. (b) The spin-down timescale is shown for the cyclic evolutions in part (a).

$$\approx 3 \times 10^{-25} \left(\frac{10 \text{kpc}}{d} \right) M_{1.4} R_6^3 \nu_{\text{kHz}}^3 \left(\frac{|c_\alpha|}{c_\alpha^{\text{th}}} \right).$$

Taking $\nu \approx \nu_{\text{max}}$ gives

$$h \propto S_{\text{ns}}^{12/11} M_{1.4}^{-1/33} R_6^2 f_{\text{dU}}^{1/11} \dot{M}^{-1/11}. \quad (2.35)$$

The maximum distance at which sources could be detected by Advanced LIGO interferometers, assuming $h_{\text{min}} = 10^{-27}$, [69] is

$$\begin{aligned} d_{\text{max}} &\approx 3 \text{ Mpc} \left(\frac{10^{-27}}{h_{\text{min}}} \right) M_{1.4} R_6^3 \nu_{\text{kHz}}^3 \left(\frac{|c_\alpha|}{c_\alpha^{\text{th}}} \right) \\ &\approx 1.5 \text{ Mpc} \left(\frac{10^{-27}}{h_{\text{min}}} \right) S_{\text{ns}}^{12/11} M_{1.4}^{-1/11} R_6^{21/11} \\ &\times T_8^{-6/11} \left(\frac{|c_\alpha|}{c_\alpha^{\text{th}}} \right). \end{aligned} \quad (2.36)$$

Eqs. (2.33) and (2.36) imply that gravitational radiation from the r-mode instability may only be detectable for sources in the Local Group of galaxies. Eq. (2.33) implies that for accretion to be able to spin up neutron stars to $\nu \gtrsim 700$ Hz, we must require $(S_{\text{ns}}/M_{1.4}R_6\sqrt{T_{8\text{in}}})^{4/11} \gtrsim 1$. Assuming this to be true, $d_{\text{max}} \lesssim 1\text{-}1.5$ Mpc. However, $t_{\text{spin-down}} \approx 1000$ yr at most, making detection unlikely for any given source. Moreover, unless S_{ns} can differ substantially from one neutron star to another, only those with ν given by Eq. (2.33) can be r-mode unstable. Slower rotators, including almost all LMXBs, are still in their stable spin-up phases.

Still more seriously, Fig. 2.3(b) shows that spin cycles are only possible for $S_{\text{ns}} \lesssim 0.50$, assuming $T_c \approx 5.0 \times 10^9$ K; Eq. (2.33) then implies $\nu \lesssim 450$ Hz. This would restrict detectable gravitational radiation to galactic sources, although the duration of the unstable phase could be longer.

Within the context of our three mode calculation, $S_{\text{ns}} > 0.50$, which is needed for explaining the fastest pulsars, would imply fast runaway. There are two possible resolutions to this problem. One is that including additional modes pre-

vents the runaway; we shall investigate this in subsequent papers. The second is that T_c is larger, or that neutron stars do not contain hyperons (e.g., because they are insufficiently dense). Fig. 2.9(a) shows the same phase plane as Fig. 2.3(b) but with $T_c = 6.5 \times 10^9$ K, and Fig. 2.9(b) shows the results for $t_{\text{spin-down}}$ analogous to Fig. 2.8. Larger T_c permits spin cycles for higher values of S_{ns} (and hence ν), but the time spent in the unstable regime is shorter.

2.6 Discussion and Concluding Remarks

In this chapter, we model the nonlinear saturation of unstable r-modes of accreting neutron stars using the triplet of modes formed from the $n = 3, m = 2$ r-mode and the the first two near resonant modes that become unstable ($n = 13, m = -3$ and $n = 14, m = 1$) by coupling to the r-mode. This is the first treatment of the spin and thermal evolution including the nonlinear saturation of the r-mode instability to provide a physical cutoff by energy transfer to other modes in the system. The model includes neutrino cooling and shear, boundary layer and hyperon bulk viscosity. We allow for some uncertainties in neutron star physics that is not yet understood by varying the superfluid transition temperature, the slippage factor that regulates the boundary layer viscosity, and the fraction of the star that is above the density threshold for direct URCA reactions. In all our evolutions we find that the mode amplitudes quickly settle into a series of quasi-stationary states that can be calculated algebraically, and depend weakly on angular velocity and temperature. The evolution continues along these sequences of quasi-steady states as long as the r-mode is in the unstable regime. The spin and temperature of the neutron star can follow several possible trajectories depending on interior physics. The first part of the evolution is the

same for all types of trajectories: the star viscously heats up at constant angular velocity.

If thermal equilibrium is reached, we find several possible scenarios. The star may follow a cyclic evolution, and spin down and cool in thermal equilibrium until the r-mode enters the stable regime. It subsequently cools at constant Ω until it reaches the initial temperature. At this point the star starts spinning up by accretion until the r-mode becomes unstable again and the cycle is repeated. The time the star spends in the unstable regime is found to vary between a few hundred years (large $S_{\text{ns}} \sim 1$) and 10^6 yr (small $S_{\text{ns}} \sim 0.05$). Our cycles are different from those previously found by Ref. [38] in that our amplitudes remain small, $\sim 10^{-5}$, which slows the viscous heating and causes the star to spend more time in the regime where the r-mode instability is active. Furthermore, we find that the star stops heating when it reaches thermal equilibrium and not when the r-mode reaches a maximum value. The cycles we find are narrow with the spin frequency of the star changing less than 10% even in the case of high spin rates ~ 750 Hz. Other possible trajectories are an evolution toward a full steady state in which the accretion torque balances the gravitational radiation emission, and a very slow thermogravitational runaway on a timescale of $\sim 10^6$ yr. These scenarios occur for very low viscosity ($S_{\text{ns}} \lesssim 0.04$). Although theoretically interesting, they do not allow for very fast rotators of ~ 700 Hz.

Alternatively, if the star does not reach thermal equilibrium, we find that it continues heating up at constant spin frequency until it enters a regime in which the r-mode is no longer unstable. This evolution is similar to that predicted by Nayyar and Owen [48]. However, the r-mode grows above its second parametric instability threshold fairly early in its evolution and at this point more iner-

tial modes should be excited and the three-mode model becomes insufficient. Modeling this scenario accurately is subject of future work.

We have focused on cases with $T_c \gtrsim 5 \times 10^9$ K. These are cases for which the nonlinear effects are substantial. In this regime, hyperon bulk viscosity is not important except for thermal runaways where we expect other mode couplings, ignored here, to play important roles. Fast rotation requires large dissipation, as has long been recognized [42, 38] and these models can only achieve $\nu \gtrsim 700$ Hz if boundary layer viscosity is very large. Alternatively, at lower $T_c \lesssim 3 \times 10^9$ K, large rotation rates can be achieved at r-mode amplitudes below the first parametric instability threshold [50]. Nayyar and Owen found that increasing the mass of the star for the same equation of state makes the hyperon bulk viscosity become important at lower temperatures [48]. Conceivably, there are accreting neutron stars with relatively low masses that have lower central densities and small hyperon populations. These could evolve as detailed here and only spin up to modest frequencies. Hyperons could be more important in more massive neutron stars leading to larger spin rates and very small steady state r-mode amplitude as found by Wagoner [50].

Our models imply small r-mode amplitudes of $\sim 10^{-5}$ and therefore gravitational radiation detectable by advanced LIGO interferometers only in the local group of galaxies up to a distance of a few Mpc. The r-mode instability puts a fairly stringent limit on the spin frequencies of accreting neutron stars of $\nu_{\max} \approx 800 \text{ Hz} [S_{\text{ns}} / (M_{1.4} R_6)]^{4/11} T_8^{-2/11}$. In order to allow for fast rotators of $\gtrsim 700$ Hz in our models a large boundary layer viscosity with $(S_{\text{ns}} / M_{1.4} R_6 \sqrt{T_{8\text{in}}})^{4/11} \sim 1$ is required. Slippage factors of order ~ 1 lead to time periods on which the r-mode is unstable with a timescale of at most 1000 yr, which is about 10^{-3} times

shorter than the accretion timescale. This would mean that only about 1 in 1000 LMXBs in the galaxy are possible LIGO sources. However, lower slippage factors lead to a longer duration of the gravitational wave emission, but also lower frequencies. We also note that in this model we have considered only very fast accretors with $\dot{M} \sim 10^{-8} M_{\odot} \text{yr}^{-1}$ and most LMXBs in our galaxy accrete at slower rates. Investigations with more accurate nuclear heating models are a subject for future work.

Our analysis could be made more realistic in several ways, such as by including the effects of magnetic fields, compressibility, multi-fluid composition [?], superfluidity, superconductivity, etc. These features would render the model more realistic, but its generic features ought to persist, since the upshot would still be a dense set of mode frequencies exhibiting three mode resonances and parametric instabilities with low threshold amplitudes. Although the behavior of the star would differ quantitatively in a model different from ours in detail, we expect the qualitative behaviors we have found to be robust, as they are well described by quasi-stationary mode evolutions whose slow variations are determined by competitions between dissipation and neutrino cooling, and accretion spin-up and gravitational radiation spin-down. In our model, it seems that three mode evolution involving interactions of the r-mode with two daughters at the lowest parametric instability threshold is often sufficient to quench the instability. Our treatment is inadequate to follow what happens when the system runs away; for this, coupling to additional modes is essential. For this regime, a generalization of the work of Brink *et al.* [51, 52, 53] that includes accretion spin-up, viscous heating and neutrino cooling would be needed. Such a calculation is formidable even in a “simple” model involving coupled inertial modes of an incompressible star.

CHAPTER 3

THE EFFECTS OF R-MODE INSTABILITY ON THE SPIN EVOLUTION OF NEWBORN NEUTRON STARS

3.1 Introduction

R-modes are driven unstable by gravitational radiation reaction via the Chandrasekhar-Friedman-Schutz (CFS) mechanism [26, 27]. They were proven to be unstable at all rotation rates in the absence of fluid dissipation [28, 29]. When dissipation is present r-modes are unstable when the gravitational driving dominates fluid dissipation. One can find a critical curve in the angular velocity - temperature ($\Omega - T$) phase space along which the gravitational driving of the $n = 3, m = 2$ r-mode is equal to the viscous dissipation (this critical curve is referred to as the r-mode stability curve in this thesis). Above the curve the r-mode is linearly unstable and grows exponentially. Young neutron stars are hot. We take an initial temperature of $T = 10^{10}$ K and assume that the star is spinning close to break-up with angular velocity $\Omega \sim 0.67 \sqrt{\pi G \bar{\rho}}$, which places it well in the unstable regime. Nonlinear effects become important when the r-mode amplitude is above its first parametric instability threshold and other inertial modes that couple to the r-mode are excited. The star can be born with an r-mode amplitude above the lowest parametric instability threshold or it can be born with a lower amplitude in which case the r-mode amplitude usually grows exponentially until it reaches parametric instability. Modeling nonlinear effects is important because they provide a natural saturation amplitude for the r-mode via energy transfer to other modes in the system and are also crucial in determining the final frequency to which the star can be spun down to.

Previous investigations that did not perform direct hydrodynamic simulations used a simple one-mode evolution model that assumes the nonlinear effects saturate the r-mode amplitude at some arbitrarily fixed value. This model was proposed by Owen *et al.* [30, 32] in 1998. Once the maximum allowed amplitude is achieved the r-mode amplitude remains constant and the star spins down at this fixed amplitude. They found that the newborn neutron star would cool to approximately 10^9 K and spin down from a frequency close to the Kepler frequency to about 100 Hz in ~ 1 yr. In their calculation they include the effects of shear viscosity and bulk viscosity for ordinary neutron star matter composed of neutrons, protons and electrons and assume modified URCA cooling.

Jones [41] and Lindblom & Owen [46] pointed out that if the star contains exotic particles such as hyperons, internal processes could lead to a very high bulk viscosity in the cores of neutron stars. They predicted that for young neutron stars this viscosity would either eliminate the instability altogether or leave a short window of instability of up to a day or so for modified URCA cooling [46, 48] that would not render the gravitational radiation detectable. Various authors [50, 71, 48] used the one-mode model to find that hyperon viscosity can stop the growth of the r-mode amplitude at low amplitudes and that in this case imposing an artificial saturation amplitude may be unnecessary. These studies mainly dealt with millisecond pulsars in Low Mass X-ray Binaries, but the idea can be extended to newborn stars [72]. The main difference is that the star is hotter and cools much faster. The star starts spinning down when the viscous heating due to the r-mode balances neutrino cooling and higher viscosity makes this balance happen at lower r-mode amplitudes.

The formalism to study the nonlinear interactions of the r-mode with other

inertial modes was developed by Schenk *et al.* [54]. They assumed a small r-mode amplitude and treated the oscillations of the modes with weakly nonlinear perturbation theory via three-mode couplings. This assumption was tested by Arras *et al.* [39] and Brink *et al.* [51, 52, 53, 73]. Arras *et al.* proposed that a turbulent cascade will develop in the strong driving regime. They studied both the newborn neutron star and the LMXB case and did not include hyperon bulk viscosity. They estimated that the r-mode amplitude was small and could have values between $10^{-1} - 10^{-4}$. Brink *et al.* computed the interactions of about 5000 modes via approximately 1.3×10^6 couplings among modes with $n \leq 30$. They modeled the star as incompressible and calculated the coupling coefficients analytically. The couplings were restricted to near resonant modes with a fractional detuning of $\delta\omega/(2\Omega) < 0.002$. Brink *et al.* showed that the nonlinear evolution saturates at amplitudes comparable with the lowest parametric instability threshold. Brink *et al.* did not include spin or temperature evolution in their model, choosing constant T and Ω .

In the previous chapter we investigated the r-mode instability for neutron stars in LMXBs including neutrino cooling and accretional spin-up. We took the mode triplet at the lowest parametric instability threshold found by Brink *et al.* and solved the coupled equations for the three modes together with the spin and temperature evolution numerically for a neutron star in an LMXB model. We found that one mode triplet was sufficient to stop thermal runaway in most scenarios and confirmed that the r-mode amplitude settled very close to its parametric instability threshold and tracked the threshold for the rest of the evolution.

In this chapter we begin a study of the nonlinear development of the r-mode

instability for newborn neutron stars. We include neutrino cooling, viscous heating and spin-down due to emitted gravitational radiation and magnetic dipole radiation. We use a simple model in which we parametrize the rate at which the star cools via neutrino emission and the rate at which the energy in inertial modes dissipates via boundary layer viscosity and bulk viscosity. In order to explore different nonlinear behavior we vary some of these parameters, including the hyperon superfluidity temperature T_h .

As before we include the three mode triplet at the lowest parametric instability threshold: the r-mode at $n = 3$ and two inertial modes at $n = 14$ and $n = 15$. This corresponds to the second lowest zero-viscosity parametric instability threshold found by Brink *et al.* The reason for not using the lowest zero-viscosity threshold is that in our case the system is strongly damped and the zero-viscosity limit is no longer a good approximation. When $\delta\omega/(\gamma_\beta + \gamma_\gamma) \ll 1$ where γ_β and γ_γ are the damping rates of the daughter modes; the parametric instability threshold amplitude $\propto \sqrt{\gamma_\beta\gamma_\gamma}/\kappa$ and is independent of $\delta\omega$. So, the lowest detuning no longer leads to the lowest parametric instability threshold and the second lowest parametric instability threshold from the zero-viscosity limit happens to be the first lowest threshold in this case because it has a large coupling coefficient. We do not include higher order corrections in angular velocity for the coupling coefficients or detuning and the exact modes and value of the coupling coefficient may change when these are included. Additionally, as the star spins down the daughter modes comprising the lowest threshold will change and different triplets of modes may become important. Modeling this is subject of future work. Brink *et al.* found typical coupling coefficients between 0.01 and 3 for $\delta\omega/(2\Omega) < 0.002$. The high n daughter modes and coupling coefficient we use ($\kappa = 1.25$) are most likely not the exact modes of the star that

get excited nor the exact coupling coefficient, but they are representative for the lowest parametric instability threshold for a dense set of modes in the strongly damped regime. We believe that the different nonlinear behaviors we obtain are robust, although the numerical values may change slightly for different three-mode parameters.

Sec. 3.2 discusses the evolution equations. We first review the equation for the three modes, the quasi-stationary solutions of the three mode system and the parametric instability threshold. The gravitational driving and viscous damping rates are discussed next. Sec. 3.3 then provides an overview that includes a discussion of each evolution scenario and input physics that leads to each scenario. Each stable evolution type is further detailed in subsections of Sec. 3.5. The runaway evolutions are discussed in detail in Sec. 3.6. The prospects of detecting gravitational radiation are considered in Sec. 3.7. We summarize the results in the conclusion. Appendix B.1 derives the frequency change in the inertial modes due to the presence of a magnetic field. Appendix B.2 details the method we use to compute the bulk viscosity timescales and compares timescales resulting from our method with those computed by Lockitch and Friedman [75]. Appendix B.4 contains a stability analysis of the evolution equations around thermal equilibrium.

3.2 Mathematical Background

3.2.1 Three-mode Evolution Equations

The evolution equations for the mode amplitudes when the $n = 3, m = 2$ r-mode couples to two near-resonant inertial modes can be written as

$$\begin{aligned}\frac{dC_\alpha}{d\tau} &= i\tilde{\omega}_\alpha C_\alpha + \frac{\gamma_\alpha}{\Omega} C_\alpha - \frac{2i\tilde{\omega}_\alpha \tilde{\kappa}}{\sqrt{\Omega}} C_\beta C_\gamma, \\ \frac{dC_\beta}{d\tau} &= i\tilde{\omega}_\beta C_\beta - \frac{\gamma_\beta}{\Omega} C_\beta - \frac{2i\tilde{\omega}_\beta \tilde{\kappa}}{\sqrt{\Omega}} C_\alpha C_\gamma^*, \\ \frac{dC_\gamma}{d\tau} &= i\tilde{\omega}_\gamma C_\gamma - \frac{\gamma_\gamma}{\Omega} C_\gamma - \frac{2i\tilde{\omega}_\gamma \tilde{\kappa}}{\sqrt{\Omega}} C_\alpha C_\beta^*.\end{aligned}\tag{3.1}$$

The scaled frequency $\tilde{\omega}_j$ is $\tilde{\omega}_j = \omega_j/\Omega$, the dissipation rates of the inertial modes, also called daughter modes, are γ_β and γ_γ , γ_α is the sum of the driving and damping rates of the r-mode $\gamma_\alpha = \gamma_{GR} - \gamma_{\alpha\nu}$, and the dimensionless coupling is $\tilde{\kappa} = \kappa/(MR^2\Omega^2)$. A derivation of the equations of motion for the three-mode system in the limit of slow rotation in terms of rotational phase τ ($d\tau = \Omega dt$) from the Lagrangian density can be found in Appendix A.1. This formalism to study the nonlinear interaction of the r-mode with other inertial modes was developed in Schenk *et al.* (in terms of the amplitude variables of Schenk *et al.* [54] and Brink *et al.* [51, 52, 53] $C_j(t) = \sqrt{\Omega(t)}c_j(t)$).

As in Ref. [74] we rescale the equations:

$$\begin{aligned}\frac{d\bar{C}_\alpha}{d\tilde{\tau}} &= \frac{i\tilde{\omega}_\alpha}{|\delta\tilde{\omega}|} \bar{C}_\alpha + \frac{\tilde{\gamma}_\alpha}{|\delta\tilde{\omega}|\tilde{\Omega}} \bar{C}_\alpha - \frac{i}{2\sqrt{\tilde{\Omega}}} \bar{C}_\beta \bar{C}_\gamma, \\ \frac{d\bar{C}_\beta}{d\tilde{\tau}} &= \frac{i\tilde{\omega}_\beta}{|\delta\tilde{\omega}|} \bar{C}_\beta - \frac{\tilde{\gamma}_\beta}{|\delta\tilde{\omega}|\tilde{\Omega}} \bar{C}_\beta - \frac{i}{2\sqrt{\tilde{\Omega}}} \bar{C}_\alpha \bar{C}_\gamma^*, \\ \frac{d\bar{C}_\gamma}{d\tilde{\tau}} &= \frac{i\tilde{\omega}_\gamma}{|\delta\tilde{\omega}|} \bar{C}_\gamma - \frac{\tilde{\gamma}_\gamma}{|\delta\tilde{\omega}|\tilde{\Omega}} \bar{C}_\gamma - \frac{i}{2\sqrt{\tilde{\Omega}}} \bar{C}_\alpha \bar{C}_\beta^*,\end{aligned}\tag{3.2}$$

where we have used the same rescaling as in Ref. [74] with $\bar{C}_j = C_j/|C_j|_0$, $\tilde{\gamma}_j = \gamma_j/\Omega_c$, and Ω_c is a fixed angular frequency chosen for reference. The rotational phase τ is rescaled by the fractional detuning as $\tilde{\tau} = \tau|\delta\tilde{\omega}|$ and the mode amplitudes scaled by the zero-viscosity parametric instability threshold

$$\begin{aligned} |C_\alpha|_0 &= \frac{|\delta\tilde{\omega}| \sqrt{\Omega_c}}{4\tilde{\kappa} \sqrt{\tilde{\omega}_\beta \tilde{\omega}_\gamma}}, & |C_\beta|_0 &= \frac{|\delta\tilde{\omega}| \sqrt{\Omega_c}}{4\tilde{\kappa} \sqrt{\tilde{\omega}_\alpha \tilde{\omega}_\gamma}}, \\ |C_\gamma|_0 &= \frac{|\delta\tilde{\omega}| \sqrt{\Omega_c}}{4\tilde{\kappa} \sqrt{\tilde{\omega}_\beta \tilde{\omega}_\alpha}}. \end{aligned} \quad (3.3)$$

3.2.2 Driving and Damping Rates

For our benchmark calculations, we adopt the neutron star model of Owen *et al.* Ref. [30] ($n = 1$ polytrope, $M = 1.4M_\odot$, $\Omega_c = 8.4 \times 10^3$ rad sec $^{-1}$ and $R = 12.5$ km) and use their gravitational driving rate for the r-mode

$$\begin{aligned} \gamma_{GR}(\Omega) &\simeq 0.05 M_{1.4} R_{12.5}^4 \left(\frac{\nu}{1 \text{ kHz}} \right)^6 \\ &\simeq \frac{\tilde{\Omega}^6}{3.26} \text{ sec}^{-1}, \end{aligned} \quad (3.4)$$

where $M_{1.4} = M/1.4M_\odot$ and $R_{12.5} = R/12.5$ km. If hyperons are present in the core of the neutron star then hyperon bulk viscosity dominates other forms of bulk viscosity. In this chapter we consider hyperon bulk viscosity and boundary layer viscosity to be the main sources of dissipation with

$$\begin{aligned} \tilde{\gamma}_{\alpha \text{ hb}} &= \frac{f_{\text{r hb}} \tau(T, T_c) A_{\text{hb}} \tilde{\Omega}^4 I_\alpha}{1 + (2\tilde{\omega}_\alpha \Omega \tau(T))^2}, \\ \tilde{\gamma}_{j \text{ hb}} &= \frac{f_{\text{d hb}} \tau(T, T_c) A_{\text{hb}} I_j}{1 + (2\tilde{\omega}_j \Omega \tau(T))^2}, \end{aligned} \quad (3.5)$$

for the r-mode and daughter modes respectively. We treat the critical temperature T_c and the coefficient A_{hb} as parameters. A_{hb} is chosen so that the peak of the r-mode stability curve is at about 1000 Hz for all our stable evolutions. We

lower it to exhibit runaway behavior. The factors f_{rhh} and f_{dhh} allow for different physical uncertainties in the r-mode and daughter mode viscosities. In this chapter we take them to be 1. The mode integral for the daughter modes is

$$I_{\text{hb}j} = \frac{1}{R^5} \int d^3x \left| \frac{\xi_j \cdot \nabla p}{p} \right|^2, \quad (3.6)$$

where the value of this integral for different inertial modes is listed in Appendix B.2. The damping rates computed via this method with modes and frequencies for the incompressible stellar model are within a factor of 2 of those computed by Lockitch and Friedman for an $n = 1$ polytope (see Appendix B.2).

The relaxation timescale

$$\tau(T, T_c) = \frac{t_1 T_9^{-2}}{R_{\text{hb}}(T/T_c)}, \quad (3.7)$$

where we use the reduction factor proposed by Ref. [47]

$$R_{\text{hb}}(T/T_c) = \frac{a^{5/4} + b^{1/2}}{2} \exp\left(0.5068 - \sqrt{0.5068^2 + y^2}\right) \quad (3.8)$$

where $a = 1 + 0.3118y^2$, $b = 1 + 0.2566y^2$ and $y = \sqrt{1.0 - T/T_c}(1.456 - 0.157\sqrt{T_c/T} + 1.764T_c/T)$. The constant is taken to be $t_1 \approx 10^{-6}$ sec.

The boundary layer viscosity is computed via Eq. (3) of Bildsten and Ushomirsky [42] and is given by

$$\gamma_{j\text{bl}}(T, \Omega) = I_j A_{\text{bl}} \tilde{\omega}^{5/2} S_{\text{ns}}^2 \frac{\sqrt{\tilde{\Omega}}}{T_9} \quad (3.9)$$

where S_{ns} is the slippage factor and I_j is the mode integral for mode j . Here the constant

$$A_{\text{bl}} = 3.68 \times 10^{-5} \left(\frac{\rho}{\rho_b} \right) \sqrt{\frac{R_{12.5}}{M_{1.4}}} \quad (3.10)$$

and the mode integral

$$I_{\text{bl}j} = \int d\cos\theta d\phi \frac{\xi_j \cdot \xi_j^*}{R^2}, \quad (3.11)$$

where ξ_j is the displacement vector for mode j (see Appendix B.3 for the list of integrals for the inertial modes in the lowest two zero-viscosity parametric instability thresholds) and the density on the boundary layer is taken to be constant $\rho_b = 1.5 \times 10^{14} \text{ g cm}^{-3}$. In this chapter we use inertial modes with $j = 592$ ($n = 15, m = -7$) and $j = 494$ ($n = 14, m = 5$).

3.2.3 Angular Momentum and Temperature Evolution

Angular momentum is lost via gravitational wave emission

$$\frac{dJ}{dt} = 2\gamma_{GR}J_{c \text{ rmode}} - \frac{I\Omega}{\tau_M}, \quad (3.12)$$

where $J_{c \text{ rmode}} = -(m_\alpha/\omega_\alpha)\epsilon_\alpha|c_\alpha|^2 = -3MR^2\Omega|c_\alpha|^2 = -3MR^2|C_\alpha|^2$, I is the moment of inertia of the star, $I\Omega/\tau_M$ is the magnetic braking torque, and τ_M is the corresponding timescale. We have adopted the simplest dipole magnetic dipole model with a timescale

$$\begin{aligned} \frac{1}{\tau_M} &= \frac{B^2R^6\Omega^2}{6c^3I} = \frac{1}{1.2 \times 10^7 \text{sec}^{-1}} \frac{R_{12.5}^4 B_{13}^2}{M_{1.4}} \left(\frac{\nu}{1 \text{kHz}} \right)^2 \\ &= \frac{B_{13}^2 \tilde{\Omega}^2}{6.7 \times 10^6 \text{sec}^{-1}}. \end{aligned} \quad (3.13)$$

Here $B_{13} = B/(10^{13} \text{ G})$. Eq. (3.12) can be rewritten in terms of the scaled variables in Eq. (3.3) as

$$\frac{dJ}{d\tilde{\tau}} = -\frac{6\tilde{\gamma}_{GR}}{\tilde{\Omega}} \frac{MR^2\Omega_c|\delta\tilde{\omega}|}{(4\tilde{k})^2\tilde{\omega}_\beta\tilde{\omega}_\gamma} |\bar{C}_\alpha|^2 - \frac{I}{|\delta\tilde{\omega}|\tau_M}. \quad (3.14)$$

Thermal energy conservation gives the temperature evolution equation

$$\begin{aligned} C(T)\frac{dT}{dt} &= \sum_j 2E_j\gamma_j - L_\nu(T) \\ &= 2MR^2\Omega(\gamma_{\alpha\nu}|C_\alpha|^2 + \gamma_\beta|C_\beta|^2 \\ &\quad + \gamma_\gamma|C_\gamma|^2) - L_\nu(T). \end{aligned} \quad (3.15)$$

Following Ref. [50], we take the neutrino luminosity to be

$$L_\nu = L_{\text{dU}}T_9^6 R_{\text{dU}}(T/T_p) + L_{\text{mU}}T_9^8 R_{\text{mU}}(T/T_p) + L_{\text{e-i}}T_9^6 + L_{\text{n-n}}T_9^8, \quad (3.16)$$

where the constants for the modified and direct URCA reactions are defined by $L_{\text{mU}} = 1.0 \times 10^{40} \text{ erg sec}^{-1}$, $L_{\text{dU}} = f_{\text{dU}} \times 10^{46} \text{ erg sec}^{-1}$ [59, 60], and the electron-ion, neutron-neutron neutrino bremsstrahlung and Cooper pairing of neutrons are given by $L_{\text{e-i}} = 9.1 \times 10^{35} \text{ erg sec}^{-1}$, $L_{\text{n-n}} \approx 10^{38} \text{ erg sec}^{-1}$. The fraction of the star f_{dU} that is above the density threshold for direct URCA reactions is in general dependent on the equation of state [62] and we take it to be 10% through most of this chapter (we set $f_{\text{dU}} = 0$ for one of the runaway cases in Sec. ??).

The proton superfluid reduction factors for the modified and direct URCA reactions are taken from Ref. [60] (see Eqs. (32) and (51) in Ref. [60]):

$$R_{\text{dU}}(T/T_p) = \left[0.2312 + \sqrt{(0.76880)^2 + (0.1438\nu)^2} \right]^{5.5} \times \exp\left(3.427 - \sqrt{(3.427)^2 + \nu^2}\right), \quad (3.17)$$

$$R_{\text{mU}}(T/T_p) = \left(0.2414 + \sqrt{(0.7586)^2 + (0.1318\nu)^2} \right)^7 \times \exp\left(5.339 - \sqrt{(5.339)^2 + (2\nu)^2}\right)$$

where the dimensionless gap amplitude ν for the singlet type superfluidity is given by

$$\nu = \sqrt{1 - \frac{T}{T_p}} \left(1.456 - 0.157 \sqrt{\frac{T_p}{T}} + 1.764 \frac{T_p}{T} \right). \quad (3.18)$$

Similar to Ref. [50], we use $T_p = 5.0 \times 10^9 \text{ K}$. In terms of the scaled variables Eq. (3.15) becomes

$$C(T) \frac{dT}{d\tilde{\tau}} = \frac{2MR^2\Omega_c^2|\delta\tilde{\omega}|}{(4\tilde{\kappa})^2\tilde{\omega}_\alpha\tilde{\omega}_\beta\tilde{\omega}_\gamma} (\tilde{\omega}_\alpha\tilde{\gamma}_{\alpha\nu}|\tilde{C}_\alpha|^2 + \tilde{\omega}_\beta\tilde{\gamma}_\beta|\tilde{C}_\beta|^2 + \tilde{\omega}_\gamma\tilde{\gamma}_\gamma|\tilde{C}_\gamma|^2) - \frac{L_\nu(T)}{\Omega_c\tilde{\Omega}|\delta\tilde{\omega}|}. \quad (3.19)$$

3.2.4 Quasi-Stationary Solutions

In terms of amplitudes and phase variables $C_j = |C_j|e^{i\phi_j}$ Eqs. (3.2) can be rewritten as

$$\begin{aligned}
\frac{d|\bar{C}_\alpha|}{d\tilde{\tau}} &= \frac{\tilde{\gamma}_\alpha}{\tilde{\Omega}|\delta\tilde{\omega}|}|\bar{C}_\alpha| - \frac{\sin\phi|\bar{C}_\beta||\bar{C}_\gamma|}{2\sqrt{\tilde{\Omega}}}, \\
\frac{d|\bar{C}_\beta|}{d\tilde{\tau}} &= -\frac{\tilde{\gamma}_\beta}{\tilde{\Omega}|\delta\tilde{\omega}|}|\bar{C}_\beta| + \frac{\sin\phi|\bar{C}_\alpha||\bar{C}_\gamma|}{2\sqrt{\tilde{\Omega}}}, \\
\frac{d|\bar{C}_\gamma|}{d\tilde{\tau}} &= -\frac{\tilde{\gamma}_\gamma}{\tilde{\Omega}|\delta\tilde{\omega}|}|\bar{C}_\gamma| + \frac{\sin\phi|\bar{C}_\alpha||\bar{C}_\beta|}{2\sqrt{\tilde{\Omega}}}, \\
\frac{d\phi}{d\tilde{\tau}} &= \frac{\delta\tilde{\omega}}{|\delta\tilde{\omega}|} - \frac{\cos\phi}{2\sqrt{\tilde{\Omega}}}\left(\frac{|\bar{C}_\beta||\bar{C}_\gamma|}{|\bar{C}_\alpha|} - \frac{|\bar{C}_\alpha||\bar{C}_\gamma|}{|\bar{C}_\beta|} - \frac{|\bar{C}_\beta||\bar{C}_\alpha|}{|\bar{C}_\gamma|}\right),
\end{aligned} \tag{3.20}$$

where we have defined the relative phase difference as $\phi = \phi_\alpha - \phi_\beta - \phi_\gamma$.

These equations have the stationary solution

$$\begin{aligned}
|\bar{C}_\alpha|^2 &= \frac{4\tilde{\gamma}_\beta\tilde{\gamma}_\gamma}{\tilde{\Omega}|\delta\tilde{\omega}|^2}\left(1 + \frac{1}{\tan^2\phi}\right), \\
|\bar{C}_\beta|^2 &= \frac{4\tilde{\gamma}_\alpha\tilde{\gamma}_\gamma}{\tilde{\Omega}|\delta\tilde{\omega}|^2}\left(1 + \frac{1}{\tan^2\phi}\right), \\
|\bar{C}_\gamma|^2 &= \frac{4\tilde{\gamma}_\alpha\tilde{\gamma}_\beta}{\tilde{\Omega}|\delta\tilde{\omega}|^2}\left(1 + \frac{1}{\tan^2\phi}\right), \\
\tan\phi &= \frac{\tilde{\gamma}_\beta + \tilde{\gamma}_\gamma - \tilde{\gamma}_\alpha}{\tilde{\Omega}|\delta\tilde{\omega}|}.
\end{aligned} \tag{3.21}$$

In the limit when $|\delta\tilde{\omega}|/\tilde{\gamma}_j \ll 1$

$$|\bar{C}_\alpha|^2 \approx \frac{4\tilde{\gamma}_\beta\tilde{\gamma}_\gamma}{\tilde{\Omega}|\delta\tilde{\omega}|^2}, \quad |\bar{C}_\beta|^2 \approx \frac{4\tilde{\gamma}_\alpha\tilde{\gamma}_\gamma}{\tilde{\Omega}|\delta\tilde{\omega}|^2}, \quad |\bar{C}_\gamma|^2 \approx \frac{4\tilde{\gamma}_\alpha\tilde{\gamma}_\beta}{\tilde{\Omega}|\delta\tilde{\omega}|^2}. \tag{3.22}$$

Assuming that the amplitudes evolve through a series of spin- and temperature-dependent steady states, i.e., $dC_i/d\tilde{\tau} \approx 0$, the spin and thermal evolution equations can be rewritten by taking $J \approx I\Omega$ and using Eqs. (3.21) in Eq.

(3.14).

$$\frac{d\tilde{\Omega}}{d\tilde{\tau}} = -\frac{6\tilde{\gamma}_{\text{GR}}}{\tilde{\Omega}^2|\delta\tilde{\omega}|} \frac{\tilde{\gamma}_\beta\tilde{\gamma}_\gamma}{4\tilde{k}^2\tilde{I}\tilde{\omega}_\beta\tilde{\omega}_\gamma} k_{\alpha\alpha} \left(1 + \frac{1}{\tan^2\phi}\right) - \frac{1}{\tau_M\Omega_c|\delta\tilde{\omega}|} \quad (3.23)$$

where $\tilde{I} = I/(MR^2)$. The thermal evolution of the system is given by

$$C(T)\frac{dT}{d\tilde{\tau}} = \frac{2MR^2\Omega_c^2}{(4\tilde{k})^2\tilde{\omega}_\alpha\tilde{\omega}_\beta\tilde{\omega}_\gamma} \frac{\tilde{\gamma}_\alpha\tilde{\gamma}_\beta\tilde{\gamma}_\gamma}{\tilde{\Omega}|\delta\tilde{\omega}|} \left(\frac{\tilde{\omega}_\alpha\tilde{\gamma}_{\alpha,v}}{\tilde{\gamma}_\alpha} + \tilde{\omega}_\beta + \tilde{\omega}_\gamma\right) \left(1 + \frac{1}{\tan^2\phi}\right) - \frac{L_\nu(T)}{\Omega_c\tilde{\Omega}|\delta\tilde{\omega}|}. \quad (3.24)$$

By setting the right hand side of the above equation to zero, one can find the Heating = Cooling ($H = C$) curve. Below, we find that Eqs. (3.23)-(3.24) describe the type I and III evolutions well throughout the stable regime. When the daughter modes are negligible the r-mode amplitude oscillates around a quasi-stationary state of its own

$$|\bar{C}_\alpha|^2 = |\bar{C}_{\text{H=C r-mode}}|^2 = \left(\frac{L_\nu}{\tilde{\gamma}_{\alpha v}}\right) \frac{(4\tilde{k})^2\tilde{\omega}_\beta\tilde{\omega}_\gamma}{2MR^2\Omega_c^3\tilde{\Omega}|\delta\tilde{\omega}|^2} \quad (3.25)$$

3.3 Brief Summary of Results

Fig. 3.1(a) and (b) show possible evolution scenarios for the spin and temperature of a newborn neutron star due to the r-mode instability. They display typical evolutionary trajectories in the angular velocity - temperature $\tilde{\Omega} - T_9$ plane, where $T = T_9 \times 10^9$ K is the core temperature, and $\tilde{\Omega} = \Omega/\Omega_c = \Omega/\sqrt{\pi G\bar{\rho}}$ with $\bar{\rho}$ the mean density of the neutron star.

The evolution can be divided into several phases:

Phase 0. The star cools at nearly constant angular velocity $\tilde{\Omega} = \tilde{\Omega}_i$. The r-mode amplitude grows exponentially. Several trajectories are possible depending on whether the amplitude first reaches its parametric instability threshold or inter-

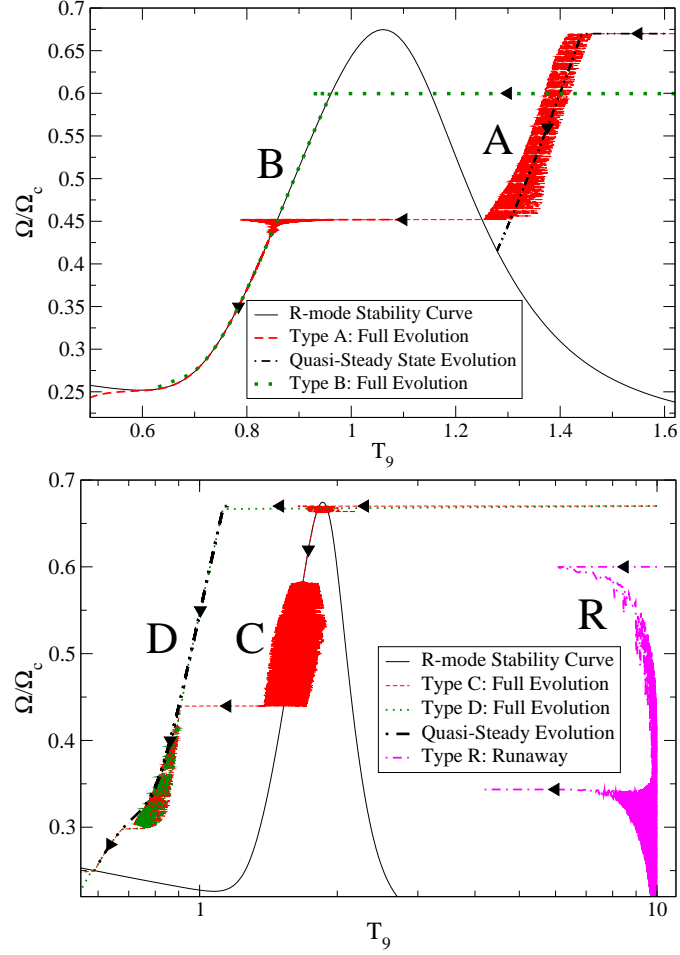


Figure 3.1: Typical trajectories for five observed evolution scenarios are shown in the $\tilde{\Omega} - T_9$ plane, where $\tilde{\Omega} = \Omega/\Omega_c$. Stable Evolutions. **Type I**: the star cools until the cooling is balanced by the viscous heating from the three modes and spins down in the first unstable region ($T_9 > T_{9\text{peak}}$) - evolution A. The average trajectory can be determined by using quasi-steady state mode amplitudes until the star intersects the r-mode stability curve. It then cools until it enters the second unstable region: $T_9 < T_{9\text{peak}}$ and spins-down along r-mode stability curve. **Type II**: the star spins down on the r-mode stability curve or oscillates around it - evolutions B and C. In evolution C the thermal oscillations become unstable and the star cools to the next thermal equilibrium region. **Type III**: the star cools until it reaches thermal equilibrium to the left of the r-mode stability curve ($T_9 < T_{9\text{peak}}$) and subsequently spins down on the quasi-steady $H = C$ curve in the second unstable region- evolution D. **Type R**: Runaway evolution. The three-mode system is not sufficient to model this evolution and more modes need to be included.

sects the r-mode stability curve.

- *Type I. Evolution A. Phase 1a.* Amplitudes settle in quasi-steady states. The r-mode grows above its parametric instability threshold exciting the daughters before the star reaches the r-mode stability curve. The triplet coupling leads to oscillations of the three-mode amplitudes around quasi-steady solutions. The star continues cooling at fixed angular velocity until the viscous heating due to the three modes temporarily stops the cooling. *Phase 2a.* The star spins-down. Some thermal oscillations at nearly constant $\tilde{\Omega}$ occur. Their amplitude depends on model parameters such as the strength of the coupling coefficients. The average trajectory in the $\tilde{\Omega} - T_9$ plane is, however, well approximated by the Heating = Cooling ($H = C$) curve computed using quasi-stationary solutions for the r-mode and daughter mode amplitudes. These quasi-stationary states can be determined algebraically and are slowly varying functions of $\tilde{\Omega}$ and T_9 . Eventually, the star reaches the r-mode stability curve. *Phase 3a* It then cools into the stable region at approximately constant angular velocity until it
 - (i) crosses to the second unstable region if the stable region is narrow enough to avoid significant dipole spin-down. It can then spin and cool down along the r-mode stability curve.
 - (ii) cools and spins down remaining in the stable region for the rest of the evolution. The r-mode and daughter mode amplitudes quickly damp to zero and the star spins down due to magnetic dipole radiation.
- (i) *Type II. Evolutions B and C. Phase 1b.* The star crosses in the stable region before the daughter are excited. The r-mode damps exponentially until

the star enters the second unstable region. The star reaches thermal equilibrium close to the r-mode stability curve.

Phase 2b. The star either continues to evolve down the stability curve (evolution B) with no thermal oscillations or oscillates around it (evolution C). The average evolution is well described by the thermal equilibrium r-mode amplitude. The daughter mode amplitudes either do not get excited at all or reach only small values relative to the r-mode amplitude.

Phase 3b. The star cools, the daughter modes get excited as temperature and hence the value of the parametric instability threshold decrease. The triplet of modes oscillate around their quasi-stationary states. The evolution then overlaps evolution D and the star spins down on an $H = C$ curve determined by all three modes.

(ii) *Type III. Evolution D. Phase 1c.* Mode amplitudes settle into quasi-steady states. The r-mode amplitude is lower than its thermal equilibrium value near the r-mode stability curve. The trajectory passes the r-mode stability curve, enters the second unstable region and the r-mode amplitude grows exponentially until it reaches parametric instability. The mode triplet settles into quasi-stationary state amplitudes.

Phase 2c Spins down on $H = C$ curve. The star continues cooling with the mode triplet close to its quasi-steady state until it reaches thermal equilibrium. It then spins down losing usually more than half of its angular velocity and cools slightly. As the star spins down the r-mode amplitude increases and can disturb the balance between heating and cooling. The star then develops thermal oscillations as it spins down. The average evolution is still well described by the Heating = Cooling ($H = C$) curve computed using the quasi-steady solutions.

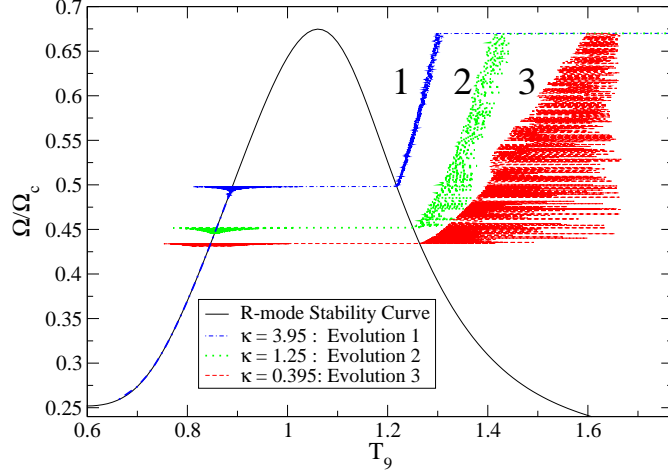


Figure 3.2: The trajectories in the $\tilde{\Omega} - T_9$ plane for evolutions with different coupling coefficients are shown for three values of κ : 3.95, 1.25 and 0.395. All other parameters are the same. The hyperon superfluidity temperature is $T_h = 6.0 \times 10^9$ K. The cooling is stopped by the heating later for larger κ and the thermal oscillations are smaller.

Phase 3c. The r-mode intersects the r-mode stability curve again and reenters the stable region. The three modes damp to zero and the star continues spinning down due to the dipole term.

- *Runaway. Evolution R.* The growth rate of the r-mode is faster than the neutrino cooling rate and the r-mode amplitude overshoots its parametric instability threshold. All three modes get excited and grow exponentially reaching amplitudes close to 1. Since the mode amplitudes are large this evolution is very short (\sim one or two hours). Our evolutions do not accurately model runaway scenarios as in this case more modes will be excited as the r-mode amplitude passes other parametric instability thresholds.

3.4 Shortcomings of the Model and Possible Improvements

We find that modeling nonlinear interactions with a single triplet of modes is sufficient to stop the instability. Our treatment is inadequate to follow what happens when the system runs away. In this case, one would include more modes.

Another simplification is that we do not include higher order corrections in angular velocity for the mode frequencies or coupling coefficients. These can be important at high spin rates and since as the star spins down the exact values for the detuning, frequencies and coupling coefficient can change. This can lead to different triplets of modes determining the lowest parametric instability threshold at different frequencies and the evolution can switch between these triplets of modes. Modeling such behavior is beyond the scope of this work. Here, we choose numbers that we think are representative for the detuning, coupling coefficient, mode frequencies and viscous damping rates and study the possible nonlinear behaviors. This study is a first step in understanding the qualitative behavior of the three mode system and we believe that the mode triplet we used is typical for this system.

The triplet we choose is the lowest parametric instability threshold at zero eccentricity in the limit of strong damping $\delta\omega/(\gamma_\beta + \gamma_\gamma) \ll 1$. The daughter modes that the r-mode couples to are $n = 15, m = 7$ and $n = 14, m = 5$. This triplet has a detuning $\delta\tilde{\omega} = 10^{-4}$ and coupling $\kappa = 1.25$. A preliminary calculation that included second order corrections in frequency and computed detunings for modes with $n < 20$ found that resonances occur for similar high n modes [76]. This is reasonable as there are more modes that satisfy the selection rules [54] at

high n and hence it is more likely for resonances to occur there. Furthermore, as long as the combination of detuning and damping rates is low enough to satisfy $\delta\omega/(\gamma_\beta + \gamma_\gamma) \ll 1$, the evolutions are independent of the exact value of the detunings. We varied the detuning by a factor of 100, between 10^{-6} and 10^{-4} , and did not observe significant changes in the evolution.

To test the dependence of the evolution on the coupling coefficient we vary it by factors of $\sqrt{10}$ between $\kappa = 0.395$ and $\kappa = 3.95$. Fig. 3.2 shows that the evolutions change but are qualitatively similar. Increasing κ decreases the amplitude of the thermal oscillations and increases the angular velocity $\tilde{\Omega}$ at which the star crosses in the stable region. The coupling coefficients found by Brink *et al.* for an incompressible stellar model for near-resonant daughter modes ($\delta\omega/(2\Omega) < 10^{-3}$) that couple to the $n = 3, m = 2$ r-mode vary roughly between 0.001 and 3 [73]. The coupling we choose, $\kappa = 1.25$, which corresponds to a mode triplet that has a low enough detuning to maintain the strong damping limit. To test the sensitivity of damping rates on mode functions we look at the lowest and second lowest ($n = 13, m = 3$ and $n = 14, m = 1$ daughter modes) zero-viscosity parametric instability thresholds. The product of the damping rates for the two daughter modes $\gamma_\beta\gamma_\gamma$ changes by factors of order 1 and the individual rates change by factors of order 2.

Another important factor that will affect the parameters is the choice of stellar model. Our model is simplified; a more realistic treatment could include compressibility, more realistic magnetic fields, differential rotation, mixtures of superfluid or superfluid and normal fluid regions. All these will affect the precise numbers for the mode frequencies, coupling coefficients, viscosity and hence the quantitative details of the evolution. However, more sophisticated

treatments should still find a dense set of modes confined to a relatively narrow frequency range. This set will exhibit three-mode resonances and hence strong nonlinear effects at small amplitudes. The principles we outline here should be quite general. The unstable region in which the star will spin down should still depend on where the neutrino cooling can be balanced by heating. Concepts such as parametric instability, competition between cooling and heating, and quasi-steady evolution ought to apply for any system of modes where nonlinear effects are important.

3.5 Stable Evolutions

In this section we examine examples of different types of stable evolutions in more detail. We assume $S_{\text{ns}} = 0.10$, $f_{\text{dU}} = 0.10$ and $T_{\text{p}} = 5.0 \times 10^9$ K.

3.5.1 Type I

In this subsection we detail two typical type I trajectories with hyperon superfluidity temperatures of $T_{\text{h}} = 6.0 \times 10^9$ K and $T_{\text{h}} = 2.0 \times 10^9$ K and the same initial conditions: $\tilde{\Omega}_i = 0.67$ and $T_{9i} = 10$. For this initial angular velocity and temperature the evolutions are independent of the initial r-mode and daughter mode amplitudes. However, this changes for the $T_{\text{h}} = 6.0 \times 10^9$ K case as $\tilde{\Omega}_i$ is lowered. For an initial $\tilde{\Omega}_i = 0.60$ an initial r-mode amplitude of $\bar{C}_\alpha(0) \geq 3.0 \times 10^{-4}$ lead to evolutions of type I, and initial r-mode amplitudes $\bar{C}_\alpha(0) < 3.0 \times 10^{-4}$ lead to the star spinning down along the r-mode stability curve (type II evolution). Roughly speaking, a type I evolution occurs when the amplitude of

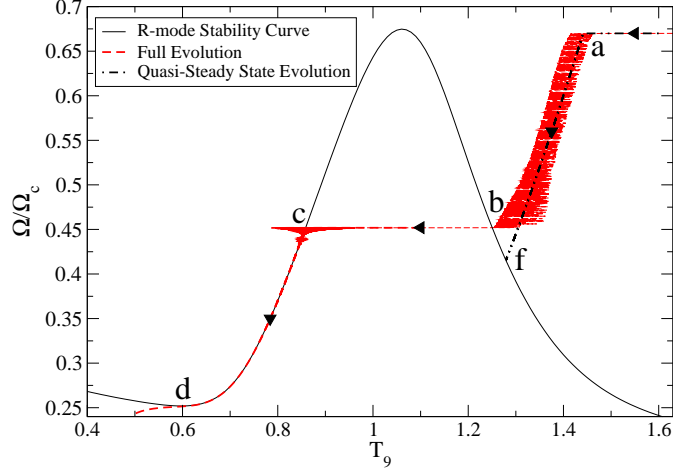


Figure 3.3: A typical type I trajectory in the $\tilde{\Omega} - T_9$ plane is shown for $T_{\text{ch}} = 6.0 \times 10^9$ K. The evolution starts at $\tilde{\Omega}_i = 0.67$, $T_{9i} = 10$. The star cools down to $T_{9a} = 1.43$ in about 10 minutes. At this point the dissipation heating of the 3-modes balances the cooling and the star spins down, oscillating around its quasi-steady solution for $t_{a \rightarrow b} \approx 0.1$ yr until it intersects the r-mode stability curve at $T_{9b} = 1.25$, $\tilde{\Omega}_b = 0.45$. It then cools down at constant $\tilde{\Omega} = \tilde{\Omega}_b$ until the cooling is again balanced by the viscous heating due to the r-mode. The daughter modes do not get excited in this part of the evolution. The star then spins and cools down in thermal equilibrium on the r-mode stability curve for $t_{c \rightarrow d} \approx 2.8$ yr until it enters the stable region again at $T_d \approx 0.60$, $\tilde{\Omega}_d \approx 0.25$.

the r-mode grows beyond its parametric instability threshold early and excites the daughters. This makes the viscous dissipation due to the three modes large enough to stop cooling on the right side of the peak of the r-mode stability curve ($T_9 > T_{9\text{peak}}$). Larger amplitudes favor type I evolutions. The sharp transition in $\bar{C}_\alpha(0)$ enforces that there is a cutoff between the different types of evolution. Evolutions of a given type are alike and changes in initial conditions do not affect the shape of the trajectory. They only affect the precursor/settling oscillations.

The first trajectory we focus on is displayed in Fig. 3.3 (This is the same as the type A evolution in Fig. 3.1(a).) The star cools down from $T_{9i} = 10$ to $T_9 \approx 2$ in the first minute or so. The r-mode and daughter mode amplitudes settle in

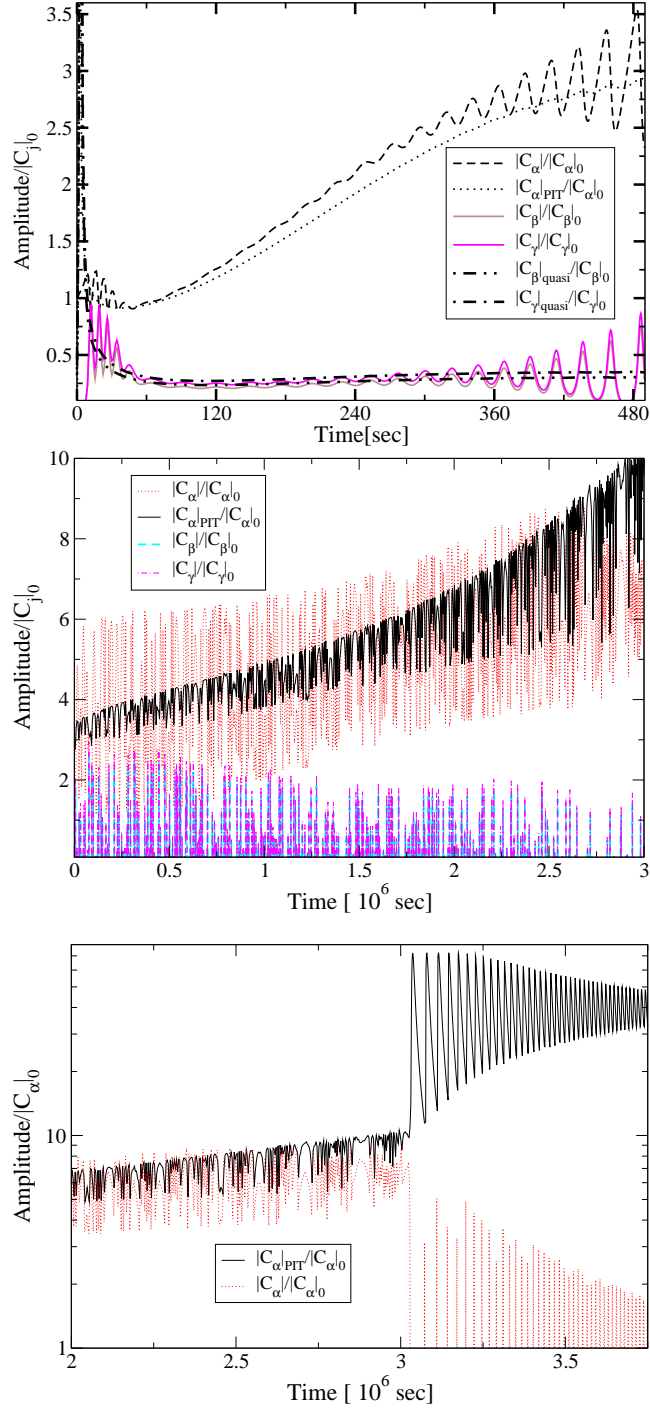


Figure 3.4: Mode amplitudes displayed as a function of time for $T_h = 6.0 \times 10^9$ K. (a) Initial evolution. The three modes settle down to their quasi-steady states in the first minute or so and then oscillate around these solutions. (b) Evolution before the r-mode stability curve is reached. (c) The r-mode and its parametric instability threshold amplitude shown as the star crosses from the right to the left side of the r-mode stability curve.

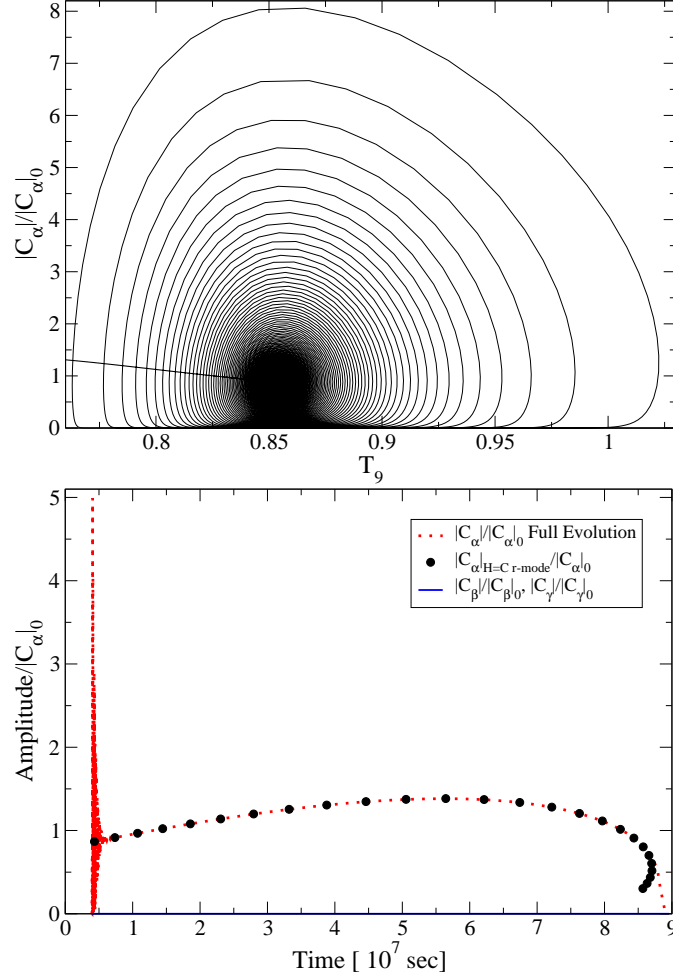


Figure 3.5: The r-mode amplitude for the second part of the evolution ($T_9 < T_{9\text{peak}}$) is shown as a function of T_9 in (a) and as a function of time in (b). Part (a) details the initial oscillation of $|C_\alpha|$ around the thermal equilibrium value $|\bar{C}_\alpha|_{\text{H=C r-mode}}$. The r-mode eventually settle to its equilibrium value and continues spinning down along the r-mode stability curve. Part (b) shows the agreement between the r-mode amplitude from the full evolution code and the thermal equilibrium r-mode amplitude computed on the r-mode stability curve $|\bar{C}_\alpha|_{\text{H=C r-mode}}(\tilde{\Omega}_{\text{CFS}}, T_{9\text{CFS}})$ with $\tilde{\Omega}$ between $\Omega_c = \Omega_b \approx 0.45$ and $\Omega_d \approx 0.25$.

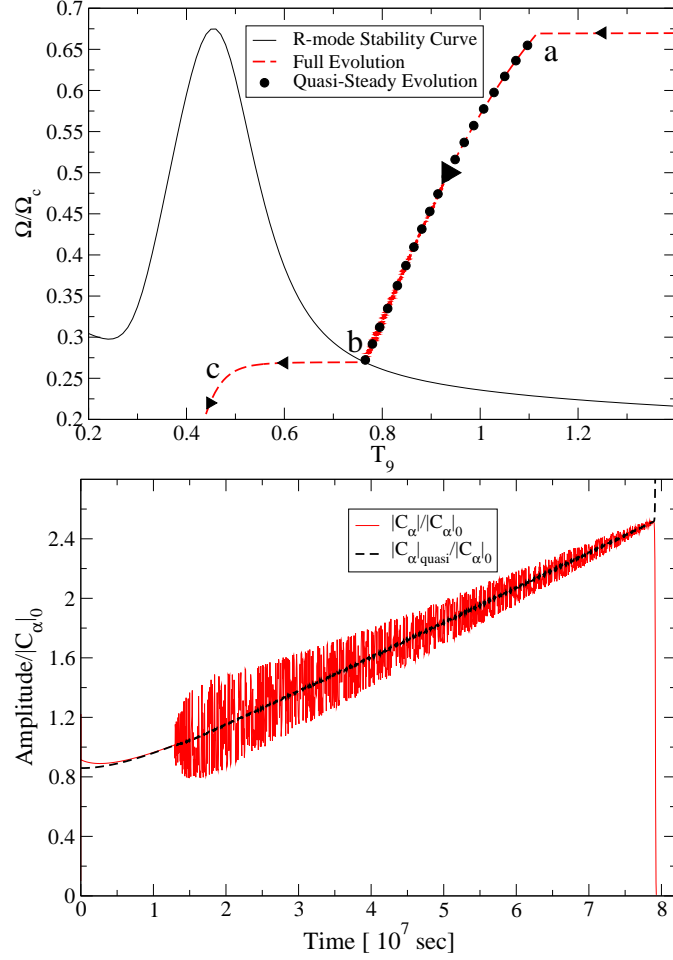


Figure 3.6: Another type I evolution is shown for a lower hyperon superfluidity temperature $T_h = 2.0 \times 10^9$ K. (a) The trajectory of the star is shown in the $\tilde{\Omega} - T_9$ plane. The star cools from $T_{9i} = 10$, $\tilde{\Omega}_i = 0.67$ to $T_{9a} \approx 1.12$ in about 10 min. At this point the viscous heating is large enough to stop the neutrino cooling. The star then spins down and cools to $\tilde{\Omega}_b \approx 0.27$, $T_{9b} \approx 0.76$ in $t_{a \rightarrow b} \approx 2.5$ yr. At point b the star intersects the r-mode stability curve and the r-mode becomes stable. The star starts cooling at constant angular velocity. At this lower spin frequency the dipole spin-down becomes important and the star spins down at $T_{9c} \approx 0.5$ never reaching the unstable region of the $\tilde{\Omega} - T_9$ plane again. (b) The r-mode and its parametric instability threshold amplitude are shown as a function of time. As before it can be seen that $|C_{\alpha}|_{\text{quasi}} = |C_{\alpha}|_{\text{PIT}}$ is a good approximation for the average r-mode amplitude until the star crosses in the stable region. The oscillations around this quasi-stationary solutions are about 6 times smaller than in the $T_h = 6.0 \times 10^9$ K evolution.

their quasi-stationary states at $T_9 \approx 2$ and subsequently oscillate around these solutions (Fig. 3.4(a)). The heating first balances the cooling at $T_{9a} \approx 1.43$. The star then starts spinning down oscillating around thermal equilibrium ($H = C$ curve in the figure). Within a time of $t_{a \rightarrow b} \approx 0.1$ yr the star spins down by more than 50% of its initial value to $\tilde{\Omega}_b \approx 0.45$, while the temperature changes slowly with a total change in the average T_9 of only $(\Delta T_{9a \rightarrow b})_{av} \approx 0.14$. The horizontal temperature oscillations have an amplitude of ≈ 0.05 . At point b, $(T_{9b}, \tilde{\Omega}_b) = (1.25, 0.45)$, the star intersects the r-mode stability curve. It then cools down at constant spin frequency and in about $t_{b \rightarrow c} = 14$ hours reaches the left side of the r-mode stability curve where $T_{9c} \approx 0.77$ and $\tilde{\Omega}_c = \tilde{\Omega}_b \approx 0.45$.

The second part of this evolution is really of type II and these evolutions will be described in further detail in the next subsection. The upshot is that the star reaches thermal equilibrium on the r-mode stability curve and spins down along it. The r-mode does not grow above its parametric instability threshold. No daughter modes are excited and the r-mode amplitude is well approximated by its thermal equilibrium value $|C_\alpha|_{r\text{-mode } H=C}$ evaluated on the r-mode stability curve (see Fig. 3.5(b)). Since the amplitude is smaller, the spin-down is slower and this part of the evolution is longer lasting, almost 3 yr.

Fig. 3.6(a) plots the trajectory in the $\tilde{\Omega} - T_9$ plane of a star with hyperon superfluidity temperature $T_h = 2.0 \times 10^9$ K. Lower T_h makes the hyperon bulk viscosity become important at lower temperatures (i.e., shifts the curve to the left). As before, the star cools at constant $\tilde{\Omega}$ until the heating dissipated by the three-modes becomes large enough to balance the cooling. As expected, in this scenario the star reaches thermal equilibrium at slightly lower temperature of $T_9 \approx 1.12$ because the viscosity is lower. The star then starts spinning down

in thermal equilibrium. Fig. 3.6(b) shows that the quasi-stationary solution remains a good approximation for the average r-mode amplitude until the evolution reaches the r-mode stability curve and the r-mode becomes stable. The r-mode amplitude stays much closer to its quasi-stationary solution with an oscillation amplitude about 6 times lower than in the $T_h = 6.0 \times 10^9$ K scenario. The spin-down time $t_{a \rightarrow b} \approx 2.5$ years and $\tilde{\Omega}$ changes by more than a factor of 2: $\tilde{\Omega}_b = 0.27$, $\Delta\tilde{\Omega} = 0.40$, $T_{9a} = 1.12$, $T_{9b} = 0.76$ and $\Delta T_{9a \rightarrow b} \approx 0.35$. Point b is at the intersection between the quasi-steady $H = C$ curve and the r-mode stability curve and can be determined analytically. Beyond this point the r-mode amplitude damps to zero and the star continues to spin down via magnetic dipole radiation.

3.5.2 Type II

We now consider evolutions in which the star reaches thermal equilibrium close to the r-mode stability curve and spins down along it. These are exemplified by evolutions B ($T_h = 6.0 \times 10^9$ K, $\Omega_i = 0.60$ and any $|\bar{C}_\alpha|(0) < 4.0 \times 10^{-5}$; for $|\bar{C}_\alpha|(0) \geq 4.0 \times 10^{-5}$ a type I evolution is obtained) and C ($T_h = 1.2 \times 10^{10}$ K, $\Omega_i = 0.67$ and any $|\bar{C}_\alpha|(0) > 5.0 \times 10^{-5}$; $|\bar{C}_\alpha|(0) \leq 5.0 \times 10^{-5}$ leads to a type III evolution) in Fig. 3.1. The initial temperature is $T_{9i} = 10$ in both cases. The second part of evolution A also falls in this category.

In the first scenario (evolution B in Fig. 3.1(a)) the r-mode never reaches its parametric instability threshold and the evolution can be adequately described by a one-mode model. The neutron star cools until the amplitude of the r-mode is large enough to generate enough viscous heating to stop the cooling. It starts

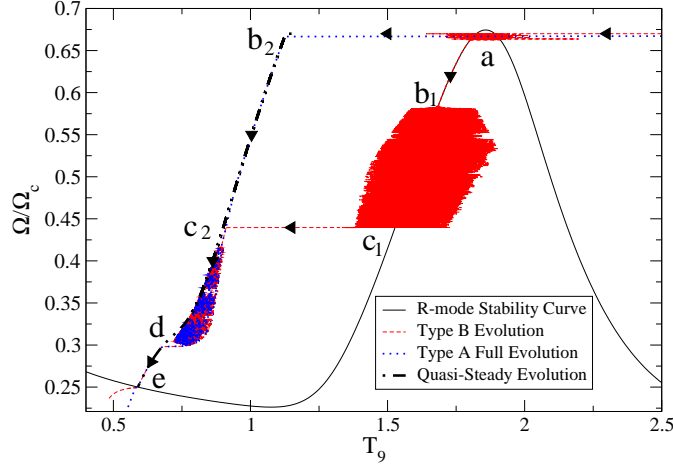


Figure 3.7: The trajectory of the neutron star in the $\tilde{\Omega} - T_9$ plane is shown for evolutions C and D of Fig. 3.1. The star cools to $T_{9a} = 1.82$ in about 6 minutes and crosses the r-mode stability curve for the second time. In evolution C the r-mode reaches large enough amplitudes for the viscous dissipation to balance the cooling. It then settles in thermal equilibrium ($H = C$) and spins down along the r-mode stability curve. It spins down to $\Omega_{b_1} = 0.58$, $T_{b_1} \approx 1.68$ in $t_{a_1 \rightarrow b_1} \approx 48$ hours. At this point the temperature of the star starts oscillating and the r-mode amplitude oscillates around the stability curve for $t_{b_1 \rightarrow c_1} = 6.7 \times 10^5$ sec until $T_{9c_1} = 1.53$, $\tilde{\Omega}_{c_1} = 0.44$. At this point it cools at constant $\tilde{\Omega}$ for $t_{c_1 \rightarrow c_2} = 1.2 \times 10^4$ sec to another thermal equilibrium region. The rest of the evolution coincides for C and D. In the case of evolution D the star cools at constant $\tilde{\Omega} = \tilde{\Omega}_i = 0.67$ to $T_{9b_2} \approx 1.13$ in about 2 hours and spins down in $t_{b_2 \rightarrow e} \approx 3$ yr on a $H = C$ curve determined by the quasi-steady states of all three modes.

spinning down oscillating around the r-mode stability curve and settles there. As the spin frequency gets lower the dipole spin-down becomes more important and the star eventually spins down into the stable region. The amplitude evolution will be similar qualitatively to Fig. 3.5. The full evolution lasts ≈ 3.2 yr and as in the second part of evolution A, after an initial precursor, the r-mode amplitude is fairly precisely determined by $|\bar{C}_\alpha|_{H=C_{r\text{-mode}}}$ evaluated on the r-mode stability curve.

In the second scenario (evolution B in Fig. 3.1) the r-mode amplitude passes its first parametric instability threshold and excites the two daughters. The hy-

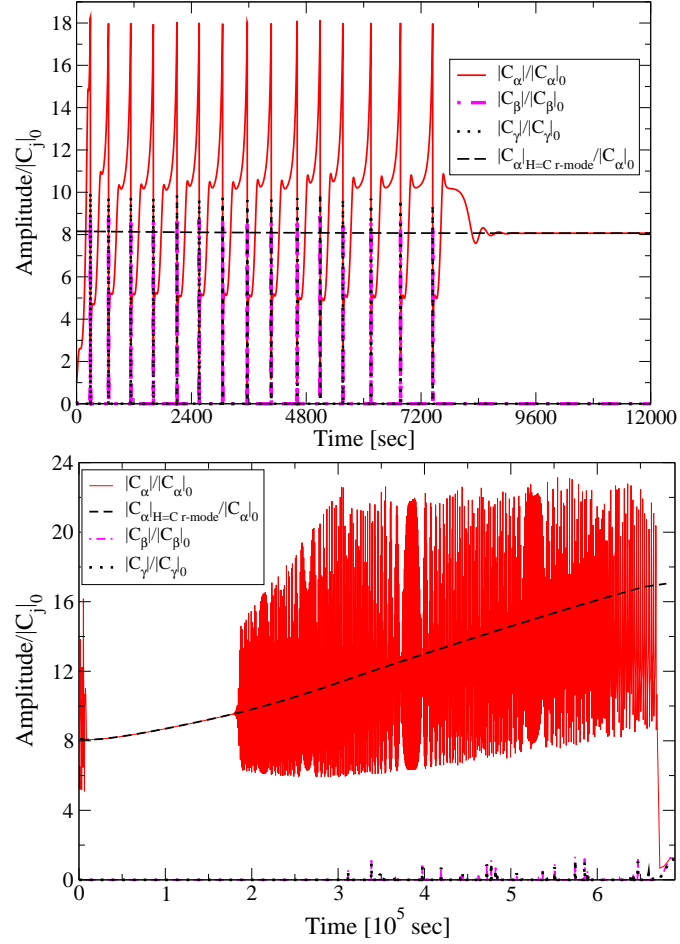


Figure 3.8: (a) The r-mode $|\bar{C}_\alpha|$ and daughter mode $|\bar{C}_\beta|$, $|\bar{C}_\gamma|$ amplitudes are displayed at the beginning of a type II evolution (evolution C in Fig 1). The r-mode is seen to settle to its equilibrium value $|\bar{C}_\alpha|_{H=C_r\text{-mode}}$ and the daughter mode oscillations damp to zero. (b) The r-mode and its thermal equilibrium solution $|\bar{C}_\alpha|_{H=C_r\text{-mode}}$ are shown for the first part of the evolution (the trajectory oscillates in the $\tilde{\Omega} - T_9$ plane around the r-mode stability curve). This equilibrium solution is seen to be a good approximation for the average r-mode amplitude.

peron bulk viscosity temperature is larger and thus to the r-mode stability curve is shifted to the right compared to the $T_h = 6.0 \times 10^9$ K case. However, the trajectory is close enough the r-mode stability curve that it is favorable for the star to return to that region of thermal equilibrium. Fig. 3.9(a) plots the initial evolution of the three mode amplitudes. It shows that the amplitude settle towards its equilibrium value $|\bar{C}_\alpha|_{H=C_r\text{-mode}}$ and subsequently oscillates around it.

3.5.3 Type III

Type III evolutions occur when the r-mode amplitude grows above its parametric instability threshold after the star cools across the stable region. This occurs at lower temperatures $T_9 < T_{9\text{peak}}$ and usually for low initial r-mode amplitudes. The r-mode amplitude needs to be low enough so that it does not provide enough dissipation to stop the cooling on its own. Once the daughters are excited they oscillate and settle to their quasi-stationary solutions. The star spins down on an $H = C$ curve determined by all three modes until it reenters the stable region. This scenario is exemplified by evolution D in Fig. 3.1(b). The star has $T_h = 1.2 \times 10^{10}$ K, $\Omega_i = 0.67$, $T_{9i} = 10$ and $|\bar{C}_\alpha|(0) = 5.0 \times 10^{-5}$. Any $|\bar{C}_\alpha|(0) \leq 5.0 \times 10^{-5}$ leads to roughly the same type III evolution. This threshold amplitude depends heavily on the initial spin frequency. Lower initial $\tilde{\Omega}$ make type III evolutions more likely.

Fig. 3.9 plots the amplitude evolution as a function of time. In Fig. 3.9(a) the initial r-mode amplitude and daughter mode amplitudes are shown settling to their quasi-stationary states in the first 40 min of the evolution. The star continues cooling and reaches thermal equilibrium at $t_{b_2} \approx 7 \times 10^5$ sec. It briefly oscillates and then settles on the quasi-steady $H = C$ curve. Fig. 3.9(b) displays the r-mode amplitude $|\bar{C}_\alpha|$ and its quasi-stationary solution, which coincides with the parametric instability threshold amplitude. The agreement between the full evolution $|\bar{C}_\alpha|$ and its quasi-steady counterpart is very good for the first 0.5 yr or so. As the star spins down it can develop some thermal oscillations: the cooling gets lower as T_9 decreases and the star heats until the cooling balances the heating again and the process repeats. The oscillations are initially unstable and growing in size. Eventually, as the star spins down and cools further, they

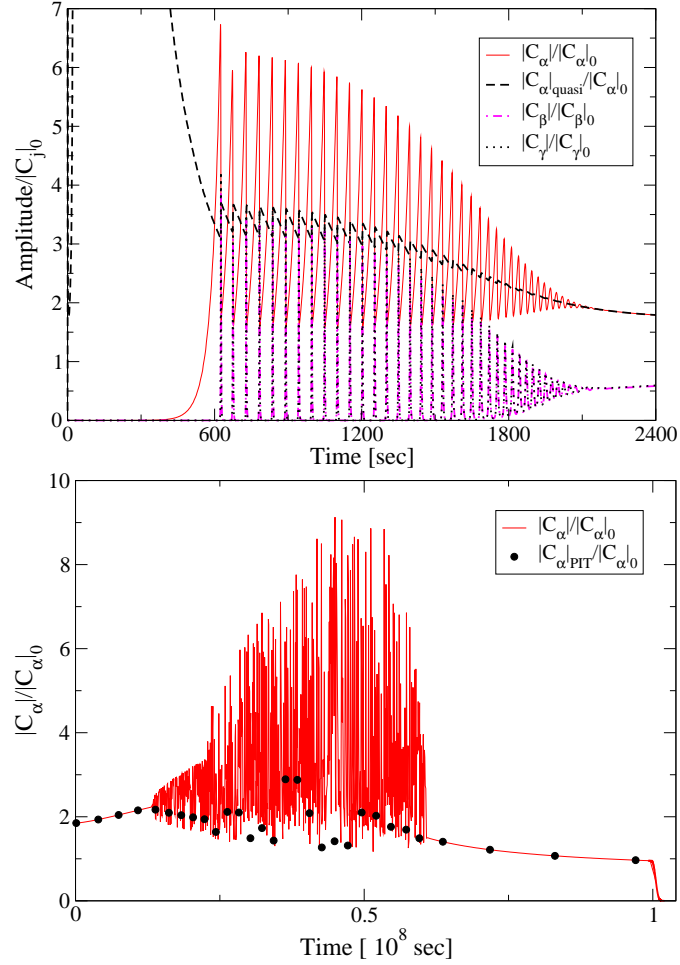


Figure 3.9: (a) The amplitudes of the r-mode $|\bar{C}_\alpha|$ and of the two daughter modes $|\bar{C}_\beta|, |\bar{C}_\gamma|$ are shown settling to their quasi-steady states in the first 40 minutes of a type III evolution (evolution D in Fig. 3.1). (b) The r-mode amplitude and its lowest parametric instability threshold (the parametric instability threshold coincides with the r-mode quasi-steady solution) is shown as a function of time for the whole evolution. The quasi-steady solution is a good approximation that maps the evolution with an almost exact agreement in the non-oscillatory part of the trajectory.

become stable. As these oscillations grow, the r-mode amplitude grows above its quasi-steady solution. It then returns to this solution and stays close to it for the rest of the evolution.

3.6 Runaway Evolutions

In Fig. 3.10 we show two evolutions: one with lower viscosity that is unstable and the other with slightly higher viscosity that is stable. The hyperon bulk viscosity is varied by changing the coefficient A_{hb} from $A_{\text{hb}} = 2.8 \times 10^3$ for the unstable evolution to $A_{\text{hb}} = 2.9 \times 10^3$ for the stable evolution. Lowering the viscosity raises the growth rate of the r-mode and makes the evolution unstable. Also, since the hyperon bulk viscosity is inversely proportional to the temperature for $T > T_{\text{peak}}$ (the hyperon bulk viscosity changes exponentially $\sim \exp(T_{\text{ch}}/T)$ for $T_{\text{h}}/T \gg 1$ and $\omega\tau \ll 1$), lowering the cooling rate makes the star spend more time at high temperatures with low viscosity and hence the evolutions are more likely to run away. Evolution R in Fig. 3.1(b) is obtained by changing f_{dU} from 0.10 to 0.0 and drastically reducing the cooling rate. Fig. 3.11 shows this unstable evolution that occurs for any $|\bar{C}_\alpha| > 7.0 \times 10^{-5}$ and a stable evolution with $|\bar{C}_\alpha| = 6.0 \times 10^{-5}$ (evolutions are stable for $|\bar{C}_\alpha| \leq 6.0 \times 10^{-5}$). Both figures show similar behavior. The unstable evolutions have $\Gamma_\alpha > \Gamma_\beta + \Gamma_\gamma$, while for the stable evolutions $\Gamma_\alpha < \Gamma_\beta + \Gamma_\gamma$. Here $\Gamma_\alpha = \gamma_\alpha / (|\delta\tilde{\omega}|\tilde{\Omega})$, $\Gamma_\beta = \gamma_\beta / (|\delta\tilde{\omega}|\tilde{\Omega})$ and $\Gamma_\gamma = \gamma_\gamma / (|\delta\tilde{\omega}|\tilde{\Omega})$.

Mathematically, one can easily see that $\Gamma_\alpha > \Gamma_\beta + \Gamma_\gamma$ corresponds to an unstable evolution by looking at the second derivative of the r-mode amplitude evolution equation:

$$\begin{aligned} \frac{d^2\bar{C}_\alpha}{d\tilde{\tau}^2} &= \frac{d\bar{C}_\alpha}{d\tilde{\tau}}(\Gamma_\alpha - \Gamma_\beta - \Gamma_\gamma) \\ &+ \bar{C}_\alpha \left[\Gamma_\alpha(\Gamma_\beta + \Gamma_\gamma) - \frac{|\bar{C}_\beta|^2 + |\bar{C}_\gamma|^2}{4\tilde{\Omega}} \right]. \end{aligned} \quad (3.26)$$

If $\Gamma_\alpha > \Gamma_\beta + \Gamma_\gamma$ then the r-mode is unstable no matter how larger the daughter modes become.

Assuming a solution of the r-mode amplitude of the form $\bar{C}_\alpha \propto \exp(st)$ and

taking the daughter modes to be constant gives the roots

$$\begin{aligned}
s_{\pm} &= \frac{1}{2}(\Gamma_{\alpha} - \Gamma_{\beta} - \Gamma_{\gamma}) \\
&\pm \frac{1}{2} \cdot \sqrt{(\Gamma_{\alpha} - \Gamma_{\beta} - \Gamma_{\gamma})^2 + 4[\Gamma_{\alpha}(\Gamma_{\beta} + \Gamma_{\gamma}) - \frac{|\bar{C}_{\beta}|^2 + |\bar{C}_{\gamma}|^2}{4\tilde{\Omega}}]} \\
&= \frac{1}{2} \left\{ (\Gamma_{\alpha} - \Gamma_{\beta} - \Gamma_{\gamma}) \pm \sqrt{(\Gamma_{\alpha} + \Gamma_{\beta} + \Gamma_{\gamma})^2 - \frac{|\bar{C}_{\beta}|^2 + |\bar{C}_{\gamma}|^2}{\tilde{\Omega}}} \right\}
\end{aligned} \tag{3.27}$$

If $\Gamma_{\alpha} < \Gamma_{\beta} + \Gamma_{\gamma}$ then the s_{-} mode is always stable and the s_{+} mode is stable only if

$$|\bar{C}_{\beta}|^2 + |\bar{C}_{\gamma}|^2 < 4\Gamma_{\alpha}(\Gamma_{\beta} + \Gamma_{\gamma})\tilde{\Omega}. \tag{3.28}$$

3.7 Detection of Gravitational Waves

We write the gravitational wave amplitude h_0 following Watts *et al.* [13] as

$$h_0^2 = \frac{5G}{2\pi^2 c^3 d^2 \nu_{GW}^2} \dot{E}_{GW}, \tag{3.29}$$

where d is the distance to the source and the GW frequency $\nu_{GW} = 4\nu//3 = (4/3) \times \Omega/(2\pi)$. Here ν and Ω are the spin frequency and angular velocity of the star.

For type II evolutions the daughter modes are not significant and the spin-down occurs in thermal equilibrium $\dot{E}_{GW} = L_{\nu}(T)$, where $T = T_{\text{CFS}}(\Omega)$ is determined by the CFS stability curve from equating $\gamma_{GR} = \gamma_{\alpha\nu}$. The gravitational wave amplitude becomes

$$h_0^2 = \frac{5GL_{\nu}(T)}{2\pi^2 c^3 d^2 \nu_{GW}^2}, \tag{3.30}$$

Assuming direct URCA dominates the cooling

$$h_0^2 \approx \frac{5GL_{dU}T_9^6 f_{dU} R_{dU}(T/T_c)}{2\pi^2 c^3 d^2 \nu_{GW}^2}, \tag{3.31}$$

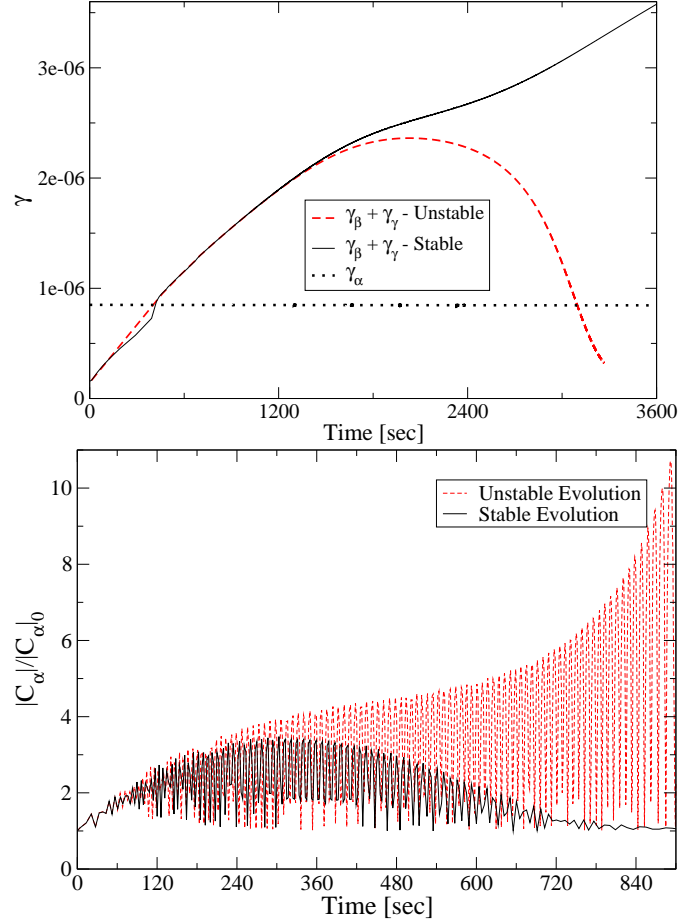


Figure 3.10: (a) The growth rate of the r-mode $\tilde{\gamma}_\alpha = \tilde{\gamma}_{GR} - \tilde{\gamma}_{\alpha v}$ and the sum of the viscous damping rates for the two daughter modes $\tilde{\gamma}_\beta + \tilde{\gamma}_\gamma$ are shown versus time. If $\tilde{\gamma}_\alpha > \tilde{\gamma}_\beta + \tilde{\gamma}_\gamma$ the evolution is unstable. (b) The r-mode amplitude $|\bar{C}_\alpha|$ is shown versus time for the two evolutions. In the unstable evolution the r-mode amplitude grows exponentially while for the stable case it oscillates and will eventually settle close to its quasi-steady state. Both evolutions have $T_h = 2 \times 10^9$ K. The viscosity is different with $A_{hb} = 2.9 \times 10^3$ for the unstable case and $A_{hb} = 2.8 \times 10^3$ for the stable case.

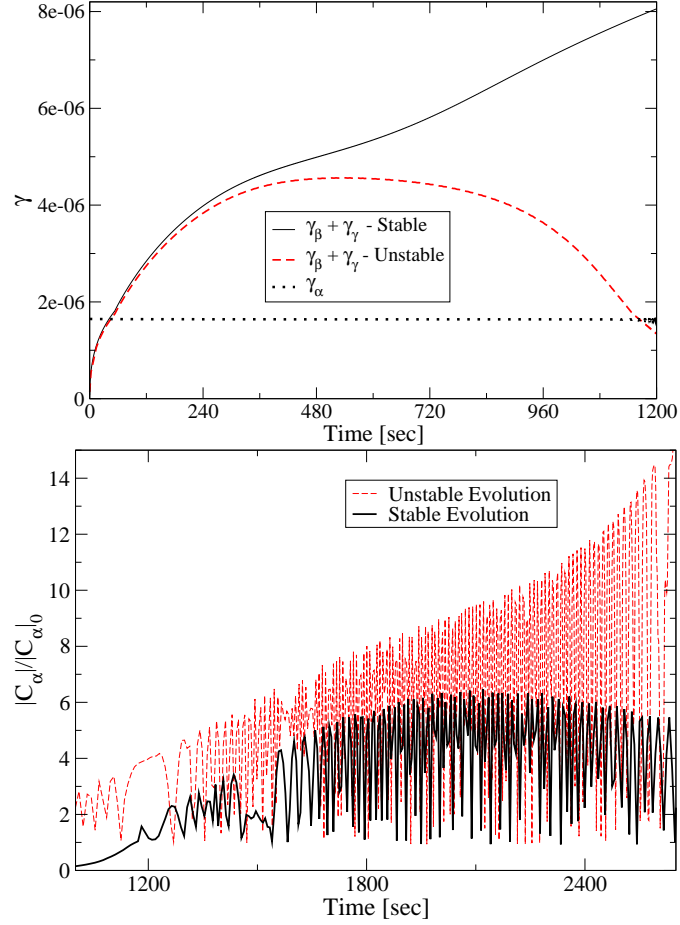


Figure 3.11: A similar runaway occurs for low cooling. Here $f_{\text{dU}} = 0.0$, $A_{\text{hb}} = 5.0 \times 10^3$ and $T_{\text{h}} = 1.2 \times 10^{10}$ K for both evolutions. The initial amplitudes are $|\bar{C}_\alpha|(0)_{\text{stable}} = 6.0 \times 10^{-5}$ and $|\bar{C}_\alpha|(0)_{\text{unstable}} = 7.0 \times 10^{-5}$.

where $L_{\text{dU}} \approx 10^{46}$ erg/sec. Taking the square root

$$\begin{aligned}
 h_0 &\approx \frac{T_9^3}{v_{\text{GW}} d} \sqrt{\frac{5GL_{\text{dU}}f_{\text{dU}}R_{\text{dU}}(T/T_c)}{2\pi^2c^3}} \\
 &\approx \frac{3T_9^3}{4vd} \sqrt{\frac{5GL_{\text{dU}}f_{\text{dU}}R_{\text{dU}}(T/T_c)}{2\pi^2c^3}}
 \end{aligned} \tag{3.32}$$

Plugging in some fiducial values

$$h_0 \approx 1.9 \times 10^{-26} \frac{T_9^3 R_{\text{dU}}}{v_{\text{kHz}}} \left(\frac{10 \text{ Mpc}}{d} \right) \left(\frac{L_{\text{dU}}}{10^{46} \text{ erg sec}^{-1}} \frac{f_{\text{dU}}}{0.10} \right)^{1/2} \tag{3.33}$$

The above analysis holds when the daughter modes are negligible. When all three modes are significant (type I and III evolutions) it is convenient to write h_0

in terms of the r-mode amplitude. Using the replacement $\dot{E}_{GW} = -(\omega_\alpha/m)\dot{J}_{GW} = 2\gamma_{GR}MR^2|C_\alpha|^2\Omega$:

$$h_0^2 = \frac{5G\gamma_{GR}MR^2|C_\alpha|^2\Omega}{\pi c^3 d^2 \nu_{GW}^2}. \quad (3.34)$$

We then use the quasi-stationary approximation for the r-mode amplitude

$$h_0^2 = \frac{5G\gamma_{GR}MR^2\Omega_c^2}{\pi c^3 d^2 \nu_{GW}^2} \frac{\tilde{\gamma}_\beta \tilde{\gamma}_\gamma}{4\tilde{\kappa}^2 \tilde{\omega}_\beta \tilde{\omega}_\gamma} \left(1 + \frac{1}{\tan \phi^2}\right). \quad (3.35)$$

In the strongly damping limit $1 \gg 1/(\tan \phi)^2$ and the gravitational wave amplitude can be written as

$$h_0^2 \approx \frac{5G\gamma_{GR}MR^2\Omega_c^2}{\pi c^3 d^2 \nu_{GW}^2} \frac{\tilde{\gamma}_\beta \tilde{\gamma}_\gamma}{4\tilde{\kappa}^2 \tilde{\omega}_\beta \tilde{\omega}_\gamma}, \quad (3.36)$$

Putting in some fiducial values

$$h_0 \approx 4.6 \times 10^{-27} \left(\frac{1 \text{ Mpc}}{d}\right) \nu_{\text{kHz}}^2 M_{1.4}^{5/2} R_{12.5}^{-3/2} \times \frac{\gamma_\beta}{10^{-7} \text{ sec}^{-1}} \frac{\gamma_\gamma}{10^{-7} \text{ sec}^{-1}}, \quad (3.37)$$

where we assume γ_β and $\gamma_\gamma \propto \rho^2$ for the mass and radius scaling.

A minimum detectable signal amplitude h_0 Ref. [13] can be written in terms of the observation time T_{obs} , number of detectors D and signal to noise ratio S_n as

$$h_0 = 11.4 \sqrt{\frac{S_n}{DT_{\text{obs}}}}. \quad (3.38)$$

For $D = 2$ detectors, $T_{\text{obs}} = 2$ weeks and a signal to noise ratio given by the broad band configurations one obtains $h_0 \approx 4 \times 10^{-26}$ for Advanced LIGO and $h_0 \approx 1 \times 10^{-26}$ for the Einstein telescope at $\nu = 900$ Hz. Here we used the noise curves

from Ref. [13]. In the first two weeks the spin frequency of the star changes by about 40% for the type II evolution detailed in Sec. 3.5.2, by $\sim 5\%$ for the $T_h = 2.0 \times 10^9$ K and the type III evolutions, and by 15% for the $T_h = 6.0 \times 10^9$ K evolution. An upper limit for the distance to which such sources could be detected is a few Mpc for type II evolutions and roughly 100 kpc for type I and type III evolutions.

3.8 Discussion and Concluding Remarks

This is a first treatment of the r-mode instability in newborn neutron stars that includes nonlinear saturation via three-mode couplings. This model provides a physical cutoff for the instability by energy transfer to other modes in the system. We vary the viscosity of the r-mode and inertial modes and explore the different nonlinear behaviors. We find that the mode triplet at the lowest parametric instability threshold is sufficient to stop the instability in most scenarios we consider. The different behaviors are determined by when the neutrino cooling is balanced by viscous heating due to the three modes. The star spins down in thermal equilibrium and this can occur before gravitational driving is balanced by viscous dissipation (to the right of the peak of the r-mode stability curve), to the left of the peak of the stability curve or on the stability curve.

We do not include higher order corrections in angular velocity in this work and preliminary calculations show that they are important at high spins. When these effects are included the evolution will most likely switch between triplets of modes as the star spins down and the modes comprising the lowest parametric instability threshold change. This chapter describes the impact of one set of

daughter modes on the r-mode instability and is a necessary first step. We use typical numbers for the coupling inertial mode viscosity and coupling coefficients. The exact numbers will change when the model is rendered more realistic. In addition to including higher order frequency corrections one can also add effects due to compressibility, multfluids and differential rotation. However, we believe that our simple model captures some of the generic features of the system. The upshot is that a dense set of modes will exhibit three-mode resonances. Their evolution is well described by quasi-stationary solutions whose slow variation depends on the competition between neutrino cooling and dissipation, gravitational radiation and magnetic dipole radiation spin-down.

CHAPTER 4

CONCLUSION

R-modes owe their origin to the Coriolis force and are a subset of a more general set of modes known as inertial modes. In the linear regime, an r-mode is unstable and grows exponentially when gravitational driving dominates fluid dissipation. Nonlinear effects become important once an unstable r-mode grows above its first parametric instability threshold and excites other near resonant modes in the system.

This thesis is a first treatment of the r-mode instability that models nonlinear saturation and includes spin and temperature evolution of the neutron star. Our model is simple. We use the eigenmodes and eigenfrequencies of an incompressible perfect fluid star. These eigenmodes are known analytically and can be expressed in terms of Legendre functions labelled by integers n and m . This simplifies the computation of shear, bulk and boundary layer viscosity and allows us to use the coupling coefficients computed by Brink *et al.* [51, 52, 53].

We apply this model to both accreting millisecond pulsars and newborn neutron stars. We model the nonlinear effects using the triplet of modes at the lowest parametric instability threshold. The triplet is comprised of the $n = 3, m = 2$ r-mode and the first two inertial modes that are excited when the r-mode amplitude crosses this first parametric instability threshold amplitude. We use simple parametrizations for viscosity and cooling to explore different nonlinear behaviors. In most scenarios we consider, we find that one triplet is sufficient to stop the growth of the r-mode instability.

In the accreting neutron star case, we observe different outcomes that can be easily predicted from initial angular velocity, neutrino cooling and viscosity parameters. The outcome of each evolution is independent of the initial values for the mode amplitudes as long as they are below the parametric instability.

The mode amplitudes settle very quickly into quasi-stationary states that change slowly as the temperature and spin frequency evolve. Once these states are reached, the mode amplitudes can be found algebraically and the system of equations is reduced from eight to two equations: spin and temperature evolution. The evolution of the neutron star's angular velocity and temperature follow easily calculated trajectories along these sequences of quasi-stationary states. The outcome of the evolution depends on whether or not the star can reach thermal equilibrium, where viscous heating is equal to neutrino cooling ($H = C$ curve; computed using quasi-stationary mode amplitudes). This curve has one maximum. Initially, the heating is much faster than accretion or gravitational spin-down and dominates the cooling. The star heats at constant angular velocity until it either reaches this $H = C$ curve or, if there is no thermal equilibrium temperature for that angular velocity (the initial angular velocity is above $\Omega_{H=C \text{ max}}$), it continues heating. The latter case corresponds to a fast runaway: the r-mode amplitude grows above several parametric instability thresholds, more inertial modes are excited and need to be included to correctly model the evolution. If the $H = C$ curve is reached, there are several possible trajectories: (1) cyclic evolution, (2) steady state and (3) slow runaway.

In a cyclic evolution, the star spins down in thermal equilibrium until the $H = C$ curve intersects the r-mode stability curve (i.e., the curve on which gravitational driving = viscous dissipation). Once this happens, the mode ampli-

tudes damp to zero and the star cools at constant angular velocity until the nuclear heating stops the cooling. The star then spins up in thermal equilibrium until it intersects the stability curve again and the cycle is repeated. The cycles we observe are narrow with changes in the spin frequency of less than 10%. In principle, this would make gravitational wave searches easier by enabling long coherent observations and maybe even targeted searches for neutron stars for which we know the spin frequency from X-ray or radio observations. For a steady state evolution, the gravitational spin-down is balanced by accretion. This happens only for low initial spin frequencies and hence low gravitational driving or when hyperon bulk viscosity is important at early temperatures. The slow runaway scenario occurs for low initial spin and slow cooling. In this case, the accretional spin-up dominates gravitational spin-down and the star spins up the $H = C$ curve. It eventually goes over the maximum of the curve and exits thermal equilibrium. Beyond this point the heating dominates the cooling again, the star heats at constant angular velocity, and the r-mode passes the second parametric instability threshold exciting more modes in the process. As in the fast runaway scenario, at this point more inertial modes need to be included to model the rest of the evolution accurately.

Since the fastest observed millisecond pulsar spins at 716 Hz, our low spin scenarios (steady states and slow runaways) are most likely ruled out by observations. Unfortunately, in cyclic evolutions, fast rotation requires large dissipation, which in turn leads to fast viscous heating and a short time for which the r-mode is unstable. In our model, neutron stars with $\nu_{\text{max}} \sim 800$ Hz lead to instability timescales of at most 1000 yr, which is about 10^{-3} shorter than the accretion timescale and this would mean that only about 1 in 1000 LMXB in our galaxy would have active r-modes.

In the newborn neutron star case, the evolution is more dynamic. We start with a hot neutron star with a temperature $T_{\text{initial}} \sim 10^{10}$ K that spins with a frequency close to the Kepler break-up frequency. The neutrino cooling is fast (direct URCA cooling $\propto T^6$) and dominates viscous heating. At high temperatures hyperon bulk viscosity dominates other forms of viscosity, assuming the star is dense enough for hyperons to appear.

Unlike in the accreting neutron star case, this evolution depends on the initial values of the mode amplitudes. At first, neutrino cooling dominates the viscous heating and is much faster than the gravitational radiation spin-down. So, the star cools at roughly constant angular velocity until the cooling is balanced by viscous heating. The point at which this happens depends on whether the r-mode has grown enough to excite other modes in the system before the r-mode stability curve is reached. This leads to a competition between the growth of the r-mode amplitude and cooling. When the viscous dissipation due to the excited modes balances the cooling, the star starts spinning down. However, the viscosity changes with spin-frequency and so the balance between heating and cooling is disturbed. The star oscillates around thermal equilibrium states as it spins down. The inertial modes that comprise the lowest parametric instability threshold change with angular velocity as well. We are using an effective three mode system with typical values of coupling coefficient and detuning. Although the details of the evolution will change as more modes are included in the calculation, we expect that we have a qualitatively correct picture of the spin-down process.

The analysis presented in this thesis could be extended in many ways. Here we include a few possible future directions. In this work we use the zero-

eccentricity values for coupling coefficients and frequencies. A first extension would be to include second order rotational effects in the frequency computation and also take into account the change of coupling coefficients with eccentricity. Additionally, including multiple triplets of modes would allow modeling of mode changes in the lowest parametric instability threshold, and following the spin-down of the star more accurately. Our evolutions are inadequate to follow what happens when the system runs away. Including additional mode-mode couplings is important to accurately model these scenarios. For accreting neutron stars our predictions are made only for fast, steady accretors with \dot{M} close to the Eddington limit. Most neutron stars in Low Mass X-ray binaries in our galaxy are transient and accrete at much slower rates. Modeling slower accretors, which would have smaller core temperatures and also higher boundary layer and shear viscosity, could be interesting. Other extensions could include making the model more realistic by adding effects such as those due to compressibility and multifluid composition.

Although there are many ways to improve our calculation, it is important to reiterate that some of the features we observe should be generic. More general treatments are still expected to find a dense set of modes confined to a narrow frequency range that will always exhibit near resonances and low parametric instability thresholds. Once a parametric instability threshold is passed inertial modes are excited, and the evolutions should still be determined by competitions between neutrino cooling and viscous heating, dissipation and gravitational driving. Some variation of the behaviors we find - (1) cycles, steady states, slow and fast runways for accreting neutron stars and (2) dynamic evolution with spin-down in different regions delimited by the r-mode stability curve and thermal oscillations around equilibrium for young neutron star - should follow.

APPENDIX A
APPENDICES TO CHAPTER 2

A.1 Equations of Motion

This appendix will sketch the derivation of Eqs. (2.1) from the Lagrangian density. We follow closely Appendix A in Schenk *et al.*, which contains the derivation of the equations of motion for constant Ω .

The Lagrangian density as given by Eq. (A1) in Schenk *et al.* [54] is

$$\mathcal{L} = \frac{1}{2}\dot{\xi} \cdot \dot{\xi} + \frac{1}{2}\dot{\xi} \cdot \mathbf{B} \cdot \xi - \frac{1}{2}\xi \cdot \mathbf{C} \cdot \xi + \mathbf{a}_{\text{ext}}(t) \cdot \xi, \quad (\text{A.1})$$

where the operators $\mathbf{B} \cdot \xi = 2\boldsymbol{\Omega} \times \xi$ and

$$\begin{aligned} \rho(C \cdot \xi)_i &= -\nabla_i(\Gamma_1 p \nabla_j \xi^j) + \nabla_i p \nabla_j \xi^j + \rho \nabla_i \delta \phi \\ &- \nabla_j p \nabla_i \xi^j + \rho \xi^j \nabla_j \nabla_i \phi + \rho \xi^j \nabla_j \nabla_i \phi_{\text{rot}} \end{aligned} \quad (\text{A.2})$$

with $\phi_{\text{rot}} = -(1/2)(\boldsymbol{\Omega} \times \mathbf{x})^2$. We are interested in a situation where the uniform angular velocity of the star changes slowly on the timescale of the rotation period itself. In order to remove the time dependence we define the new displacement and time variables

$$\xi = \frac{\tilde{\xi}}{\sqrt{\Omega}}, \quad d\tau = \Omega dt. \quad (\text{A.3})$$

In terms of these new variables the Lagrangian density can be written as

$$\begin{aligned} \tilde{\mathcal{L}} &= \frac{1}{2}\tilde{\xi}' \cdot \tilde{\xi}' + \frac{1}{2}\tilde{\xi}' \cdot (\tilde{\mathbf{B}} \cdot \tilde{\xi}) + \frac{(\sqrt{\Omega})''}{2\sqrt{\Omega}}|\tilde{\xi}|^2 \\ &- \frac{1}{2}\tilde{\xi} \cdot \tilde{\mathbf{C}} \cdot \tilde{\xi} + \frac{\mathbf{a}_{\text{ext}}(t)}{\Omega^{3/2}} \cdot \tilde{\xi}, \end{aligned} \quad (\text{A.4})$$

where the primes denote derivatives with respect to τ , $\tilde{\mathbf{B}} = \Omega^{-1}B$ and $\tilde{\mathbf{C}} = \Omega^{-2}C$.

The momentum canonically conjugate to $\tilde{\xi}$ is

$$\tilde{\pi} = \frac{\partial \mathcal{L}}{\partial \tilde{\xi}'} = \tilde{\xi}' + \hat{\Omega} \times \tilde{\xi}. \quad (\text{A.5})$$

The associated Hamiltonian density is

$$\mathcal{H} = \frac{1}{2} \left| \tilde{\pi} - \frac{1}{2} \tilde{\mathbf{B}} \cdot \tilde{\xi} \right|^2 - \frac{(\sqrt{\Omega})''}{2\sqrt{\Omega}} |\tilde{\xi}|^2 + \frac{1}{2} \tilde{\xi} \cdot \tilde{\mathbf{C}} \cdot \tilde{\xi} - \frac{\mathbf{a}_{\text{ext}}}{\Omega^{3/2}} \cdot \tilde{\xi}. \quad (\text{A.6})$$

Hamilton's equations of motions can be written as

$$\tilde{\zeta}' = T \cdot \tilde{\zeta} + \mathbf{F}(\tau), \quad (\text{A.7})$$

where

$$\tilde{\zeta} = \begin{pmatrix} \tilde{\xi} \\ \tilde{\pi} \end{pmatrix},$$

the operator T is $T = T_0 + T_1$ with

$$T_0 = \begin{pmatrix} -\frac{1}{2} \tilde{\mathbf{B}} & 1 \\ \frac{1}{4} \tilde{\mathbf{B}}^2 - \tilde{\mathbf{C}} & -\frac{1}{2} \tilde{\mathbf{B}} \end{pmatrix}$$

and

$$T_1 = \begin{pmatrix} 0 & 0 \\ \frac{(\sqrt{\Omega})''}{\sqrt{\Omega}} & 0 \end{pmatrix},$$

and

$$\mathbf{F}(\tau) = \begin{pmatrix} 0 \\ \frac{\mathbf{a}_{\text{ext}}}{\Omega^{3/2}} \end{pmatrix}.$$

We assume solutions of the form $\tilde{\zeta}(\tau, \mathbf{x}) = e^{i\tilde{\omega}\tau} \tilde{\zeta}(\mathbf{x})$. Specializing to the case of no forcing term $a_{\text{ext}} = 0$ leads to the eigenvalue equation

$$(T_0 - i\tilde{\omega}) \tilde{\zeta}(\mathbf{x}) = 0. \quad (\text{A.8})$$

Since the operator T_0 is not Hermitian it will have distinct right and left eigenvectors. Similar to Schenk *et al.* [54] we label the right eigenvectors of T as $\tilde{\zeta}_A$,

and the associated eigenfrequencies as $\tilde{\omega}_A = \omega_A/\Omega$, and the eigenvalue equation above becomes

$$(T_0 - i\tilde{\omega}_A)\tilde{\zeta}_A(\mathbf{x}) = 0. \quad (\text{A.9})$$

The left eigenvectors χ_A satisfy

$$(T_0^\dagger - i\tilde{\omega}_A^*)\tilde{\chi}_A = 0, \quad (\text{A.10})$$

where

$$T_0^\dagger = \begin{pmatrix} \frac{1}{2}\tilde{\mathbf{B}} & \frac{1}{4}\tilde{\mathbf{B}}^2 - \tilde{\mathbf{C}} \\ 1 & \frac{1}{2}\tilde{\mathbf{B}} \end{pmatrix}$$

For simplicity, in this appendix we specialize to the case of no Jordan chains when the set of right eigenvectors forms a complete basis. The orthonormality relation between right and left eigenvectors is

$$\langle \tilde{\chi}_A, \tilde{\zeta}_B \rangle = \int d^3\mathbf{x} \rho(\mathbf{x}) \tilde{\chi}_A^\dagger \cdot \tilde{\zeta}_B = \delta_{AB}. \quad (\text{A.11})$$

We can expand $\zeta(\tau, \mathbf{x})$ in this basis as

$$\zeta(\tau, \mathbf{x}) = \sum_A C_A(\tau) \zeta_A(\mathbf{x}), \quad (\text{A.12})$$

where the coefficients C_A are given by the inverse of this mode expansion

$$C_A(\tau) = \langle \tilde{\chi}_A, \tilde{\zeta}(\tau, \mathbf{x}) \rangle. \quad (\text{A.13})$$

Using Eqs. (B-2,A.9,A.11) in Eq. (A.7) leads to the equations of motion for the mode amplitudes

$$\begin{aligned} C'_A - i\tilde{\omega}_A C_A &= g(\tau) \sum_B C_B^* \left\langle \tilde{\chi}_A, \begin{pmatrix} 0 \\ \tilde{\zeta}_B \end{pmatrix} \right\rangle \\ &+ \langle \tilde{\chi}_A, F(\tau) \rangle, \end{aligned} \quad (\text{A.14})$$

where $g(\tau) = (\sqrt{\Omega})''/\sqrt{\Omega}$. Following Sec. IV of Schenk *et al.* [54] we replace the externally applied acceleration by the nonlinear acceleration given by Eq.

(4.2) of Ref. [54]. The inner product can be written in terms of the displacement variable $\tilde{\xi}$. The left eigenvectors are

$$\tilde{\chi}_A = \begin{pmatrix} \tilde{\sigma}_A \\ \tilde{\tau}_A \end{pmatrix},$$

where $\tilde{\tau}_A$ can be chosen to be proportional to $\tilde{\xi}_A$ because they satisfy the same matrix equation.

$$\tilde{\tau}_A = -i\tilde{\xi}_A/\tilde{b}_A, \quad (\text{A.15})$$

which corresponds to Eq. (A-45) in Schenk *et al.* [54] with the proportionality constant $\tilde{b}_A = \Omega^{-1}b_A = MR^2/\tilde{\omega}_A$ (also given by Eq. (2.36) of Ref. [54]).

The equations of motion for the mode amplitudes become

$$\begin{aligned} C'_A - i\tilde{\omega}_A C_A &= \frac{ig(\tau)}{\tilde{b}_A} \sum_B C_B \int d^3\mathbf{x} \tilde{\xi}_A^* \cdot \tilde{\xi}_B \\ &+ \frac{iMR^2}{\tilde{b}_A} \sum_{BC} \tilde{\kappa}_{ABC}^* C_B^* C_C^*, \end{aligned} \quad (\text{A.16})$$

where the nonlinear coupling $\tilde{\kappa}_{ABC} = \kappa_{ABC}/(MR^2\Omega^2)$ and κ_{ABC} is explicitly give by Eq. (4.20) of Ref. [54]. The $g(\tau)$ integral mixes only modes with $m_A = m_B$ because of the $e^{im\phi}$ dependence of the displacement eigenvectors $\tilde{\xi}$. ($\int_0^{2\pi} d\phi e^{i(m_A - m_B)\phi} = 0$ if $m_A \neq m_B$.) So, this term will be zero for our mode triplet. Also, in the case of a single mode triplet there is only one coupling and Eqs. (A.16) take the form of Eqs. (2.1).

A.2 Stability Around Equilibrium at Constant Angular Velocity

In this appendix we study the behavior of the mode amplitudes and temperature near equilibrium assuming constant angular velocity. We are performing a first order expansion of Eqs. (2.5) and (2.18). Each of the five variables is expanded about its equilibrium $(X_j)_e$ as follows

$$X_j(\tilde{\tau}) = \{|\bar{C}_\alpha|, |\bar{C}_\beta|, |\bar{C}_\gamma|, \phi, T_8\} = (X_j)_e [1 + \zeta_j(\tilde{\tau})] \quad (\text{B-1})$$

where the perturbation $|\zeta_j| \ll 1$ and $j = \alpha, \beta, \gamma, T$. The expansion leads to a first order differential equation for each ζ_j

$$\begin{aligned} \frac{d\zeta_\alpha}{d\tilde{\tau}} &= \frac{(\tilde{\gamma}_\alpha)_e}{\tilde{\Omega}|\delta\tilde{\omega}|} \left[\zeta_\alpha - \zeta_\beta - \zeta_\gamma - \left(\frac{\phi}{\tan\phi} \right)_e \zeta_\phi \right. \\ &\quad \left. - \left(\frac{T_8}{\tilde{\gamma}_\alpha} \right)_e \left(\frac{\partial\tilde{\gamma}_\alpha}{\partial T_8} \right)_e \zeta_T \right], \\ \frac{d\zeta_\beta}{d\tilde{\tau}} &= \frac{(\tilde{\gamma}_\beta)_e}{\tilde{\Omega}|\delta\tilde{\omega}|} \left[\zeta_\alpha - \zeta_\beta + \zeta_\gamma + \left(\frac{\phi}{\tan\phi} \right)_e \zeta_\phi \right. \\ &\quad \left. - \left(\frac{T_8}{\tilde{\gamma}_\beta} \right)_e \left(\frac{\partial\tilde{\gamma}_\beta}{\partial T_8} \right)_e \zeta_T \right], \\ \frac{d\zeta_\gamma}{d\tilde{\tau}} &= \frac{(\tilde{\gamma}_\gamma)_e}{\tilde{\Omega}|\delta\tilde{\omega}|} \left[\zeta_\alpha + \zeta_\beta - \zeta_\gamma + \left(\frac{\phi}{\tan\phi} \right)_e \zeta_\phi \right. \\ &\quad \left. - \left(\frac{T_8}{\tilde{\gamma}_\gamma} \right)_e \left(\frac{\partial\tilde{\gamma}_\gamma}{\partial T_8} \right)_e \zeta_T \right], \\ \frac{d\zeta_\phi}{d\tilde{\tau}} &= \frac{1}{\phi_e \tan\phi_e} \left(\zeta_\alpha \frac{\tilde{\gamma}_\alpha + \tilde{\gamma}_\beta + \tilde{\gamma}_\gamma}{\tilde{\Omega}|\delta\tilde{\omega}|} + \zeta_\beta \frac{-\tilde{\gamma}_\alpha - \tilde{\gamma}_\beta + \tilde{\gamma}_\gamma}{\tilde{\Omega}|\delta\tilde{\omega}|} \right. \\ &\quad \left. + \zeta_\gamma \frac{-\tilde{\gamma}_\alpha + \tilde{\gamma}_\beta - \tilde{\gamma}_\gamma}{\tilde{\Omega}|\delta\tilde{\omega}|} \right)_e + \frac{(\tilde{\gamma}_\alpha - \tilde{\gamma}_\beta - \tilde{\gamma}_\gamma)_e}{\tilde{\Omega}|\delta\tilde{\omega}|} \zeta_\phi, \\ \frac{d\zeta_T}{d\tilde{\tau}} &= \frac{MR^2\Omega_c^2\tilde{\gamma}_\alpha\tilde{\gamma}_\beta\tilde{\gamma}_\gamma}{2\tilde{\kappa}^2\tilde{\omega}_\alpha\tilde{\omega}_\beta\tilde{\omega}_\gamma\tilde{\Omega}|\delta\tilde{\omega}|C(T_e)T_{8e}} \left(1 + \frac{1}{\tan\phi_e^2} \right) \\ &\quad \times \left[2 \left(\tilde{\omega}_\alpha \frac{\tilde{\gamma}_{\alpha v}}{\tilde{\gamma}_\alpha} \zeta_\alpha + \tilde{\omega}_\beta \zeta_\beta + \tilde{\omega}_\gamma \zeta_\gamma \right) \right. \\ &\quad \left. + T_{8e} \left(\tilde{\omega}_\alpha \frac{1}{\tilde{\gamma}_\alpha} \frac{\partial\tilde{\gamma}_\alpha}{\partial T_8} + \tilde{\omega}_\beta \frac{1}{\tilde{\gamma}_\beta} \frac{\partial\tilde{\gamma}_\beta}{\partial T_8} + \tilde{\omega}_\gamma \frac{1}{\tilde{\gamma}_\gamma} \frac{\partial\tilde{\gamma}_\gamma}{\partial T_8} \right)_e \zeta_T \right] \end{aligned} \quad (\text{B-2})$$

$$- \left(\frac{dL_\nu}{dT_8} \right)_e \frac{1}{\Omega_c \tilde{\Omega} |\delta \tilde{\omega}| C(T_e)} \zeta_T,$$

where the equilibrium amplitudes $|C_j|_e$ have been written in terms of the corresponding driving and damping rates using Eqs. (2.6). Eq. (B-2) can be written in matrix form as

$$\frac{d\zeta_j}{d\tilde{\tau}} = A^{ij} \zeta_i. \quad (\text{B-3})$$

Let $\zeta_j \propto \exp(\lambda \tilde{\tau})$. The determinant $\|A^{ij} - \lambda \delta^{ij}\| = 0$ leads to the eigenvalue equation

$$\lambda^5 + a_4 \lambda^4 + a_3 \lambda^3 + a_2 \lambda^2 + a_1 \lambda + a_0 = 0. \quad (\text{B-4})$$

The coefficients a_j with $j = 0, 4$ are

$$\begin{aligned} a_4 &= 2 \tan \phi_e = \frac{\tilde{\gamma}_\beta + \tilde{\gamma}_\gamma - \tilde{\gamma}_\alpha}{\tilde{\Omega} |\delta \tilde{\omega}|}, \\ a_3 &\approx \frac{2}{\tan \phi_e^2} \frac{\tilde{\gamma}_\beta^2 + \tilde{\gamma}_\gamma^2 + \tilde{\gamma}_\alpha^2}{(\tilde{\Omega} |\delta \tilde{\omega}|)^2} + \tan \phi_e^2 - 1, \\ a_2 &\approx \frac{\tilde{\gamma}_\alpha \tilde{\gamma}_\beta \tilde{\gamma}_\gamma}{(\tilde{\Omega} |\delta \tilde{\omega}|)^3} \left(\frac{12}{\tan \phi_e^2} + 1 \right), \\ a_1 &\approx \frac{4 \tilde{\gamma}_\alpha \tilde{\gamma}_\beta \tilde{\gamma}_\gamma}{(\tilde{\Omega} |\delta \tilde{\omega}|)^3} \left(\frac{1}{\tan \phi_e} + \tan \phi_e \right), \\ a_0 &\approx \frac{2MR^2 \Omega_c^2}{\tilde{\kappa}^2 \tilde{\omega}_\alpha \tilde{\omega}_\beta \tilde{\omega}_\gamma C(T_e)} \frac{(\tilde{\gamma}_\alpha \tilde{\gamma}_\beta \tilde{\gamma}_\gamma)^2}{(\tilde{\Omega} |\delta \tilde{\omega}|)^4} \frac{1}{\tan \phi_e} \left(1 + \frac{1}{\tan \phi_e^2} \right) \\ &\quad \times \left[\frac{\tilde{\omega}_\alpha}{\tilde{\gamma}_\alpha} \left(\frac{\partial \tilde{\gamma}_\alpha}{\partial T_8} \right)_e + \frac{\tilde{\omega}_\beta}{\tilde{\gamma}_\beta} \left(\frac{\partial \tilde{\gamma}_\beta}{\partial T_8} \right)_e + \frac{\tilde{\omega}_\gamma}{\tilde{\gamma}_\gamma} \left(\frac{\partial \tilde{\gamma}_\gamma}{\partial T_8} \right)_e \right] \\ &\quad - \frac{4 \tilde{\gamma}_\alpha \tilde{\gamma}_\beta \tilde{\gamma}_\gamma}{(\tilde{\Omega} |\delta \tilde{\omega}|)^3} \frac{1}{\tan \phi_e} \frac{1}{\tilde{\Omega} |\delta \tilde{\omega}| C(T_e)} \left(\frac{dL_\nu}{dT_8} \right)_e. \end{aligned} \quad (\text{B-5})$$

The eigenvalues can be approximated as

$$\begin{aligned} \lambda_{1,2} &\approx -\frac{a_4}{2} - \epsilon \pm i \sqrt{\frac{a_1}{\epsilon^2 + w^2} - \left(\frac{a_4}{2} + \epsilon \right)^2}, \\ \lambda_{3,4} &\approx \epsilon \pm iw, \\ \lambda_5 &\approx -\frac{a_0}{a_1}, \end{aligned} \quad (\text{B-6})$$

where $\epsilon = (a_2 - a_3 a_4)/a_4$ and $w = \sqrt{a_1/a_3}$. The system is unstable when $a_2 - a_3 a_4 > 0$ or $a_0 < 0$. The first two eigenvalues will have a negative real part as long as

$\tilde{\gamma}_\beta + \tilde{\gamma}_\gamma > \tilde{\gamma}_\alpha$. If the heating compensates the cooling of the star $a_0 \approx 0$ and becomes negative if the star can not reach thermal equilibrium. The other critical stability condition $a_2 - a_3 a_4 = 0$ can be written as

$$\left(\frac{\tilde{\gamma}_\alpha}{\tilde{\Omega}|\delta\tilde{\omega}|} \right)^3 [1 + \Gamma_\beta + \Gamma_\gamma - (\Gamma_\beta^2 + \Gamma_\gamma^2) - (\Gamma_\beta - \Gamma_\gamma)^2(\Gamma_\beta + \Gamma_\gamma)] = 0, \quad (\text{B-7})$$

where $\Gamma_\beta = \gamma_\beta/\gamma_\alpha$ and $\Gamma_\gamma = \gamma_\gamma/\gamma_\alpha$. Note that we have ignored the smaller terms of order $O([\tilde{\gamma}_\alpha/(\tilde{\Omega}|\delta\tilde{\omega}|)]^5)$. This condition can be rewritten by defining variables $D_1 = \Gamma_\beta + \Gamma_\gamma$ and $D_2 = \Gamma_\beta - \Gamma_\gamma$

$$2 + 2D_1 - D_1^2 - D_2^2 - 2D_2^2 D_1 = 0. \quad (\text{B-8})$$

If $D_2 = 0$ then the equation has one solution $D_1 = 1 + \sqrt{3}$ for $D_1 > 2$, which corresponds to $\Gamma = \Gamma_\beta = \Gamma_\gamma = 1.37$ and matches the result of Wersinger *et al.* [56]. For the viscosity we consider (see Sec. 2.2.4) $a_2 - a_3 a_4 < 0$.

APPENDIX B
APPENDICES TO CHAPTER 3

B.1 Changes in Mode Frequencies due to Magnetic Fields

In this appendix we follow Morsink and Rezania [35] to obtain the frequency corrections due to the presence of a magnetic field. These corrections are added perturbatively.

They define a dimensionless magnetic coupling

$$\kappa_{AB} = M^{-1} \langle \xi_A, \rho^{-1} \mathbf{F}_B \rangle, \quad (\text{B-1})$$

where \mathbf{F} is the Lorentz force created by the fluid motion. The coefficients can be thought of as the ratio of the work done by the perturbed Lorentz force to the total magnetic energy stored in the equilibrium star.

The dominant part of the magnetic coupling coefficients is

$$\kappa_{AB}^{(1)} = \int \nabla \times (\xi_A^* \times \mathbf{B}) \cdot \nabla \times (\xi_B \times \mathbf{B}) d^3x \quad (\text{B-2})$$

Assuming the off-diagonal entries are small [35], the frequency corrections are given by

$$\omega_{\text{new}} = \omega_{\text{old}} \left(1 - \frac{\mathcal{M}}{2\mathcal{T}} \kappa_{AA} \right), \quad (\text{B-3})$$

where the ratio of magnetic field energy to rotational kinetic energy

$$\mathcal{T} = \epsilon = MR^2\Omega^2$$

Assuming a constant magnetic field of the form

$$B_x = B_0 \sin \alpha \quad (\text{B-4})$$

$$B_y = 0$$

$$B_z = B_0 \cos \alpha.$$

For an $n = m + 1$ r-mode

$$\begin{aligned} |\kappa_{AA}| &= \int d^3x \sin^2 \alpha \{ \cos^2 \phi (|\partial_{\varpi} \xi_{\varpi}|^2 + |\partial_{\varpi} \xi^{\phi}|^2 + |\partial_{\varpi} \xi_z|^2) \\ &+ (\sin^2 \phi / \varpi^2) [(1 + m^2)(|\xi^{\varpi}|^2 + |\xi^{\phi}|^2) + m^2 |\xi^z|^2 - 4m |\xi^{\phi} \xi^{\varpi}|] \\ &+ \cos^2 \alpha (|\partial_z \xi^z|^2 + |\partial_z \xi^{\varpi}|^2 + |\partial_z \xi^{\phi}|^2) \end{aligned} \quad (\text{B-5})$$

Using an incompressible stellar model (we use Eq. (3.18) together with the recursion relations Eq. (A.1-5) in [73].) we obtain

$$|\kappa_{AA}| = \frac{4\pi(m+1)(2m+3)}{12} \left(1 + \sin^2 \alpha \frac{m^2 + m - 3}{2} \right). \quad (\text{B-6})$$

B.2 Bulk Viscosity Integrals and Viscous Damping Timescales

The two sets of daughter modes at the two lowest zero-viscosity parametric instability thresholds have: $j = 414$ ($n = 13, m = -3$) and $j = 538$ ($n = 14, m = 1$) for the lowest threshold and $j = 494$ ($n = 14, m = -5$) and $j = 592$ ($n = 15, m = 3$) for the second lowest threshold.

The mode number j is a way of labeling hybrid inertial modes so that each mode is given a unique number that is a function of principal Legendre index n ($n : 2 \rightarrow \infty$), azimuthal number m ($m : 0 \rightarrow n - 1$) and frequency index k

($k : 1 \rightarrow n - m$ if $m \neq 0$ and $1 \rightarrow n - m - 1$ if $m = 0$).

$$j = \frac{(n-1)n(n+1)}{6} + \frac{(n-m-1)(n-m)}{2} + k - 1 \quad (\text{B-7})$$

The bulk viscosity integral for inertial modes is computed using Eq. (3.6):

$$I_{414} \approx 2\pi \times 50.3, \quad I_{538} \approx 2\pi \times 100.1, \quad (\text{B-8})$$

$$I_{494} \approx 2\pi \times 142.4, \quad I_{592} \approx 2\pi \times 103.1.$$

The r-mode integral is computed using Eqs. (55-56) of Nayyar and Owen [48]

$$I_4 = I_\alpha = 0.211 \quad (\text{B-9})$$

Table B.1 compares the bulk viscosity timescales for several different inertial modes of $n = 1$ polytrope computed by Lockitch and Friedman [75] with those computed in this work using an incompressible model. The difference is small; typically about a factor of two or less. For the computations in this table we used n-p-e bulk viscosity with a bulk viscosity coefficient

$$\zeta = 6 \times 10^{25} \left(\frac{\text{Hz}}{\omega} \right)^2 \left(\frac{\rho}{10^{15} \text{ g cm}^{-3}} \right)^2 T_9^6 \text{ g cm sec}^{-1}. \quad (\text{B-10})$$

B.3 Boundary Layer Viscosity Integrals

The mode integrals are calculated using Eq. (3.11).

For the r-mode this gives

$$I_4^{\text{incompressible}} = 2\pi \times 10.5, \quad I_4^{n=1 \text{ polytrope}} \approx 2\pi \times 21.8, \quad (\text{B-11})$$

where we have used the incompressible ($\rho = \text{constant}$) value in this work.

Table B.1: Bulk viscosity timescales computed using incompressible stellar modes ($\tau_{\text{bulk } n=0}$; used in this work with a different bulk viscosity coefficient) and $n = 1$ polytrope ($\tau_{\text{bulk } n=1}$) inertial modes for an n-p-e gas. The $n = 1$ polytrope calculation was performed by Lockitch and Friedman [75]. Note that, mathematically, the bulk viscosity damping rate is zero for incompressible stars. We adopt the attitude that the dissipation timescale is computed to leading order in Γ_1 and take $\Gamma_1 = 2$ (for incompressible stars $\Gamma_1 \rightarrow \infty$). The timescales for the two models are roughly within a factor of 2 of each other.

j	n	m	$\tau_{\text{bulk } n=0}$	$\tau_{\text{bulk } n=1}$
12	4	2	7.03×10^9 sec	3.32×10^9 sec
14	4	1	9.68×10^9 sec	5.86×10^9 sec
44	6	2	7.00×10^9 sec	4.79×10^9 sec
47	6	1	2.51×10^9 sec	2.57×10^9 sec
70	7	2	6.62×10^9 sec	5.32×10^9 sec

For the daughter modes at first two parametric instability thresholds the integrals are calculated also using the modes for an incompressible star

$$I_{414} \approx 2\pi \times 92.99, \quad I_{538} \approx 2\pi \times 376.2, \quad (\text{B-12})$$

$$I_{494} \approx 2\pi \times 241.8, \quad I_{592} \approx 2\pi \times 140.1.$$

B.4 Oscillations Around Thermal Equilibrium: One Mode Evolution

Consider the one-mode evolution equations

$$\begin{aligned} \frac{d|C_\alpha|^2}{dt} &= 2(\gamma_{GR} - \gamma_{\alpha v})|C_\alpha|^2 \\ C(T)\frac{dT}{dt} &= 2MR^2\Omega|C_\alpha|^2\gamma_{\alpha v} - L_v(T). \end{aligned} \quad (\text{B-13})$$

We expand each variable to first order around its equilibrium value

$$|C_\alpha|^2 = |C_{\alpha e}|^2(1 + \zeta_\alpha) \quad (\text{B-14})$$

$$T = T_e(1 + \zeta_T).$$

This leads to the coupled equations

$$\begin{aligned}\frac{d\zeta_\alpha}{dt} &= 2(\gamma_{GR} - \gamma_{\alpha v})_e \zeta_\alpha - 2T_e \left(\frac{\partial \gamma_{\alpha v}}{\partial T} \right)_e \zeta_T, \\ \frac{d\zeta_T}{dt} &= \frac{2E_{\alpha e} \gamma_{\alpha v}(\Omega, T_e)}{T_e C(T)} \zeta_\alpha \\ &\quad + \left[\frac{2E_{\alpha e}}{C(T)} \left(\frac{\partial \gamma_{\alpha v}}{\partial T} \right)_e - \frac{1}{C(T)} \left(\frac{dL_v}{dT} \right)_e \right] \zeta_T,\end{aligned}\tag{B-15}$$

where $E_{\alpha e} = MR^2 \Omega |C_\alpha|_e^2$. In equilibrium

$$\begin{aligned}\gamma_{GR}(\Omega) - \gamma_{\alpha v}(\Omega, T_e) &= 0 \\ 2E_{\alpha e} \gamma_{\alpha v}(\Omega, T_e) &= L_v(T_e).\end{aligned}\tag{B-16}$$

Using these the coupled equations simplify to

$$\begin{aligned}\frac{d\zeta_\alpha}{dt} &= -2T_e \left(\frac{\partial \gamma_{\alpha v}}{\partial T} \right)_e \zeta_T, \\ \frac{d\zeta_T}{dt} &= \frac{L_v(T_e)}{T_e C(T_e)} \zeta_\alpha \\ &\quad + \left[\frac{1}{\gamma_{\alpha v e}} \left(\frac{\partial \gamma_{\alpha v}}{\partial T} \right)_e - \frac{1}{L_v(T_e)} \left(\frac{\partial L_v}{\partial T} \right)_e \right] \frac{L_v(T_e)}{C(T_e)} \zeta_T.\end{aligned}\tag{B-17}$$

We can now write the second order eigenvalue equation for this system

$$\lambda^2 - \lambda \left(\frac{\partial \ln \gamma_{\alpha v}}{\partial T} - \frac{\partial \ln L_v}{\partial T} \right)_e \frac{L_v(T_e)}{C(T_e)} + \frac{2L_v(T_e)}{C(T_e)} \left(\frac{\gamma_{\alpha v}}{\partial T} \right)_e = 0\tag{B-18}$$

with solutions

$$\lambda_{1,2} = \frac{\gamma_0}{2} \pm \frac{1}{2} \sqrt{\gamma_0^2 - \frac{8L_v(T_e)}{C(T_e)} \left(\frac{\gamma_{\alpha v}}{\partial T} \right)_e}.\tag{B-19}$$

Here

$$\gamma_e = \left(\frac{\partial \ln \gamma_{\alpha v}}{\partial T} - \frac{\partial \ln L_v}{\partial T} \right)_e \frac{L_v(T_e)}{C(T_e)}.\tag{B-20}$$

Fixed points on the right side of the r-mode stability curve $T > T_{\text{peak}}$ have a viscosity with negative slope $(\partial \gamma_{\alpha v} / \partial T)_e < 0$ and are always unstable (one eigenvalue is positive). While fixed points on the left side of the r-mode stability curve $T < T_{\text{peak}}$ have $(\partial \gamma_{\alpha v} / \partial T)_e > 0$ are stable if $\gamma_e < 0$ and unstable if $\gamma_e > 0$.

In order to gain a better understanding of the thermal cycles around the stability curve we write the viscous heating U as fraction of the cooling and subsequently study the evolution of f .

$$U = 2\gamma_{\alpha v}E_{\alpha} = f(t)L_v(T), \quad (\text{B-21})$$

where $0 \leq f \leq 1$ and we have neglected the viscous heating due to the daughter modes as their amplitudes are much smaller than that of the r-mode in this scenario. The thermal evolution of the system can now be written as

$$C(T)\frac{dT}{dt} = U - L_v(T) = (f - 1)L_v(T). \quad (\text{B-22})$$

To find the evolution of f we take the time derivative of Eq. (B-21). We can then write

$$\frac{1}{f} \frac{df}{dt} = \frac{1}{U} \frac{dU}{dt} - \frac{(f - 1)}{C(T)} \frac{\partial L_v}{\partial T} \quad (\text{B-23})$$

and

$$\frac{1}{U} \frac{dU}{dt} = \frac{1}{\gamma_{\alpha v}} \frac{\partial \gamma_{\alpha v}}{\partial T} \frac{(f - 1)L_v(T)}{C(T)} + 2(\gamma_{GR} - \gamma_{\alpha v}). \quad (\text{B-24})$$

Plugging Eq. (B-24) in Eq. (B-23) we can write

$$\frac{1}{f} \frac{df}{dt} = \frac{(f - 1)L_v(T)}{C(T)} \left(\frac{1}{\gamma_{\alpha v}} \frac{\partial \gamma_{\alpha v}}{\partial T} - \frac{1}{L_v} \frac{\partial L_v}{\partial T} \right) + 2(\gamma_{GR} - \gamma_{\alpha v}). \quad (\text{B-25})$$

Labeling the term in parenthesis as γ we obtain

$$\frac{1}{f} \frac{df}{dt} = \frac{(f - 1)L_v(T)}{C(T)} \gamma + 2(\gamma_{GR} - \gamma_{\alpha v}), \quad (\text{B-26})$$

where

$$\gamma = \frac{1}{\gamma_{\alpha v}} \frac{\partial \gamma_{\alpha v}}{\partial T} - \frac{1}{L_v} \frac{\partial L_v}{\partial T}. \quad (\text{B-27})$$

Initially, the star is very hot $T \sim 10^{10}$ K and cools fast: $\gamma < 0$ (the slope of the r-mode stability curve is negative for $T > T_{\text{peak}}$), $f \ll 1$ and $\gamma_{GR} > \gamma_{\alpha v}$. So, the right hand side of Eq. (B-26) is positive and f grows exponentially. If the r-mode

amplitude does not grow above its parametric instability threshold and is not large enough for $f = 1$ (as fast cooling $\propto T^6$ we do not observe evolutions for which the viscous heating balances the cooling for $T > T_{\text{peak}}$ before parametric instability; in the phase space we studied this balance occurs on the right side of the r-mode stability curve only for r-mode amplitudes of order unity or greater), then the star continues to cool at approximately constant angular velocity until it crosses the r-mode stability curve. As discussed above all fixed points on the $T > T_{\text{peak}}$ side of the r-mode stability curve are unstable. So, the star keeps cooling through the stable regime until it crosses the r-mode stability curve again. This time the slope of the curve is positive. The star then can find thermal equilibrium $f \approx 1$ in a one mode evolution only close to the r-mode stability curve $\gamma_{GR} \approx \gamma_{\alpha v}$. Typically, $f = 1$ slightly off the stability curve for $T > T_{CFS}$. Once this happens, the right hand side of Eq. (B-26) becomes positive ($f = 1$ and $\gamma_{GR} > \gamma_{\alpha v}$) and makes f increase (the star heats) again. The neutrino cooling ($\propto T^6$) eventually balances the heating as the temperature increases. This balance happens in the stable region $\gamma_{GR} < \gamma_{\alpha v}$. At this point ($f = 1$ and $\gamma_{GR} < \gamma_{\alpha v}$) the right hand side of Eq. (B-26) is negative and f starts decreasing (the star cools). The star enters the unstable region again and thermal oscillation repeats. In this time the angular velocity of the star decreases slowly.

In other words, the thermal equilibrium points (fixed points) on the left side of the r-mode stability curve ($T < T_{\text{peak}}$; positive slope) are initially stable and the r-mode stability curve acts as an attractor. The star exhibits thermal oscillations at constant angular velocity around this curve with the oscillations becoming smaller and smaller until the trajectory of the star coincides with the r-mode stability curve. As the star spins down the viscosity decreases and the heating is slower. If the thermal equilibrium becomes unstable, then the thermal oscilla-

tions restart with growing amplitude until the return to thermal equilibrium is no longer possible. The star cools until the daughter modes are excited and the viscosity due to all three modes balances the cooling. Otherwise, the star continues cooling and spinning down on the r-mode stability curve. Eventually, the star enters the stable regime again after boundary layer viscosity dominates bulk viscosity and the slope of the r-mode stability curve changes.

BIBLIOGRAPHY

- [1] A. P. Lundgren, R. Bondarescu, D. Tsang and M. Bondarescu, Phys. Rev. D **77**, 042003 (2008). [arXiv:0710.3808].
- [2] J. Balakrishna, R. Bondarescu, G. Daues, F. S. Guzman and E. Seidel, Class. Quant. Grav. **23**, 2631 (2006). [arXiv:gr-qc/0602078].
- [3] J. Balakrishna, R. Bondarescu, G. Daues, F. S. Guzman and E. Seidel, Phys. Rev. D **77**, 024028 (2008). [arXiv:0710.4131].
- [4] D. C. Backer *et al.*, Nature **300**, 615 (1982).
- [5] J. M. Lattimer and M. Prakash, Science **304**, 536 (2004).
- [6] D. R. Lorimer, F. Camilo, P. Freire, M. Kramer, and A. G. Lyne, R. N. Manchester and N. D'Amico, Astron. Soc. of the Pacific Conf. Ser. **302**, 363 (2003).
- [7] <http://chandra.harvard.edu/photo/2005/47tuc/>.
- [8] R. Wijnands, and M. van der Klis, Nature **394**, 344 (1998).
- [9] C. O. Heinke, P. G. Jonker, R. Wijnands, R. E. Taam, Astrophys. J. **660**, 1424 (2007). astro-ph/0612232.
- [10] D. Chakrabarty *et al.*, Nature **424**, 42 (2003).
- [11] D. Chakrabarty, Astron. Soc. Pac. Conf. Series **328**, 279 (2005).
- [12] D. Altamirano, P. Casella, A. Patruno, R. Wijnands, M. van der Klis, Astrophys. J. **674**, L45 (2008).
- [13] A. L. Watts, B. Krishnan, L. Bildsten, B. Schutz, arXiv:0803.4097.
- [14] P. Kaaret, E. H. Morgan, R. Vanderspek, and J. A. Tomsick, Astrophys. J., **638**, 963 (2006).
- [15] F. K. Lamb and S. Boutloukos, arXiv:0705.0155.
- [16] G. B. Cook, S. L. Shapiro, and S. A. Teukolsky, Astrophys. J **423** L117 (1994).

- [17] G. B. Cook, S. L. Shapiro, and S. A. Teukolsky, *Astrophys. J* **424** 823 (1994).
- [18] J. W. T. Hessels *et al.* *Science* **311** 1901 (2006).
- [19] J. E. Grindlay, *Science* **311**, 1876 (2006).
- [20] D. A. Green, S. P. Reynolds, K. J. Borkowski, U. Hwang, I. Harnett, and R. Petre, *MNRAS* **387**, L54 (2008).
- [21] A. G. Lyne, R. S. Pritchard and F. Graham Smith, *MNRAS* **265**, 1003 (1993).
- [22] C. Wang, D. Lai, and J. L. Han, *astro-ph/0509484*.
- [23] C.-A. Faucher-Giguere and V. Kaspi, *ApJ* **643**, 931 (2006).
- [24] R. Perna., R. Soria, D. Pooley and L. Stella, *MNRAS* **384**, 1638 (2008). [arXiv: 0712.1040].
- [25] An alternative explanation for the relatively low spins of newborn neutron stars that will not be discussed in this work assumes that the core and the envelope of the progenitor rotate at different rates. The core loses angular momentum via some mechanism and then the neutron star can be born with a period in the observed range.
- [26] S. Chandrasekhar, *Phys. Rev. Lett.* **24**, 611 (1970).
- [27] J. L. Friedman and B. F. Schutz, *Astrophys. J.* **222**, 281 (1978). J. L. Friedman and B. F. Schutz, *Astrophys. J.* **221**, 937 (1978).
- [28] N. Andersson, *Astrophys. J.* **502**, 708 (1998).
- [29] J. Friedman and S. Morsink, *Phys. Rev. D* **80**, 4843 (1998).
- [30] L. Lindblom, B. J. Owen, and S. M. Morsink, *Phys. Rev. Lett* **80**, 4843 (1998).
- [31] N. Andersson, K. Kokkotas, and B. F. Schutz, *Astrophys. J.* **510**, 846 (1999).
- [32] B. J. Owen, L. Lindblom, C. Cutler, B. F. Schutz, A. Vecchio, and N. Andersson, *Phys. Rev.* **D58**, 084020 (1998).
- [33] L. Lindblom, G. Mendell, and B. J. Owen, *Phys. Rev.* **D60**, 64006 (1999).

- [34] W. Ho and D. Lai, *Astrophys. J.* **543**, 386 (2000). astro-ph/9912296.
- [35] S. M. Mornsink and V. Rezanian, *Astrophys. J.* **574**, 908 (2002).
- [36] D. Lai, *MNRAS* **307**, 1001 (1999).
- [37] A. Passamonti, B. Haskell, N. Andersson, D. I. Jones and I. Hawke, arXiv:0807.3457.
- [38] Y. Levin, *Astrophys. J.* **517**, 328 (1999).
- [39] P. Arras *et al.*, *Astrophys. J.* **591**, 1129 (2003).
- [40] J. Heyl, *Astrophys. J.* **574**, L57 (2002).
- [41] P. B. Jones, *Astrophys. Lett.* **5**, 33 (1970). P. B. Jones, *Proc. Roy. Soc. (London)* **A323**, 111 (1971). P. B. Jones, *Phys. Rev. Lett.* **86**, 1384 (2001). P. B. Jones, *Phys. Rev.* **D64**, 084003 (2001).
- [42] L. Bildsten and G. Ushomirsky, *A&A* **529**, L33 (2000).
- [43] Y. Levin and G. Ushomirsky, *MNRAS* **322**, 515 (2001).
- [44] S. Yohida and U. Lee, *Astrophys. J.* **546**, 1121 (2001).
- [45] K. Glampedakis and N. Andersson, astro-ph/0607105, astro-ph/0411750.
- [46] L. Lindblom and B. J. Owen, *Phys. Rev.* **D65**, 063006 (2002), astro-ph/0110558.
- [47] P. Haensel, K. P. Levenfish, and D. G. Yakovlev, *Astron. and Astrophys.* **381**, 1080 (2002), astro-ph/0110575.
- [48] M. Nayyar and B. J. Owen, *Phys. Rev. D* **73** (2006) 084001, astro-ph/0512041.
- [49] N. Andersson, D. I. Jones, and K. D. Kokkotas, *MNRAS* **337**, 1224 (2002).
- [50] R. Wagoner, *Astrophys. J.* **578**, L63 (2002).
- [51] J. Brink, S. A. Teukolsky, and I. Wasserman, *Phys. Rev.* **D70** (2004) 121501, gr-qc/0406085.

- [52] J. Brink, S. A. Teukolsky, and I. Wasserman, Phys. Rev. **D70** (2004) 124017, gr-qc/0409048.
- [53] J. Brink, S. A. Teukolsky, and I. Wasserman, Phys. Rev. **D71** (2005) 064029, gr-qc/0410072.
- [54] A. K. Schenk, P. Arras, E. E. Flanagan, S. A. Teukolsky, I. Wasserman, Phys.Rev. **D65** (2002) 024001, gr-qc/0101092.
- [55] Y. S. Dimant, Phys. Rev. Lett. **84**, 622 (2000).
- [56] J. Wersinger, J. Finn, and E. Ott, Phys. Fluids **23**, 1142 (1980).
- [57] E. F. Brown, Ap. J **531**, 988 (2000).
- [58] H. Schatz, Phys. Rep. **294**, 167 (1998).
- [59] D. G. Yakovlev and K. P. Levenfish, Astron. Astrophys. **297**, 717 (1995).
- [60] D. G. Yakovlev and K. P. Levenfish, and Yu. A. Shibano, Soviet Phys.-Uspekhi, **42**, 737 (1999).
- [61] D. G. Yakovlev, A. D. Kaminker, and O. Y. Gnedin, A&A, **379**, L5 (2001).
- [62] D. G. Yakovlev, and C. J. Pethick, Ann. Rev. Astron. Astrophysics, **42**, 169 (2004).
- [63] G. Bryan, Philos. Trans. R. Soc. London **A180**, 187 (1889).
- [64] C. J. Pethick, D. G. Ravenhall, C. P. Lorenz, Nucl. Phys. **A584**, 675 (1995).
- [65] C. Cutler and L. Lindblom, Astrophys. J **314**, 234 (1987).
- [66] K. D. Kokkotas and N. Stergioulas, Astron. and Astrophys. **341**, 110 (1999).
- [67] J. B. Kinney and G. Mendell, Phys.Rev. **D67** 024032 (2003).
- [68] R. V. Wagoner, J. F. Hennawi, J. Liu, Proceedings of the 20th Texas Symposium on Relativistic Astrophysics, 781 (2001), astro-ph/0107229.

- [69] P. R. Brady, T. Creighton, C. Cutler, B. F. Schutz, *Phys. Rev. D* **57**, 2101 (1998), gr-qc/9702050. P. R. Brady, T. Creighton, *Phys. Rev. D* **61**, 082001 (2000), gr-qc/9812014.
- [70] B. J. Owen and L. Lindblom, *Class.Quant.Grav.* **19**, 1247-1254 (2002), gr-qc/0111024.
- [71] A. Reisenegger and A. Bonacic, *Phys. Rev. Lett.* **91** (2003) 201103, arXiv: astro-ph/0303375.
- [72] A. Reisenegger and A. Bonacic, "International Workshop On Pulsars, AXPs And SGRs Observed With BeppoSAX And Other Observatories" proceedings, Marsala, Sicily, Italy, September 2002. arXiv: astro-ph/0303454.
- [73] Jeandrew Brink, Ph. D. Thesis. Cornell University.
- [74] R. Bondarescu, S. Teukolsky and I. Wasserman, *Phys. Rev. D* **76**, 064019 (2007), arXiv:0704.0799.
- [75] K. H. Lockitch and J. L. Friedman *Astrophys. J.* **521**, 764 (1999). arXiv:gr-qc/9812019.
- [76] Sharon Morsink private communication.